2004-09

Sidelobe canceller jamming using hot-clutter

Oruc, Ercan

Monterey California. Naval Postgraduate School

NAVAL POSTGRADUATE SCHOOL

MONTEREY, CALIFORNIA

THESIS

SIDELOBE CANCELLER JAMMING USING HOT-CLUTTER

by

Sargun Goktun
and
Ercan Oruc

September 2004

Thesis Advisor: D. Curtis Schleher
Second Reader: David Jenn

Approved for public release; distribution is unlimited

THIS PAGE INTENTIONALLY LEFT BLANK

REPORT DOCUMENTATION PAGE			Form Approved OMB No. 0704-0188

1. AGENCY USE ONLY *(Leave blank)*	2. REPORT DATE	3. REPORT TYPE AND DATES COVERED
	September 2004	Master's Thesis

4. TITLE AND SUBTITLE: Sidelobe Canceller Jamming using Hot-clutter	5. FUNDING NUMBERS
6. AUTHOR(S) Sargun Goktun and Ercan Oruc	
7. PERFORMING ORGANIZATION NAME(S) AND ADDRESS(ES) Naval Postgraduate School Monterey, CA 93943-5000	8. PERFORMING ORGANIZATION REPORT NUMBER
9. SPONSORING /MONITORING AGENCY NAME(S) AND ADDRESS(ES) N/A	10. SPONSORING/MONITORING AGENCY REPORT NUMBER

11. SUPPLEMENTARY NOTES The views expressed in this thesis are those of the author and do not reflect the official policy or position of the Department of Defense or the U.S. Government.

12a. DISTRIBUTION / AVAILABILITY STATEMENT	12b. DISTRIBUTION CODE
Approved for public release; distribution is unlimited.	

13. ABSTRACT (maximum 200 words)

Coherent Sidelobe Cancellation (CSLC) is a coherent processing technique that has the potential of reducing noise jamming through the antenna side lobes. Present CSLCs have the capability of reducing the noise jamming by 25 to 35 dB. The maximum number of side lobe jammers that can be handled by a CSLC is equal to the number of auxiliary antennas.

The performance of CSLC is governed by nonlinear stochastic differential equations that are not solvable by analytic means. Therefore this thesis employs simulation techniques to solve these equations.

The CSLC becomes saturated as the number of jammers in different directions exceeds the number of loops. Jammer multipath adds an additional degree of freedom for each multipath signal that has a direction different than that of the main jammer.

The objective of this thesis was to determine the effect that these multipath or hot clutter signals have on a CSLC. It was found that hot clutter produced substantial degradations on single, double and triple CSLCs. The effect was most pronounced for single cancellers where multipath with a magnitude of 1% of the jamming signal reduced the cancellation ratio by 18 dB. Comparable numbers for double and triple cancellers were 11 dB.

14. SUBJECT TERMS	15. NUMBER OF PAGES
Sidelobe Canceller, Hot-clutter	129
	16. PRICE CODE

17. SECURITY CLASSIFICATION OF REPORT	18. SECURITY CLASSIFICATION OF THIS PAGE	19. SECURITY CLASSIFICATION OF ABSTRACT	20. LIMITATION OF ABSTRACT
Unclassified	Unclassified	Unclassified	UL

NSN 7540-01-280-5500 Standard Form 298 (Rev. 2-89)
Prescribed by ANSI Std. 239-18

THIS PAGE INTENTIONALLY LEFT BLANK

Approved for public release; distribution is unlimited

SIDELOBE CANCELLER JAMMING USING HOT-CLUTTER

Sargun Goktun
Major, Turkish Air Force
B.S., Turkish Air Force Academy, 1990

Ercan Oruc
Lieutenant Junior Grade, Turkish Navy
B.S., Turkish Naval Academy, 1998

Submitted in partial fulfillment of the
requirements for the degree of

MASTER OF SCIENCE IN SYSTEMS ENGINEERING

from the

NAVAL POSTGRADUATE SCHOOL
September 2004

Authors: Sargun Goktun

Ercan Oruc

Approved by: D. Curtis Schleher
Thesis Advisor

David Jenn
Second Reader

Dan C. Boger
Chairman, Department of Information Sciences

THIS PAGE INTENTIONALLY LEFT BLANK

ABSTRACT

Coherent Sidelobe Cancellation (CSLC) is a coherent processing technique that has the potential of reducing noise jamming through the antenna side lobes. Present CSLCs have the capability of reducing the noise jamming by 25 to 35 dB. The maximum number of side lobe jammers that can be handled by a CSLC is equal to the number of auxiliary antennas.

The performance of CSLC is governed by nonlinear stochastic differential equations that are not solvable by analytic means. Therefore this thesis employs simulation techniques to solve these equations.

The CSLC becomes saturated as the number of jammers in different directions exceeds the number of loops. Jammer multipath adds an additional degree of freedom for each multipath signal that has a direction different than that of the main jammer.

The objective of this thesis was to determine the effect that these multipath or hot clutter signals have on a CSLC. It was found that hot clutter produced substantial degradations on single, double and triple CSLCs. The effect was most pronounced for single cancellers where multipath with a magnitude of 1% of the jamming signal reduced the cancellation ratio by 18 dB. Comparable numbers for double and triple cancellers were 11 dB.

THIS PAGE INTENTIONALLY LEFT BLANK

TABLE OF CONTENTS

LIST OF FIGURES

THIS PAGE INTENTIONALLY LEFT BLANK

LIST OF TABLES

THIS PAGE INTENTIONALLY LEFT BLANK

ACKNOWLEDGMENTS

The authors would like to extend their thanks to thesis advisor Professor D. Curtis Schleher, Naval Postgraduate School, Monterey, CA for his patience, guidance, and flexibility throughout the thesis process. His insights, expert knowledge and condor on the issue were invaluable to this study. The authors also would like to thank to Professor David C. Jenn for agreeing to be the second reader to the thesis. The precious time they took to educate us on the points of electromagnetism, antenna theory, and radar theory are sincerely appreciated.

The author Sargun Goktun is most grateful to his wife Aysun and the author Ercan Oruc is most grateful to his wife Filiz for their endless love, support, encouraging, and understanding to complete their Master’s Degree and this thesis.

Additionally, the authors would like to thank to their family members for their continuing love and support.

Finally, the authors would like to express their sincere gratitude to their country Turkey, Turkish Air Force and Turkish Navy for giving them the opportunity to undertake this study.

THIS PAGE INTENTIONALLY LEFT BLANK

I. INTRODUCTION

A major operational form of noise jamming is called stand-off or support jamming. The objective of this form of jamming is to shield an operational force by injecting interference into the radars side lobes (also the main lobe if geometrically feasible). Support jamming aircraft that are capable of carrying large amounts of jamming resources while employing a directional antenna are dedicated to this purpose. The jammer has the advantage that its signal is attenuated in proportion to the second power of range, while the radar signal is attenuated by the fourth power of range and the back-scattering characteristics of the radar target. The radar has the advantage that the stand-off jammer must generally attack through the radar's sidelobes and also that the target is generally closer to the radar than is the jammer. The current radar trend is to maximize its advantage through ultra-low sidelobes and the use of sidelobe noise-cancellation techniques (sidelobe cancellers)[1].

Coherent Sidelobe Cancellation (CSLC) is a coherent processing technique that has the potential of reducing noise jamming through the antenna side lobes and is employed in a number of operational radars for this purpose. Present CSLCs have the capability of reducing the noise jamming by 25 to 35 dB, but their theoretical performance is potentially much higher. CSCLs operate by supplementing the main radar antenna with ancillary receiving antennas having the same angular coverage but displaced laterally to provide directional sensitivity. The purpose of the auxiliaries is to provide replicas of

jamming signals that are intercepted in the main antenna pattern for cancellation. An ancillary receiving antenna is required for each jammer to be canceled. Hence the maximum number of side lobe jammers that can be handled is equal to the number of auxiliary antennas.

Many current operational surveillance radars employ CSLCs using the analog Howells-Applebaum cancellation approach. In this approach weights are generated using feedback loops connected to each auxiliary antenna. The weights are then applied to the jamming signals intercepted by each auxiliary antenna, summed and then subtracted from the jamming signals received in the sidelobes of the main antenna. This process can also be viewed as generating nulls in the main antenna's receiving pattern in the direction of each jammer. Interaction of the multiple loops generally restricts the number of loops employed to a maximum of 4 with two and three loops being more common [2].

As is well-known the CSLC becomes saturated as the number of jammers in different directions exceeds the number of loops. Jammer multipath from objects in proximity of the radar add an additional degree of freedom for each multipath signal that has a direction significantly different than that of the main jammer. This provides an opportunity for the jammer to disturb the CSLC by directing its jamming signal so that it illuminates both the radar and also the surface in front of the radar. This form of operation is sometimes referred to as "hot clutter."

The objective of this thesis was to determine the effect that these multipath or hot clutter signals have on the operation of a CSLC. It was found that hot clutter

produced substantial degradations on single, double and triple CSLCs. The effect was most pronounced for single cancellers where multipath with a magnitude of 1% of the jamming signal reduced the cancellation ratio by 18 dB. Comparable numbers for double and triple cancellers were 11 dB.

The performance of a CSLC is governed by nonlinear stochastic differential equations that are not solvable by analytic means [2]. Therefore this Thesis employs simulation techniques to solve these equations. The simulation is accomplished using Simulink. Complete Simulink models are supplied for single, double, and triple CSLCs.

THIS PAGE INTENTIONALLY LEFT BLANK

II. JAMMING SIDELOBE CANCELLERS

Radar is one of the most powerful and most important sensors in the battlefield. Preventing the proper operation of a radar system is one of the major objectives of a jamming operation. Different jamming techniques can be employed against radars. Standoff jamming and escort jamming are the most useful noise jamming techniques. The noise jamming of radar through its antenna pattern sidelobes arises from the nature of standoff jamming. Since a standoff jammer can be employed outside the threat zone of enemy weapon systems, it is a safe jamming technique for the jammer platform. However a high jamming signal power must be introduced into the sidelobes of the radar antenna to be effective at long ranges.

Current radars use advanced sidelobe canceller systems to defend against sidelobe jamming, but their effectiveness is restricted to the number of sidelobe canceller loops, which is also known as the “degrees of freedom” of the canceller system. It is known that once the degrees of freedom is exceeded using multiple jamming sources (i.e. hot-clutter), the sidelobe canceller system begins to lose its effectiveness.

The hot-clutter effect is economical since the number of degrees of freedom of the sidelobe cancellers can be easily overloaded. It is more efficient to use hot-clutter effects instead of using much more expensive multiple stand-off or escort jammers in different locations. Multi-path reflected signals arising from one jamming source, reduce the cancellation performance dramatically, especially when they are very powerful and distributed in

different angles. This effect improves jamming effectiveness, and is the main theme of this research study.

The computer simulation of hot-clutter effects on sidelobe canceller units caused a large degradation of up to 36.2 dB in the cancellation performance. These simulation results also showed that the relative operating range of the radar can be decreased a maximum of 87% by using hot-clutter effects. This demonstrates that hot-clutter is a major threat to the operation of radar systems as well as sidelobe canceller systems.

The time-varying nature of hot-clutter further affects sidelobe cancellers, where the response time and loop-noise compete with each other. The canceller loop should be implemented with a very fast response time to track these time-varying jamming signals. Computer simulation experiments proved that very fast responsive canceller loops can be designed, but in the steady state condition the loop noise effects degrades the canceller performance by a considerable amount. The loop should be designed with very strict error tolerances to overcome this problem. This is very costly and difficult owing to performance limitations of real-time correlation loops.

Since hot-clutter introduces closely spaced replicas of jamming signals into a radar system, it is necessary to insert multiple nulls to effectively mitigate hot-clutter effects. The multiple sidelobe canceller computer simulation verifies the improvement of cancellation performance by up to 20.43 dB by increasing the number of degrees of freedom up to four. In the presence of more than one jamming source, it is necessary to increase the number

of sidelobe canceller loops. Under these circumstances using the hot-clutter effect increases the required number of sidelobe canceller loops. Due to design considerations, it is not easy to build a system with many sidelobe cancellers, so using the hot clutter effect presents a serious problem for the radar designer.

As a result, jammers present a special problem due to multipath (i.e. reflection of the jammer interference off the earth into the radar), especially when the jammer is located in the sidelobes of the radar. In regions where the Earth is very smooth (e.g., smooth sea) this multipath may appear at the same azimuth as the direct jammer interference.

THIS PAGE INTENTIONALLY LEFT BLANK

III. CANCELLER LOOP DESIGN AND COMPUTER SIMULATION

A. OVERVIEW

In this chapter, a conventional Howells-Applebaum analog correlation loop has been designed and simulated with a MATLAB Simulink software package.

First, one sidelobe canceller with only one auxiliary antenna is simulated to validate the design. In fact, a single canceller loop represents only one amplitude and phase change on the auxiliary antenna signal. So, a sidelobe canceller system with only one auxiliary antenna is unable to cancel more than one jamming signal. Cancellation of more interference signals from different directions requires different weights to be used for each interference signal. Using more than one auxiliary antenna with a correlation loop attached to each one can approach the problem of canceling interference from multiple jamming signals at different angular locations. The number of maximum jamming signals that the system can cancel is equal to the number of auxiliary antennas and attached control loops, which is also known as the degrees of freedom of a canceller system.

A single jamming signal from one jammer arrives at the radar via two paths: a direct path and a surface-reflected path, which is due to reflections from the earth’s surface. Surface-reflected jamming signals are distributed at different angles as a result of surface roughness. Surface-reflected signals differ from the original jamming signal in amplitude and phase due to the surface reflection coefficient and the slight range difference between the direct path and the surface-reflected path.

The Howells-Applebaum implementation of the multiple sidelobe canceller system is shown in Figure 1, where there is a correlation loop attached to each auxiliary antenna.

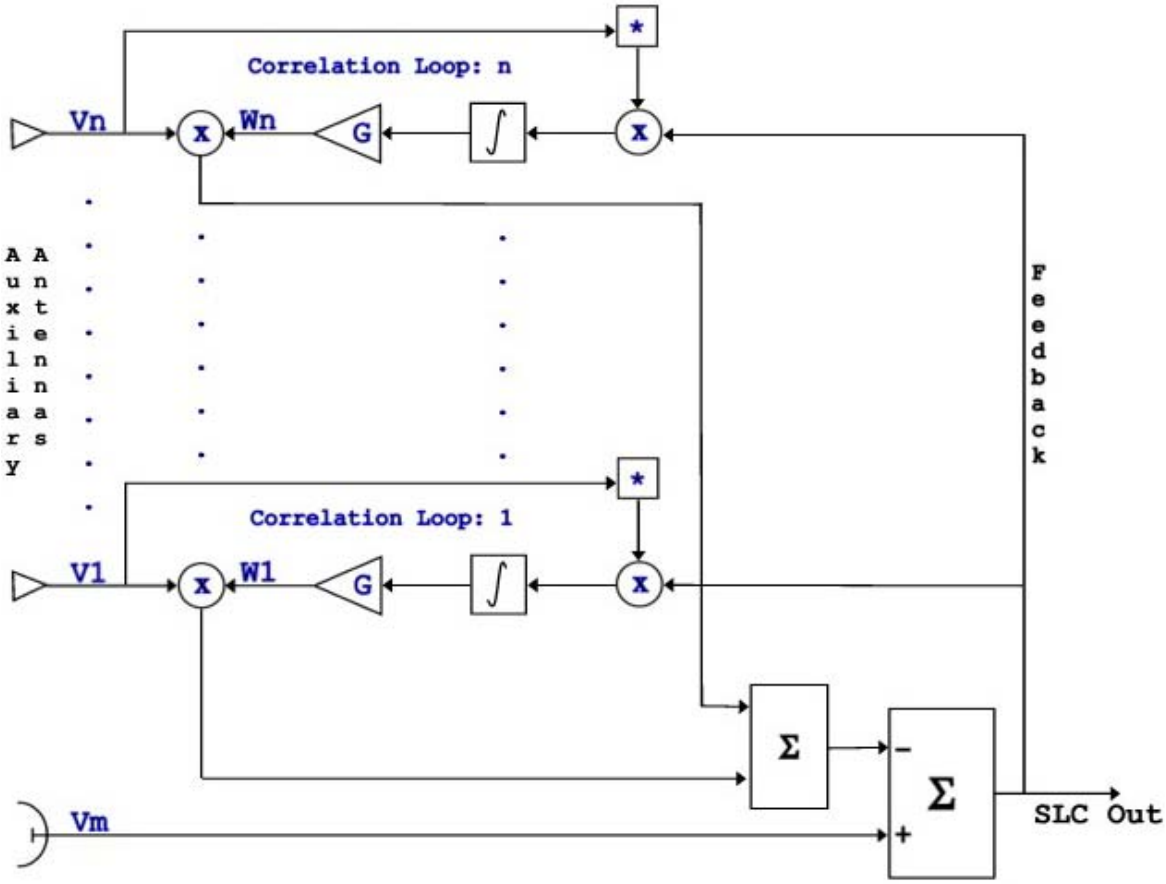

Figure 1. Howells-Applebaum Implementation of Multiple SLC

In Figure 1, V_m denotes the signal coming from the main antenna and $V_1 \ldots V_n$ denote the signals coming from the auxiliary antennas. Amplifier outputs $W_1 \ldots W_n$ denote the complex weights generated by each control loop. Also, the complex weight of each channel determines the amplitude and phase change applied to each auxiliary antenna signal. These weights are used to correlate the auxiliary channel signals with the main channel signal.

The sidelobe canceller output signal is fed back to the correlation loops.

B. CANCELLER LOOP DESIGN AND IMPLEMENTATION

The conventional Howells-Applebaum control loop is designed according to the trade-off analysis in Appendix B sections D1-c and d. The Howells-Applebaum control loop theory is explained in Appendix B section D1 and schematically drawn in Figure 47.

The receiver channel bandwidth, BW_c, is simulated as 100 kHz, $BW_c = 100$ kHz. The receiver filter time constant, τ_c, is

$$\tau_c = \frac{1}{2\pi BW_c}$$
$$\tau_c = \frac{1}{200,000\pi}. \qquad (3.1)$$

The canceller loop bandwidth, BW_{SLC}, is chosen not to exceed one-tenth of the receiver channel bandwidth.

$$BW_{SLC} \leq \frac{BW_c}{10}, \tau_{SLC} \geq 10\tau_c. \qquad (3.2)$$

$$\tau_{SLC} \geq \frac{1}{20,000\pi}. \qquad (3.3)$$

A good average of the weight process is obtained by choosing the maximum canceller loop bandwidth as 10 kHz, $BW_{SLC} = 10$ kHz.

A hard-limiter is used to reduce the dependence of the loop performance on the intensity of the external noise field. Then the amplitude variations in the conjugate signal are removed, and only the phase variations remain.

Thus, the canceller loop is more sensitive to the phase variations of the input signal rather than to the amplitude variations.

The weight *W* reaches its optimum value with the transient time constant of the canceller loop being [21]

$$\tau_{SLC} = \frac{\tau_{LPF}}{\left(1 + G\left|\bar{V}_a\right|\right)}. \tag{3.4}$$

The minimum canceller loop time constant, from Equation (3.3), is

$$\tau_{SLC_{min}} = \frac{1}{20,000\pi}. \tag{3.5}$$

The low-pass filter time constant, τ_{LPF}, and amplifier gain, G, are chosen to keep the canceller loop time constant, τ_{SLC}, within its limits, as defined by Equation (3.3) and Equation (3.5).

The main jammer signal power is normalized at 1 W. So the receiver self-noise power is adjusted to simulate different Jammer-to-noise Ratio values.

The closed-loop gain reaches its minimum value when all the receiver noises are removed from the system. The minimum value of the voltage coming from the auxiliary antenna channel, $\left(\left|\bar{V}_a\right|\right)_{min}$, is

$$\left(\left|\bar{V}_a\right|\right)_{min} = 1.696 \tag{3.6}$$

where the auxiliary antenna gain is twice the main antenna gain. The minimum closed-loop gain is

$$\left(G\left|\bar{V}_a\right|\right)_{min} = G\left(\left|\bar{V}_a\right|\right)_{min}. \tag{3.7}$$

The weight reaches its ideal value when $G\left|\bar{V}_a\right| \gg 1$ [21]. The amplifier gain, G, is chosen to satisfy this condition when voltage coming from the auxiliary antenna is at its minimum value of 1.696

$$\left(G\left|\bar{V}_a\right|\right)_{min} = G \times 1.696 . \tag{3.8}$$

The minimum closed-loop gain, $\left(G\left|\bar{V}_a\right|\right)_{min}$, is chosen to be 10,000 to satisfy the condition of $G\left|V_a\right| \gg 1$. Thus

$$G \times 1.696 = 10,000 . \tag{3.9}$$

The minimum value of the amplifier gain is 5,896.226 to keep the minimum closed-loop gain, $\left(G\left|\bar{V}_a\right|\right)_{min}$, at 10,000. The amplifier gain is chosen to be 5,900, so the minimum closed-loop gain is

$$\left(G\left|\bar{V}_a\right|\right)_{min} = 10,006.4 . \tag{3.10}$$

The minimum closed loop gain is 10,006.4, which always satisfies $G\left|\bar{V}_a\right| \gg 1$.

The voltage coming from the auxiliary channel approaches its maximum value as the receiver self-noise is added to the system. The maximum value of the voltage from the auxiliary antenna channel is

$$\left(\left|\bar{V}_a\right|\right)_{max} = 1.896 . \tag{3.11}$$

The maximum value of the closed-loop gain is

$$\left(G\left|\bar{V}_a\right|\right)_{max} = 11,186.4 . \tag{3.12}$$

The canceller loop time constant reaches its minimum value when the closed-loop gain reaches its maximum value of 11,186.4. The low-pass filter time constant is chosen to

keep the closed-loop time constant within its limits, as defined by Equation (3.3) and Equation (3.5)

$$\tau_{SLC_{min}} = \frac{\tau_{LPF}}{1 + \left(G\left|\bar{V}_a\right|\right)_{max}} \tag{3.13}$$

$$\tau_{LPF_{min}} = \frac{1}{1.7877\pi}. \tag{3.14}$$

This is the minimum value of the low-pass filter time constant to satisfy the closed-loop time constant, which is always greater than $\frac{1}{20,000\pi}$. The low-pass filter time constant is chosen to be $\frac{1}{1.5\pi}$. Therefore the minimum value of closed-loop time constant is

$$\tau_{SLC_{min}} = \frac{1}{16,781.1\pi}, \tag{3.15}$$

which always satisfies Equation (3.3).

1. Implementation of Howells-Applebaum Control Loop in MATLAB Simulink Software

The functional block diagram of Howells-Applebaum control-loop and its implementation in MATLAB Simulink software are shown in Figure 2 and Figure 3, respectively.

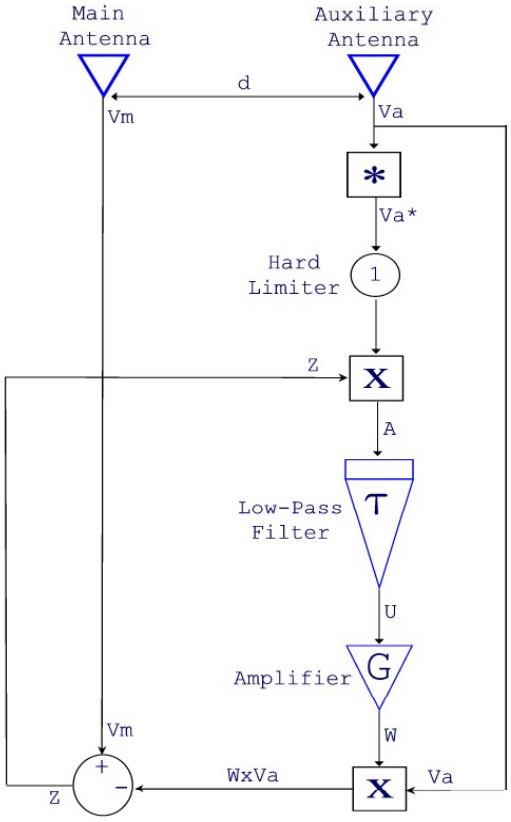

Figure 2. Conventional Howells-Applebaum Control Loop

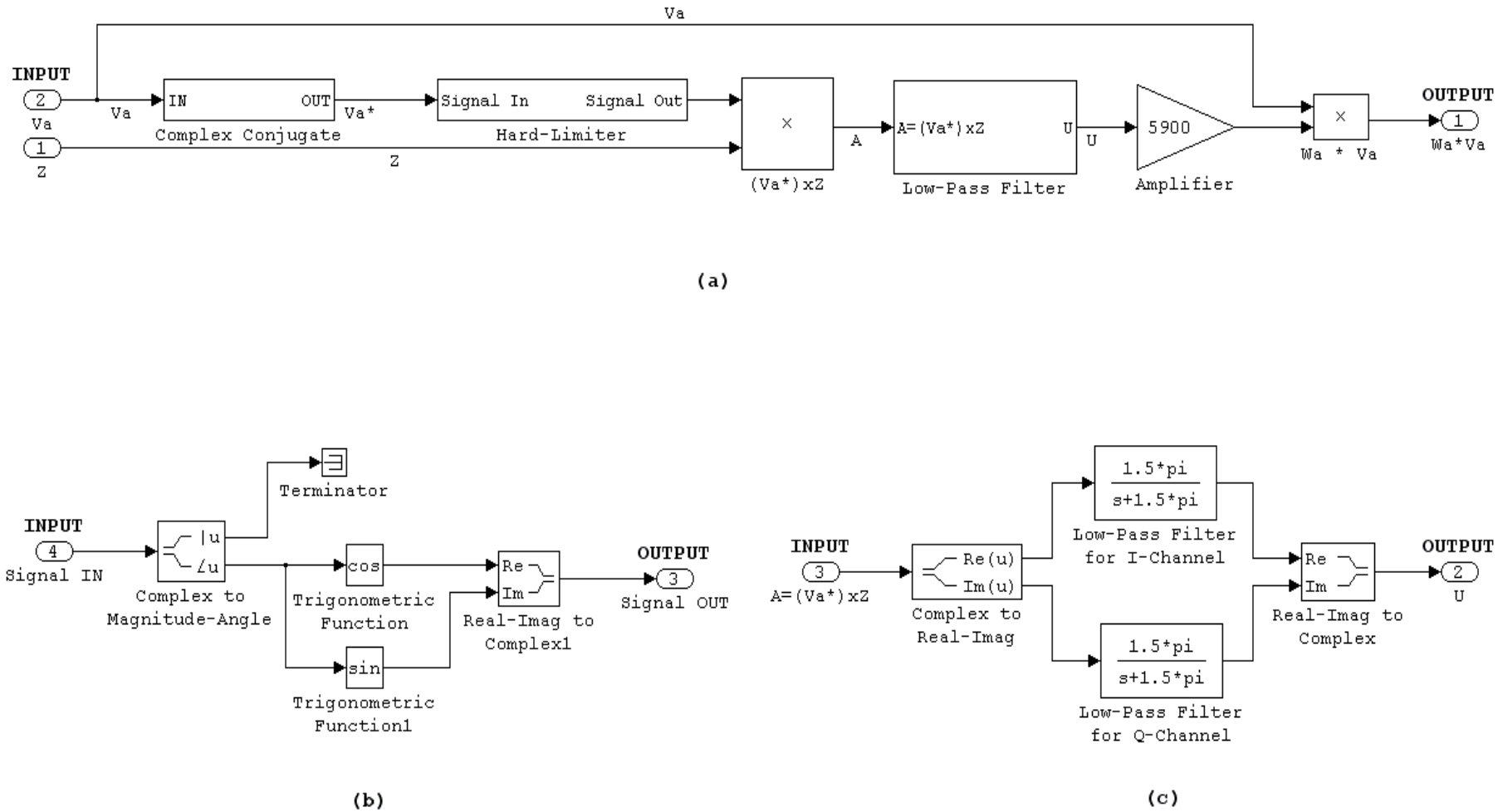

Figure 3. (a)Implementation of Howells-Applebaum Control Loop in MATLAB Simulink Software. (b)Implementation of Hard-limiter. (c)Implementation of Low-Pass Filter

The canceller loop block accepts the auxiliary antenna output, V_a, and the canceller system output, Z, as input signals and calculates the complex weight, W_a, for the auxiliary channel signal input. The block output is the multiplication of the auxiliary channel signal with the calculated weight, $W_a \times V_a$. A low-pass filter is implemented by using the s-domain transfer function and applied to real and imaginary parts of the signal separately. The first-order Butterworth low-pass filter transfer function is defined as $\frac{1}{s\tau_{LPF} + 1}$. The transfer function of the filter is implemented as $\frac{1.5\pi}{s + 1.5\pi}$, since $\tau_{LPF} = \frac{1}{1.5\pi}$.

The implementation of the Howells-Applebaum control loop is used as a block in the sidelobe canceller block diagram. It is named the Canceller Loop—N, where N denotes the number of the canceller loop.

2. Sidelobe Canceller System Implementation

All individual canceller loop outputs are summed and then subtracted from the main channel signal to obtain the sidelobe canceller system output. This output is fed back in parallel to all canceller loop inputs for the next operation cycle. The canceller system block diagram is shown in Figure 4.

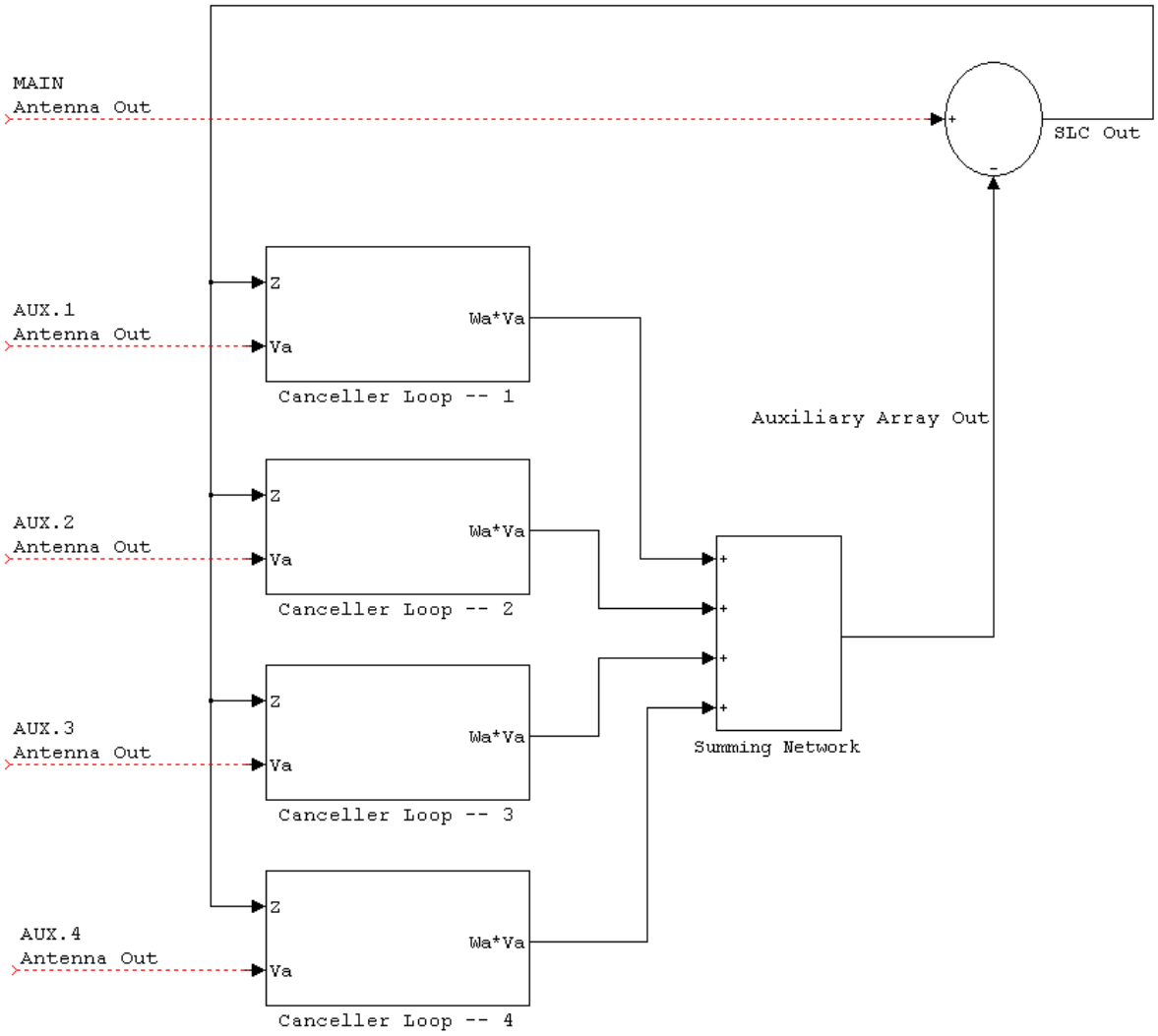

Figure 4. Sidelobe Canceller System Block Diagram

C. MODELING OF JAMMING SIGNALS

The mathematical model of the free-space jammer is

$$a(t)\cos\left[\omega t + \delta(t)\right] \tag{3.16}$$

where $a(t)$ and $\delta(t)$ represent the amplitude and phase modulation terms respectively, and ω represents the angular frequency of the signal [21]. The signal produced in the main channel is

$$G_{sl}a(t)\cos\left[\omega t + \delta(t)\right] \tag{3.17}$$

where G_{sl} is the voltage gain of the radar antenna sidelobe in the jammer direction. The signal produced in the first auxiliary antenna is

$$G_A a(t) \cos\left[\omega t + \phi + \delta(t)\right] \tag{3.18}$$

where G_A is the voltage gain of the auxiliary antenna in the jammer direction of arrival and ϕ is the phase difference term due to an extra path length, $d \sin\theta$, with respect to the radar antenna phase center, traveled by the jamming signal to reach the auxiliary antenna [21]. The phase difference term is explained in Appendix B section C1 by Equation (B.4).

The free space jamming signals are modeled as zero-mean Gaussian random variables. Since it is convenient to express Equation (3.16) as the real part of the complex number, the signals received by the main and the auxiliary antennas are

$$\begin{aligned} V_M(t) &= G_{SL} j(t) + n_M(t) \\ V_A(t) &= G_A j(t) s_1 + n_A(t) \end{aligned} \tag{3.19}$$

where $j(t)$ is the free-space jamming signal with power P_J. $n_M(t)$ and $n_A(t)$ are the thermal noises in the main and the auxiliary receiving channels with power P_N [21]. The receiver thermal noises are modeled as zero-mean Gaussian random variables. The s_1 denotes the phase shift of the jamming signal between the main and the auxiliary receiver channel due to the extra path length, $d \sin\theta$, which is explained in Appendix B section C4 by Equation (B.9).

The calculation of the phase shifted jamming signals is shown in Figure 5.

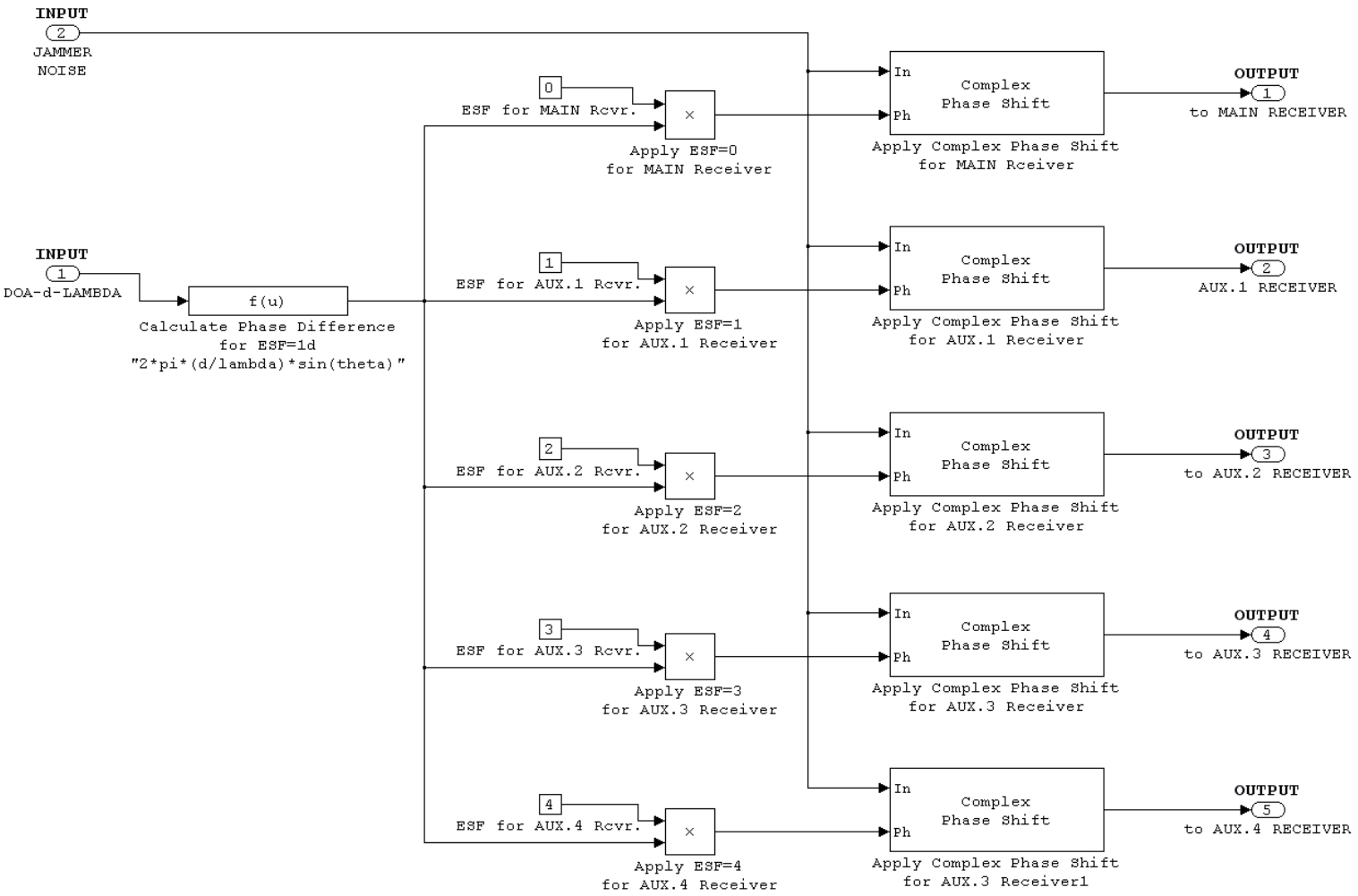

Figure 5. Application of Phase Differences to Jamming Signals

One block is built to calculate phase-shifted jamming signals arriving at antenna elements, as in Figure 5. This block accepts the jammer noise signal in a complex form. It accepts the direction of the arrival of the jammer in radians, the antenna element spacing (d) in meters, and the operating wavelength (λ) in meters as inputs.

The phase shift for the first auxiliary antenna is calculated, where ESF = 1d, and this unit phase shift is multiplied by 0, 1, 2, 3 and 4 to calculate the phase shifts for the main antenna, first auxiliary, second auxiliary, third auxiliary and fourth auxiliary antennas, respectively. These phase-shifts are applied to the jammer signal by using a complex phase shift block. Consequently, the total signal arrives to the antennas.

1. The Main Jammer Noise Generator

The main jammer noise generator block is drawn in Figure 6.

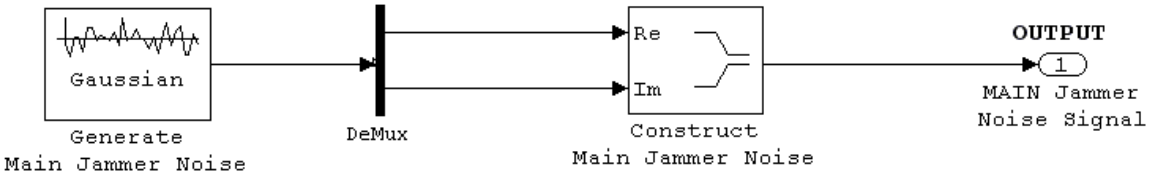

Figure 6. Generation of Main Jamming Signal

The Gaussian noise generator block is used to generate the zero-mean Gaussian random variable with 1 W power. Real and imaginary parts of the jammer noise are generated with different seeds. These parts are then combined to construct the complex main jammer noise signal.

2 Distributed Jammers Noise Generator

The distributed jammer noise generator block is drawn in Figure 7.

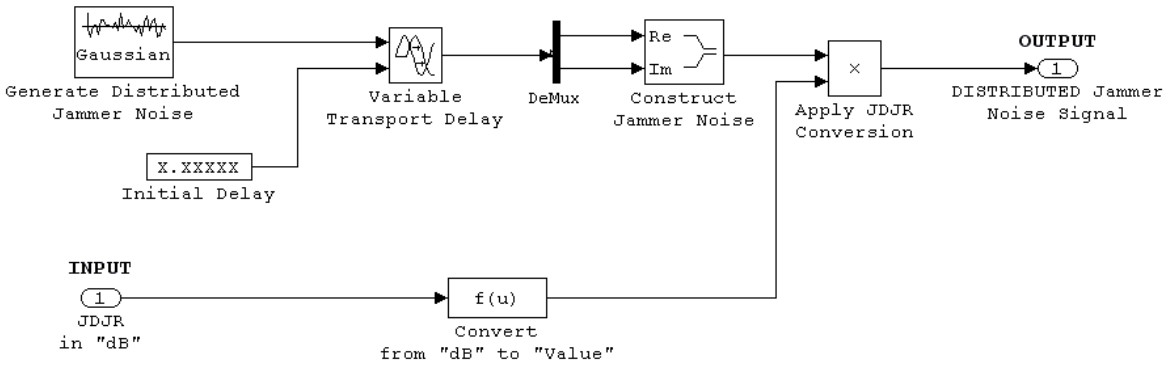

Figure 7. Generation of Distributed Jamming Signal

This block accepts the jammer-to-distributed jammer ratio (JDJR in dB) as input. The zero-mean Gaussian random variable is generated with a Gaussian noise generator block. The variable transport time delay is applied to the noise signal to uncorrelate the distributed jammer noise signal from the main jammer signal. Real and imaginary parts are also combined to obtain the complex distributed jammer noise signal with 1 W power. The noise signal is multiplied by the jammer-to-distributed jammer ratio. So, the power is adjusted according to the JDRJ. The variation of distributed jamming signal powers is simulated, which is due to different scattering coefficients of the earth's surface.

The jamming signals at each antenna element are calculated by combining Figure 5, Figure 6 and Figure 7. The distance between the antenna elements (d in meters), the operating wavelength (λ in meters), the directions of arrival of jammers (DOA in degrees), and the jammer-to-distributed jammer ratio (JDJR in dB) are also included.

Thus $\frac{d}{\lambda} = 0.5$ is chosen as a compromise value. These implementations are shown in Figure 8.

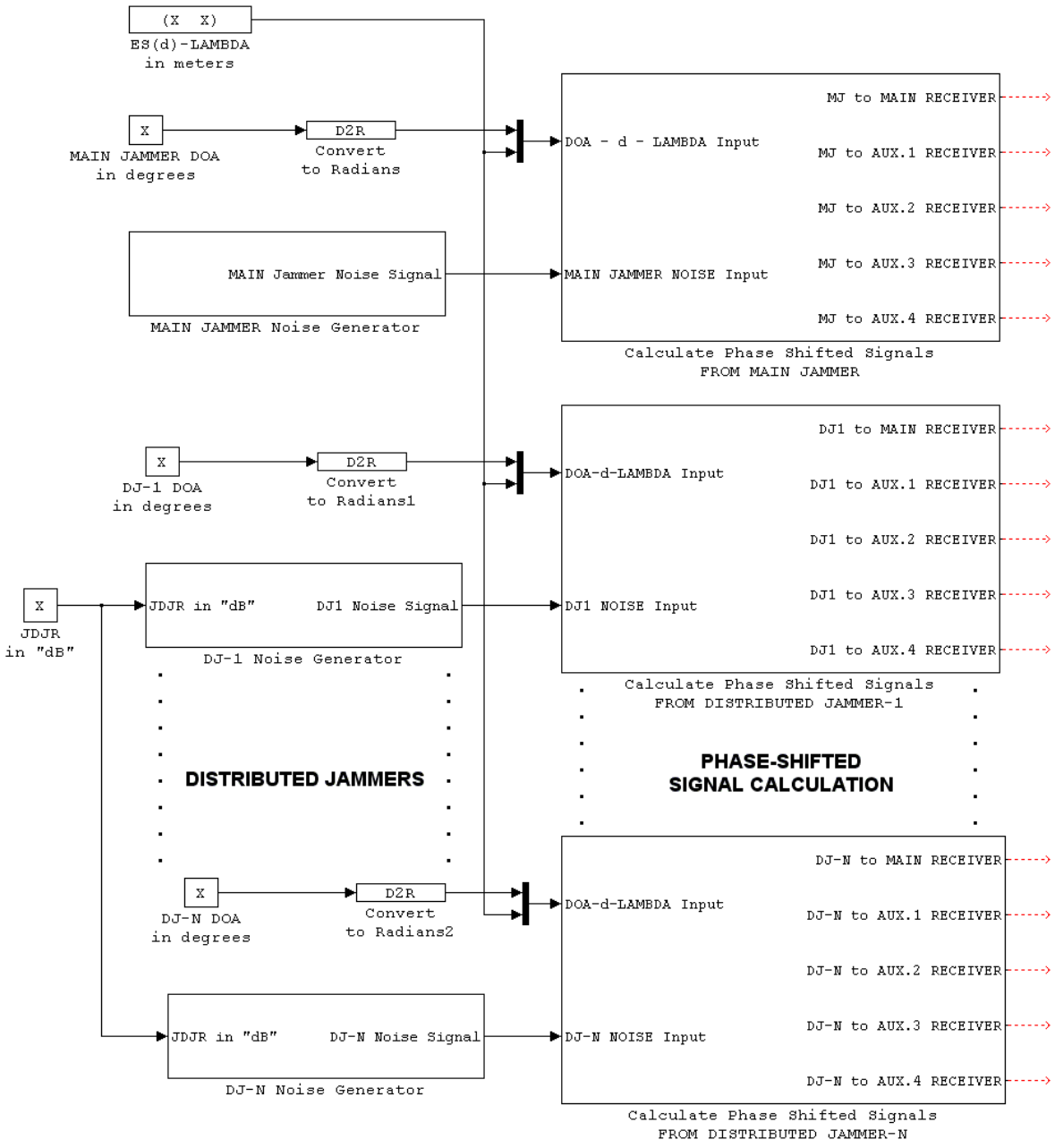

Figure 8. Generation and Calculation of Jamming Signals Arriving at Each Antenna Element

D. MODELING OF RECEIVER NOISES

The main and auxiliary receivers thermal noises, n_M and n_A, are modeled as zero-mean Gaussian random variables. The receivers noise generator block is shown in Figure 9.

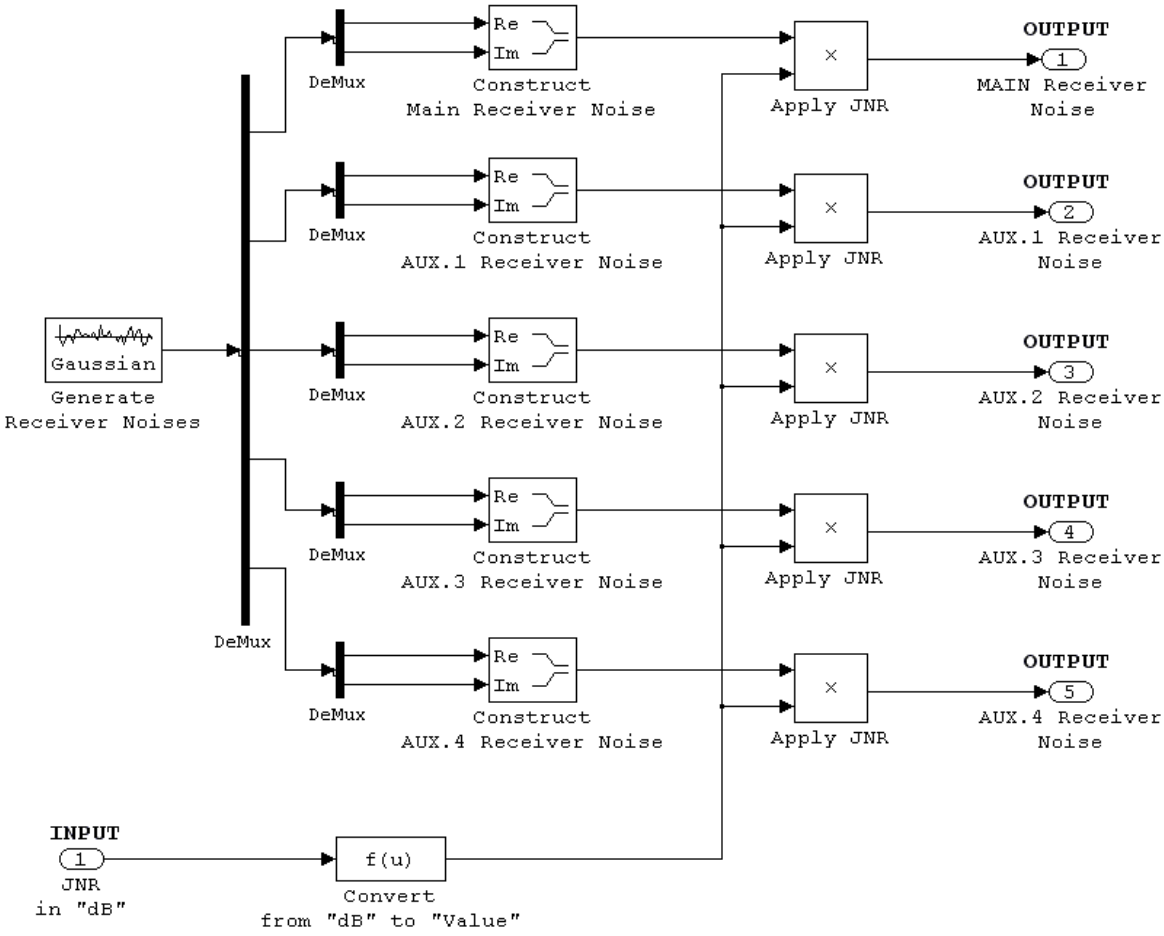

Figure 9. Generation of Receiver Self Noises

This block accepts the jammer-to-noise ratio (JNR in dB) as the input variable. Real and imaginary parts of all receiver noises are generated with the Gaussian noise generator block as zero-mean Gaussian random variables, all with different initial seeds and 1 W power. Also, the real and imaginary parts are combined to construct each receiver's self-noise signal. All the receivers' noise

signals are multiplied by the jammer-to-noise ratio to simulate different JNRs.

E. ANTENNAS AND RECEIVER CHANNEL BANDWIDTH

One main and four auxiliary antennas are modeled. The main antenna sidelobe gain is assumed to be unity and the auxiliary antenna gains are assumed to be twice the main antenna gain in the direction of the arrival of the jamming signals. In the steady state of the canceller loop, a large value of auxiliary antenna gain margin is desirable, in which case the weights of the auxiliary channels would be small and the corresponding internal noise power values in the auxiliary channels would be attenuated. However, in the transient state of the canceller loop, the transient sidelobes are proportional to the auxiliary antenna gain margin; therefore, a low value of the gain margin would be advisable. Auxiliary antenna gains are chosen to be 2 as a compromise value. Receiver self-noises are added to the received signals in the antenna block. The Simulink antenna model implementation is shown in Figure 10.

Receiver channel bandwidths are chosen to be 100 kHz. This is due to strict computational time restrictions. To implement higher receiver channel bandwidths, the sampling frequency of the jammer signal should also be increased to satisfy the Nyquist sampling theorem. This process requires very long processing times on today’s digital computers. Receiver channel bandwidth is implemented by using an s-domain transfer function of the first-order Butterworth low-pass filter. The filters are placed at the antenna outputs.

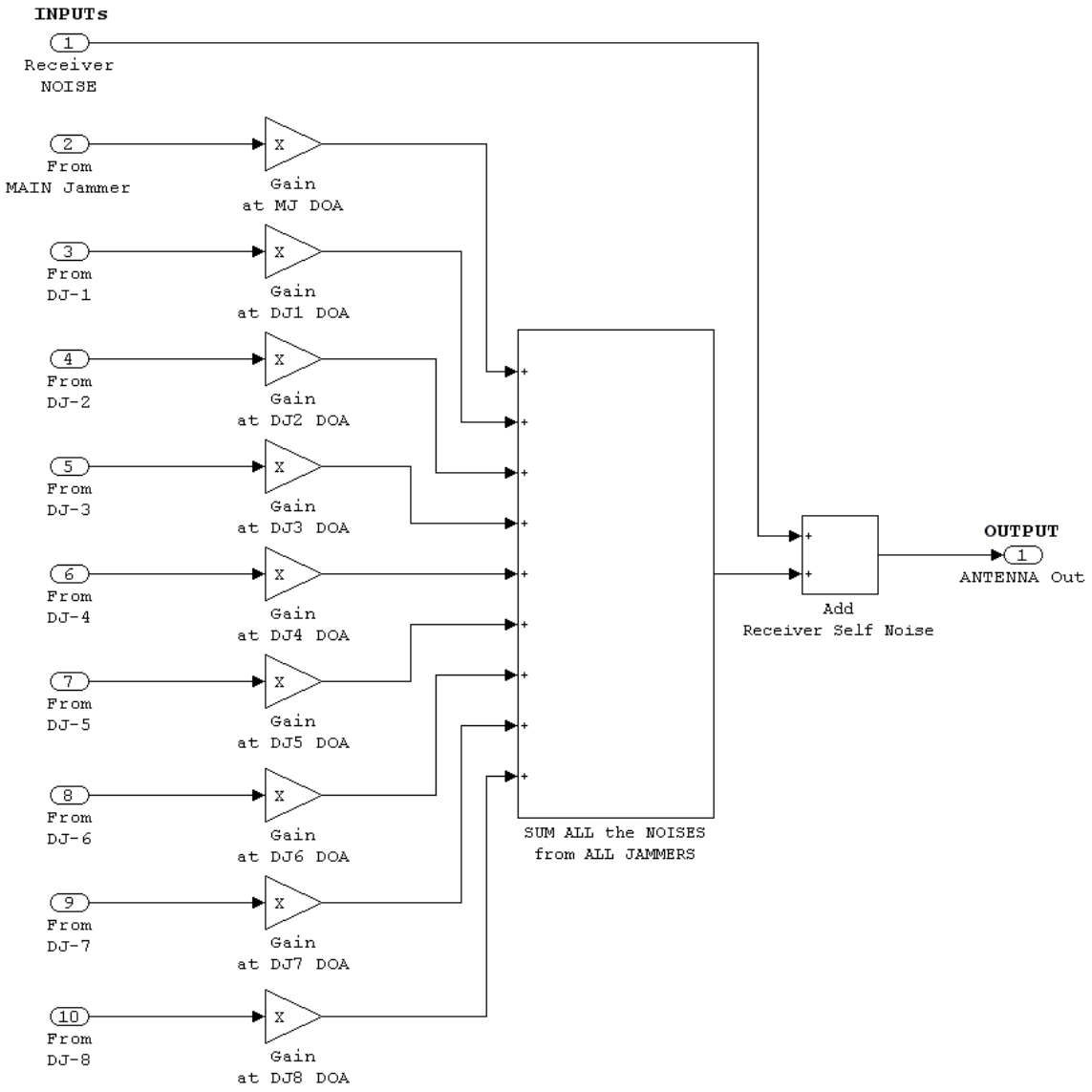

Figure 10. Antenna Implementation in Simulink Software

The antenna block accepts 11 inputs: one receiver self-noise input, one main jammer signal input and eight distributed jammer signal inputs. Receiver noises are generated, as in Figure 9, and jammer signals at the antenna elements are determined, as in Figure 8. Jammer signal inputs are multiplied with antenna gain in the direction of the arrival of the jamming signals and then summed together. The gain is 1 for the main antenna and 2

for the auxiliary antennas. Receiver self noise is added to the summation of the received jamming signals. This total signal determines the output of the antenna. Each antenna output is filtered with receiver channel bandwidth. The output of each antenna and filter combination is equal to $V_M, V_1..V_n$, shown in Figure 1. The auxiliary channel signals go into the canceller loop input after the filtering.

F. CALCULATION OF CANCELLATION RATIO

The average power levels of the main jamming signal and sidelobe canceller system output are calculated independently. These power levels are converted to decibels (dB) and then the sidelobe canceller output power is subtracted from the main jamming signal power. The cancellation ratio is obtained in dB. The block diagram of this calculation block is shown in Figure 11.

The cancellation ratio calculator block accepts the main jammer signal, the sidelobe canceller output signal, and the step size as inputs. The step size of the simulation is used to calculate the number of signal samples. This number is used when calculating the average power levels of the input signals. Since the signal powers are calculated in dB, the sidelobe canceller output power is subtracted from the main jammer signal power to obtain the cancellation ratio. The output is connected to a display to read the cancellation ratio easily during simulation.

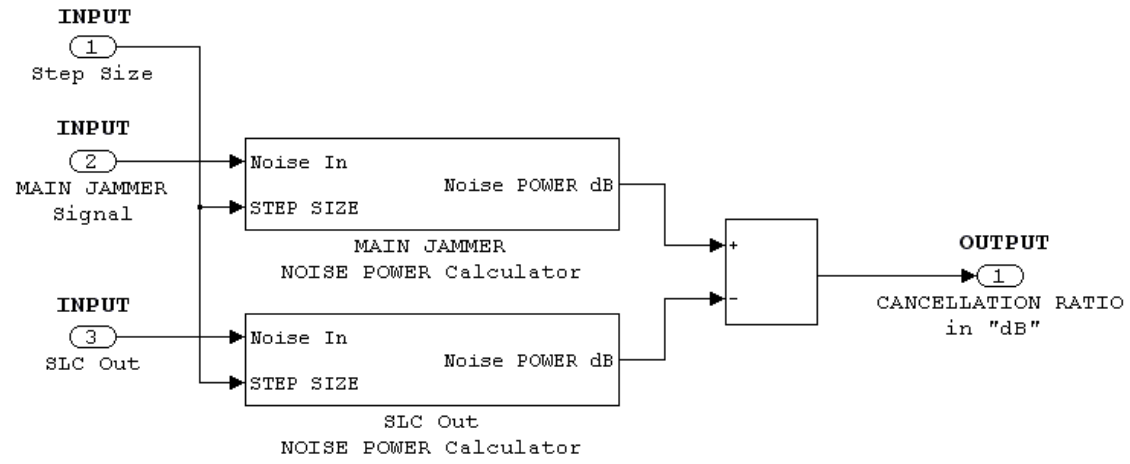

(a)

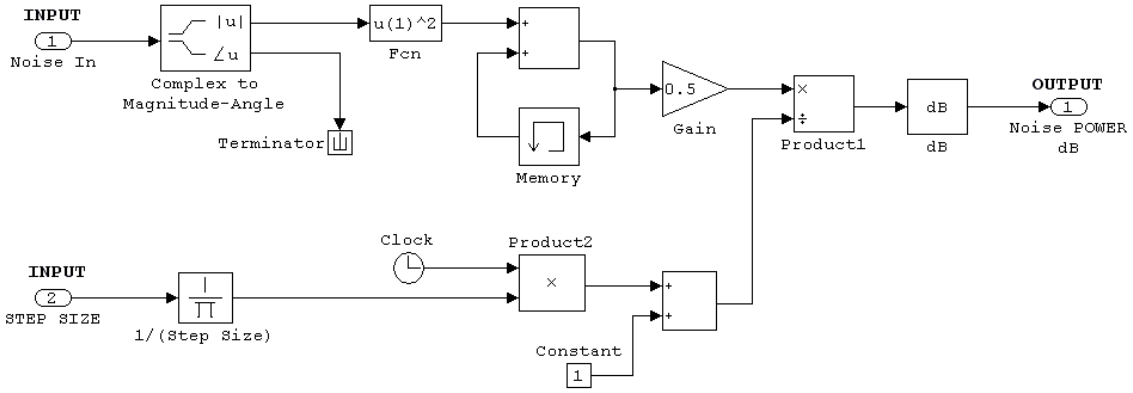

(b)

Figure 11. (a) Cancellation Ratio Calculator Block (b) Noise Power Calculator Block

IV. COMPUTER SIMULATION RESULTS

A. OVERVIEW OF COMPUTER SIMULATION

An analog multiple sidelobe canceller system is simulated using the conventional Howells-Applebaum adaptive control loop theory. This design was simulated on a computer using MATLAB Simulink software, which is one of the most suitable software packages for simulating an analog circuit. A 100 kHz receiver bandwidth was used due to computational time limitations, which was directly limited by the computer resources (i.e. cpu speed). The sampling frequency of the jamming signal was 1 MHz that was wide enough to cover the whole receiver bandwidth.

First, the sidelobe canceller design was tested to ensure its proper operation according to the theory. The control loop bandwidth was chosen to not exceed one-tenth of the receiver channel bandwidth, even under extreme jamming conditions. This provides a good average of weight processing in the steady state condition. Fast response time is obtained to track non-stationary jammers. A robust sidelobe canceller system is designed to provide a fast response time and a high steady state cancellation ratio.

Hot-clutter effects were injected into the system after the suitability of the sidelobe canceller design was tested with different jamming scenarios. Different power levels of multi-path reflected signals were applied to simulate different scattering properties of the terrain between the jammer and the receiver. Multi-path jamming signals were simulated through distribution at different angles each having the same power level.

B. SUMMARY OF SIMULATION AND PERFORMANCE EVALUATION

The hot-clutter effect was simulated on single and multiple sidelobe canceller systems with up to four canceller loops. The single sidelobe canceller system was tested against one main jammer and five multi-path jamming signals. A large decrease of up to 36.2 dB was obtained in the cancellation performance as a result of hot-clutter.

A double sidelobe canceller system was tested against one main jammer and six distributed jammers. The number of distributed jammers was increased by one for the simulation results to be comparable with each other. The second canceller loop helped to decrease the effect of hot clutter by up to 8.2 dB, but the hot-clutter effect still reduced the cancellation performance significantly by up to 28 dB.

The number of sidelobe canceller loops was increased to three and then four while the number of distributed jammers was increased to seven and eight, respectively. The hot-clutter effect on the canceller system was reduced due to the increasing number of degrees of freedom of the canceller system. The third canceller loop decreased the hot clutter effect by up to 18.4 dB. But despite this the hot-clutter managed to reduce canceller performance by 17.8 dB. In the case of four canceller loops, which is the practical limit for today’s sidelobe canceller systems due to design problems, the maximum improvement in the canceller performance was just 1.63 dB as compared to three canceller loop performance. The benefit of using four canceller loops is a maximum 20.03 dB increase in the cancellation performance, which means that hot-clutter can still be useful for reducing the canceller performance by up to 16.17 dB.

The summary of the simulation results proved that hot-clutter played a considerable role in degrading the sidelobe canceller performance. A strong hot-clutter effect decreased the cancellation performance of a quadruple sidelobe canceller by up to 16.17 dB. Hot-clutter was much more effective in degrading the cancellation performances of single and double canceller systems by causing a performance loss of up to 36.2 dB.

This effect directly and significantly affected the operating range of radar. The reduction of the relative operating range of the radar versus the interference plus noise-to-noise ratio is plotted in Figure 12.

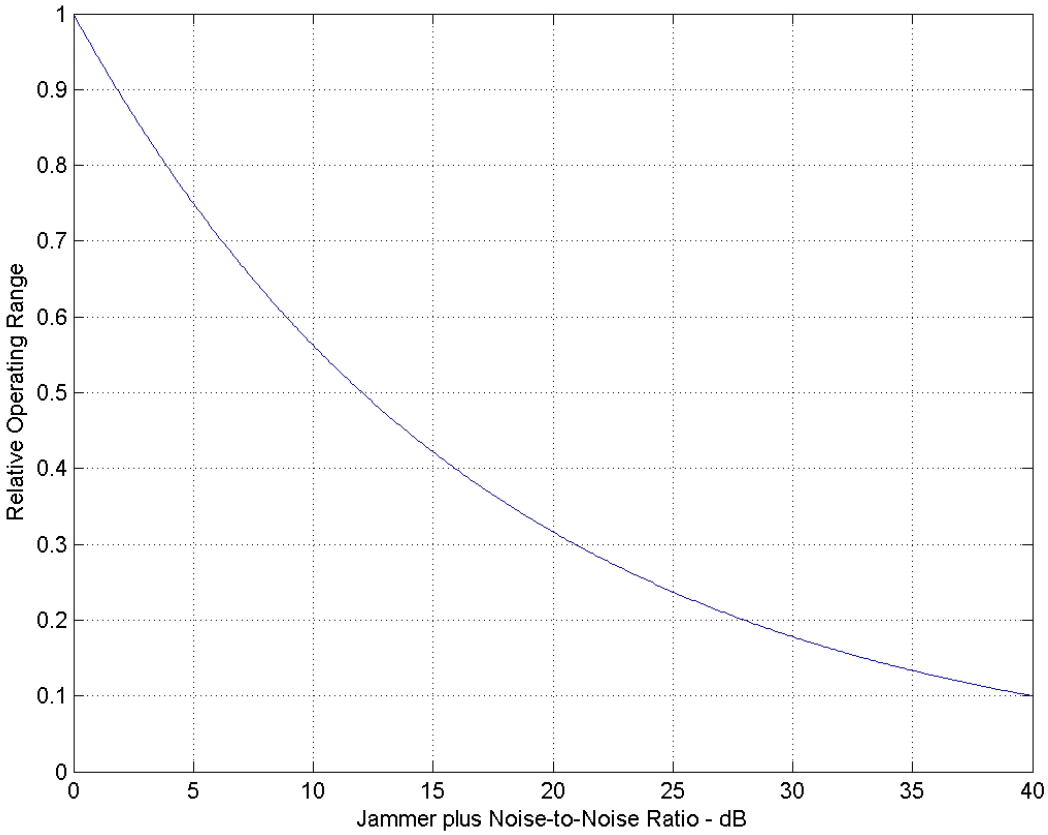

Figure 12. Relative Operating Range of Radar versus Interference plus Noise-to-noise Ratio

A single sidelobe canceller reduced the JNR from 40 dB to 1.36 dB without the hot-clutter effect. This corresponded to a 38.64 dB cancellation ratio. In this case, the canceller increased the relative operating range of the radar from 0.1 units to 0.9247 units. This corresponded to an 824.7% increase in the relative operating range of the radar. Clearly, the canceller did not perform as satisfactorily when hot-clutter was included in the scenario. Hot-clutter reduced the cancellation performance easily by overloading the number of degrees of freedom of the sidelobe canceller. The maximum effect of hot-clutter reduced the cancellation ratio from 38.64 dB to 2.44 dB, which corresponded to a 36.2 dB performance loss. Thus, the relative operating range was reduced to 0.1151 units with 37.56 dB JNR. The maximum effect of hot-clutter decreased the relative operating range of the radar by 87.55%. The minimum effect of hot-clutter reduced the cancellation performance by 2.9 dB, and the cancellation ratio dropped from 38.64 dB to 35.74 dB. The minimum effect of hot-clutter was a 15.37% decrease in the relative operating range of the radar.

The summary of the analysis results proved that hot-clutter was one of the most effective methods to limit single and multiple sidelobe canceller performances. The number of degrees of freedom of the sidelobe canceller system was easily overloaded with the hot-clutter effect owing to its nature of disturbance at different angles. This negative effect of hot-clutter on sophisticated sidelobe canceller systems makes it a major concern in the jamming arena.

C. ANALYSIS OF COMPUTER SIMULATION RESULTS

The effects of hot-clutter on different sidelobe canceller configurations were analyzed in the following scenarios, which are then discussed in detail below:

1. Jamming effects on single sidelobe canceller performance without hot-clutter
2. Effects of hot-clutter on single sidelobe canceller performance
3. Effects of hot-clutter on double sidelobe canceller performance
4. Effects of hot-clutter on triple sidelobe canceller performance
5. Effects of hot-clutter on quadruple sidelobe canceller performance

The jamming effect on a single sidelobe canceller was analyzed to obtain an overview of the cancellation performance without the hot-clutter effect. The drop in performance of the canceller system in the intense hot-clutter environment can be evaluated quantitatively in the following simulations.

1. Jamming Effects on Single Sidelobe Canceller Performance without Hot-clutter

A carefully designed single sidelobe canceller reduced the JNR by up to 50.36 dB. This allows the radar to work well in a high-power jamming environment. The simulation results of this configuration are tabulated in Table 1 and the cancellation ratio of a single sidelobe canceller versus jammer-to-receiver noise ratio (JNR) is plotted in Figure 13.

JNR (in dB)	CR (in dB)
5	3.996
10	8.955
20	18.93
30	28.9
40	38.64
50	46.6
60	49.85
70	50.36

Table 1. Single Sidelobe Canceller Performance without Hot-clutter

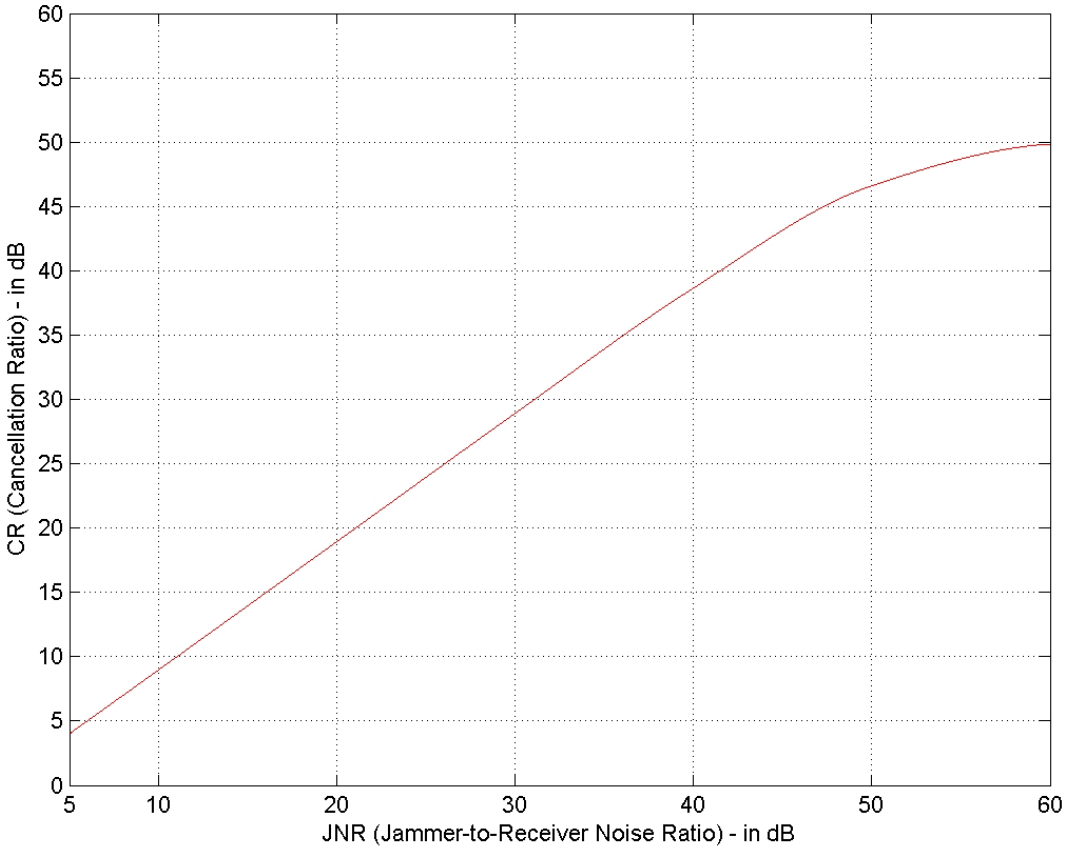

Figure 13. Cancellation Ratio versus JNR for Single Sidelobe Canceller without Hot-clutter

A simulation was performed for different values of JNR as in Table 1. The cancellation ratio curve was obtained by interpolating these simulation results with the cubic interpolation method.

The single sidelobe canceller performed well against one jammer without the hot-clutter effect. The canceller loop correlated the auxiliary channel signal with the main channel signal with a high degree of correlation. A large amount of jammer energy was denied and the radar system performed much better when this highly correlated auxiliary channel signal was subtracted from the main channel signal. This analysis proves that a well-designed sidelobe canceller decreased the jamming effectiveness greatly and jamming was ineffective without the hot-clutter effect. One may conclude that hot-clutter must be used to increase the jamming effectiveness against the sidelobe canceller systems.

It was proven that the maximum achievable cancellation ratio was limited to the JNR value. The cancellation ratio began to converge its final value of 50.36 dB and remained at this level with increasing JNR. This is because the convergence time, the weight variance, and the weight mean remained almost at their own values with increasing JNR, since the receiver self-noise was decreased to simulate the increasing JNR values. This convergence began as the JNR reached the canceller loop’s maximum interference power level. This design can handle about 40 dB interference power level above the quiescent receiver noise level.

The sidelobe canceller output versus time, and weight magnitude versus time are plotted in Figure 14, and Figure 15,respectively. Both figures are plotted for JNR = 40 dB.

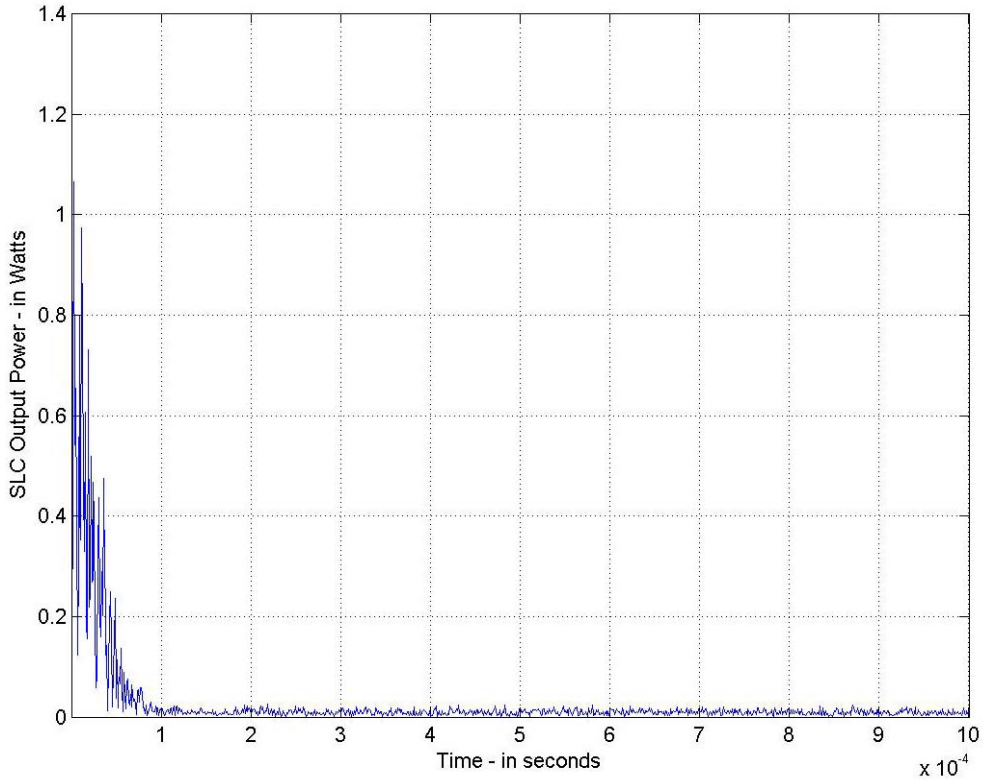

Figure 14. Single Sidelobe Canceller Power Output versus Time without Hot-clutter

The plot in Figure 14 showed that the single sidelobe canceller reached the steady state condition very quickly. The output power is very small in the steady state condition and it does not fluctuate around its mean value very much. This provided good steady state cancellation, which was caused by good estimation and calculation of weight average and weight variance by the canceller loop.

The canceller loop performed outstandingly well against one jammer without hot-clutter.

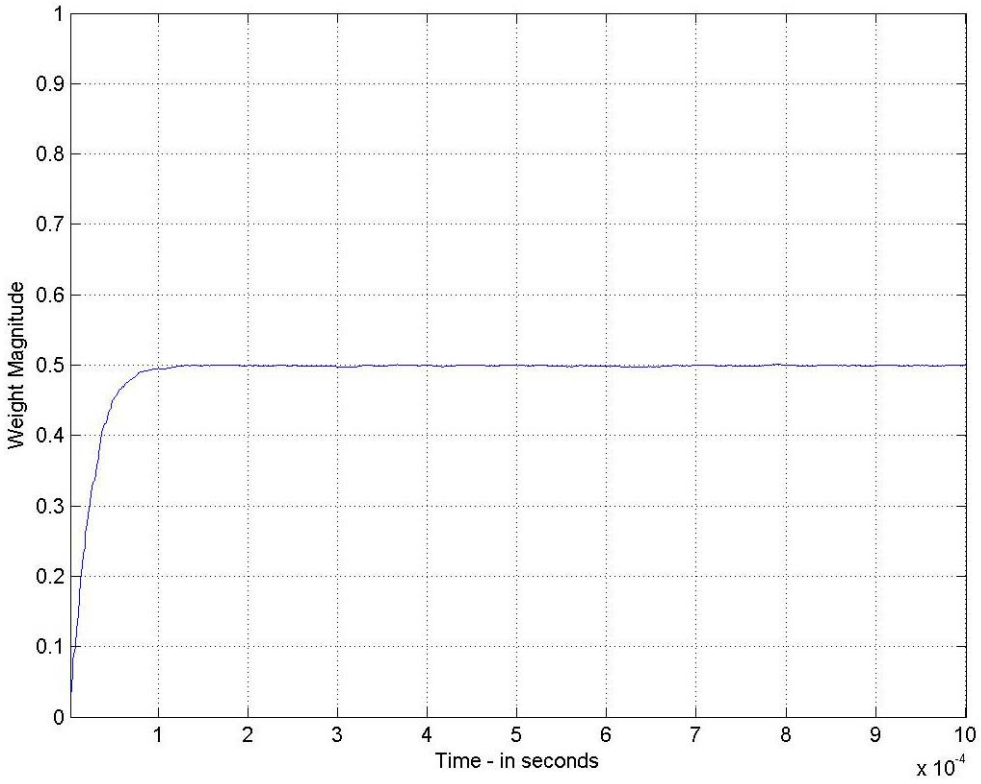

Figure 15. Weight Magnitude versus Time for Single Sidelobe Canceller without Hot-clutter

The weight reaches its average value of 0.5 very fast. The weight variance is very small. So, the weight does not fluctuate around its mean value very much. The single canceller loop is very effective in calculating the optimum weight for the auxiliary channel and thus, suppressing the hot-clutter effect. The fast calculation of weight mean and the small variance of weight provided the canceller output to be quite stable as shown in Figure 14.

The plots in Figure 14, and Figure 15 served to validate proper and successful operation of the canceller loop, which was designed in Chapter 3.

2. Effects of Hot-clutter on Single Sidelobe Canceller Performance

The hot-clutter effect was simulated with five multi-path reflected jamming signals. All these reflected jamming signals have equal power, but they were distributed in different directions of arrivals. The varying powers of the reflected signals were also simulated. The simulation results are tabulated in Table 2 and the hot-clutter effect on the cancellation performance of a single sidelobe canceller is plotted in Figure 16.

JDJR = 5 dB	
JNR (in dB)	**CR (in dB)**
5	0.1743
10	1.588
20	2.348
30	2.432
40	2.44

JDJR = 10 dB	
JNR (in dB)	**CR (in dB)**
5	1.885
10	4.18
20	5.679
30	5.862
40	5.881

JDJR = 20 dB	
JNR (in dB)	**CR (in dB)**
5	3.658
10	7.944
20	13.31
30	14.53
40	14.67

JDJR = 30 dB	
JNR (in dB)	**CR (in dB)**
5	3.959
10	8.838
20	17.88
30	23.18
40	24.37

JDJR = 40 dB	
JNR (in dB)	**CR (in dB)**
5	3.992
10	8.943
20	18.81
30	27.85
40	33.1

Table 2. Triple Sidelobe Canceller Performance with the Existence of Hot-Clutter

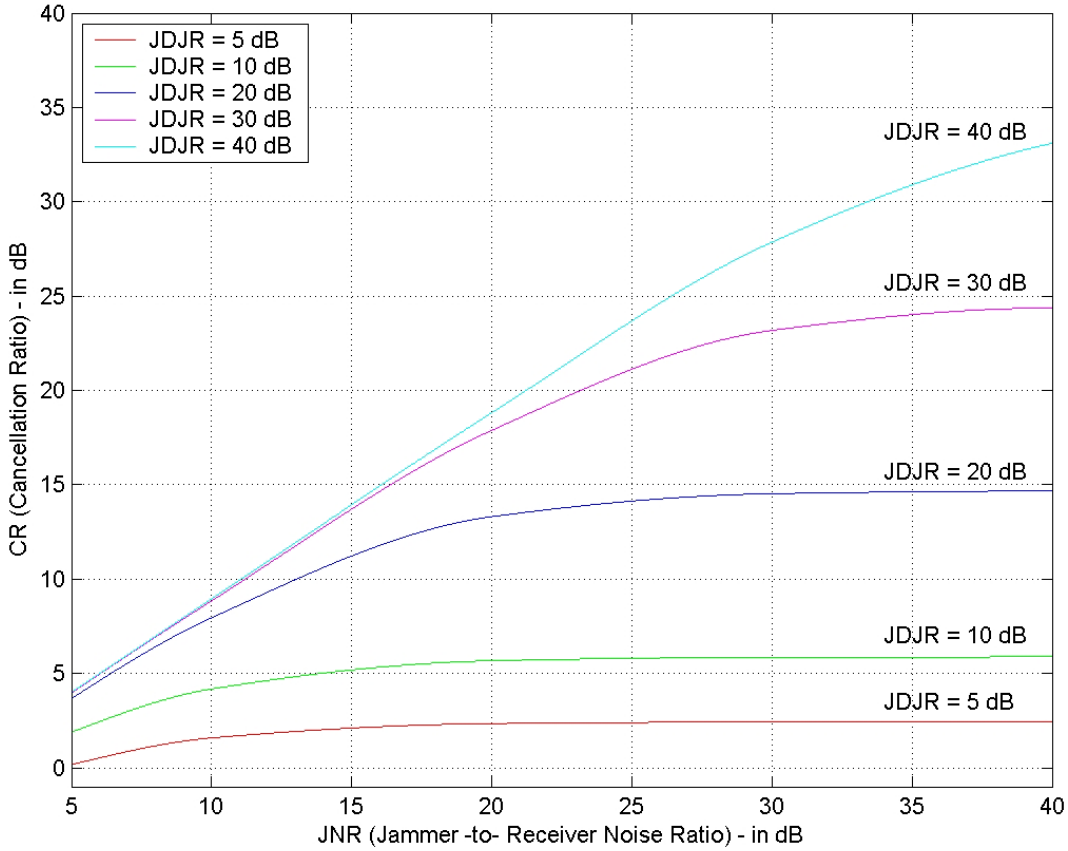

Figure 16. The Hot-clutter Effect on Single Sidelobe Canceller Performance

The term JDJR denotes the jammer-to-distributed jammer ratio, where JDJR = 20 dB indicates that all the distributed jammer powers are 20 dB below the main jammer power.

The variation of the powers of the distributed jammer signals was due to different terrain scattering coefficients. A higher scattering coefficient of the terrain increased the multi-path reflected signal power, in which case the JDJR decreased in the simulation. The highest power of multi-path reflected jamming signals was considered to be 5 dB below the main jammer power, which states that JDJR = 5 dB.

The sidelobe canceller output versus time, and weight magnitude versus time are plotted in Figure 17, and Figure 18, respectively. Both figures are plotted for JNR = 40 dB and JDJR = 20 dB.

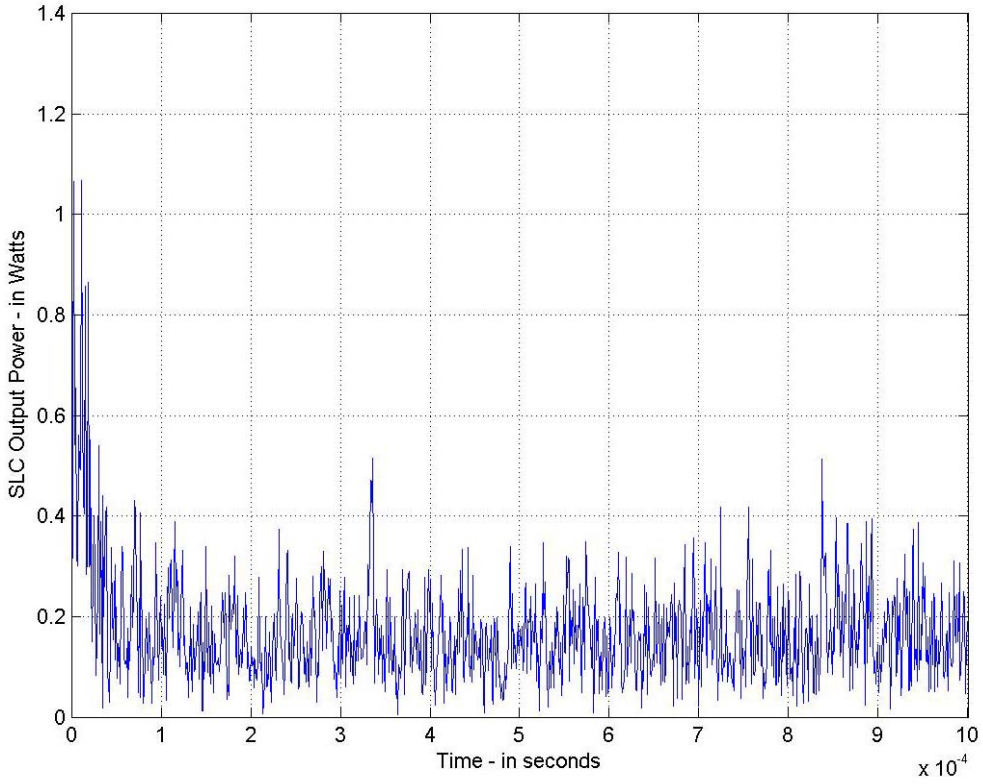

Figure 17. Single Sidelobe Canceller Power Output versus Time with Hot-clutter

The single sidelobe canceller output power is not stable when the hot-clutter is included. The canceller loop is unstable because of the existence of distributed jamming signals in different directions. The average output power level is higher than previous simulation, which is plotted in Figure 14. The output power also fluctuates around its mean value more. This is due to the high weight variance calculated by the canceller loop.

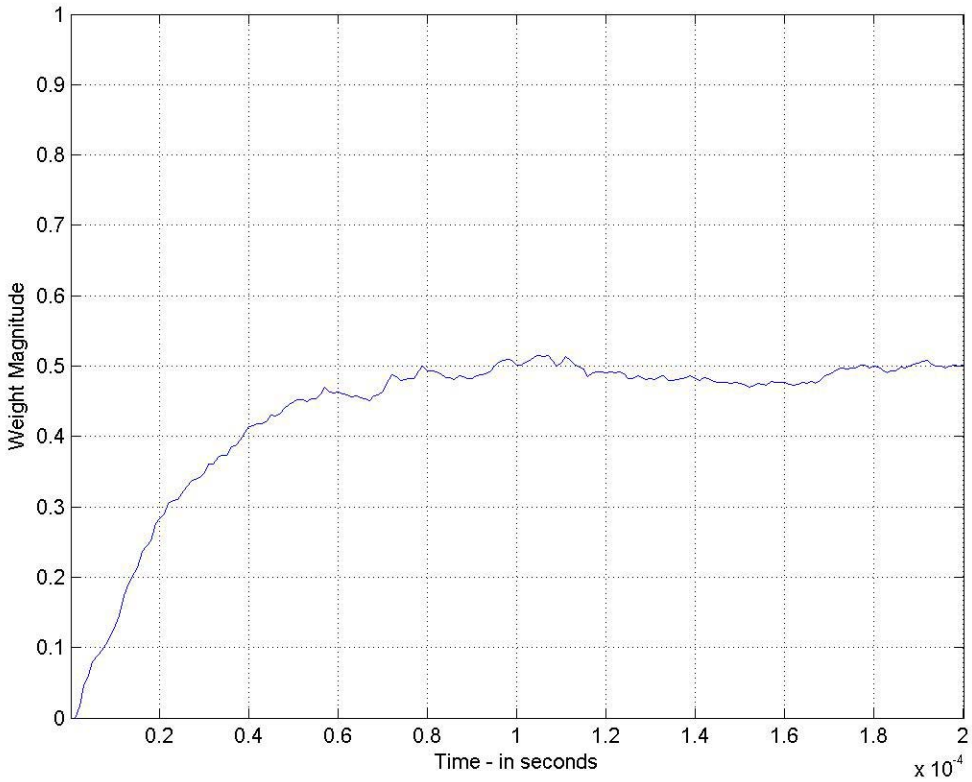

Figure 18. Weight Magnitude versus Time for Single Sidelobe Canceller with Hot-clutter

The weight reaches its mean value fast, but it fluctuates around the mean value more than the weight obtained in previous simulation, which was plotted in Figure 15. The fast response is due to hard-limiter, which is used in the design. The response time does not depend on external excitation conditions when the hard-limiter is used. The weight fluctuation around its mean value is due to distributed jamming signals, which makes the canceller loop less stable and weight variance higher. This high variance of the weight causes worse cancellation, as explained in Appendix B sections D-1-a/b and as seen in Figure 17.

The degradation effect of hot-clutter on the single sidelobe canceller performance can be seen by comparing Figure 13 and Figure 16. This degradation effect is plotted in Figure 19.

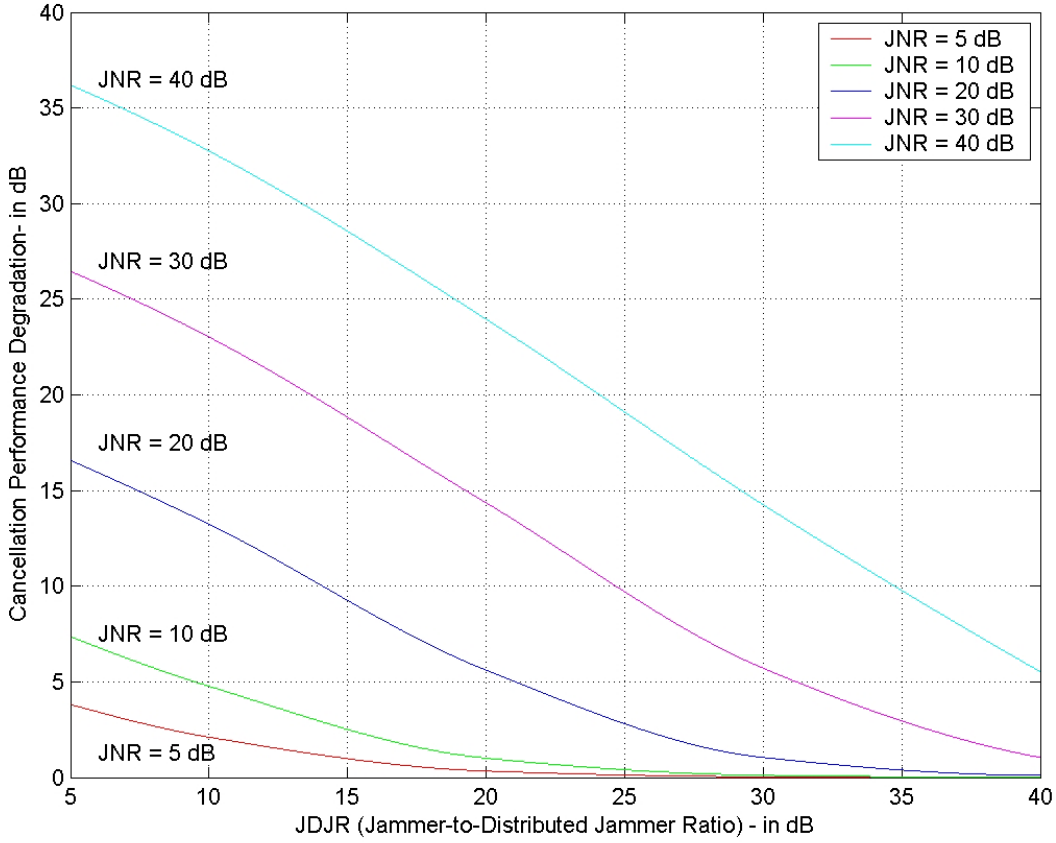

Figure 19. Performance Degradation Effects of Hot-clutter on Single Sidelobe Canceller

The hot-clutter effect degraded the single canceller performance by up to 36.2 dB. Hot-clutter became relatively less effective with decreasing JNRs. This was due to the change of weight variance in the steady state of the canceller with a changing JNR. The degradation effects of hot-clutter were 26.468 dB, 16.582 dB, 7.367 dB and 3.8217 dB for 30 dB, 20 dB, 10 dB and 5 dB of JNRs, respectively.

The minimum effect of hot-clutter was 5.54 dB performance degradation for 40 dB JNR.

The hot-clutter effect rose with the increasing powers of multi-path reflected signals. The effects of increasing powers of multi-path reflected signals on cancellation performance of a single sidelobe canceller are plotted in Figure 20.

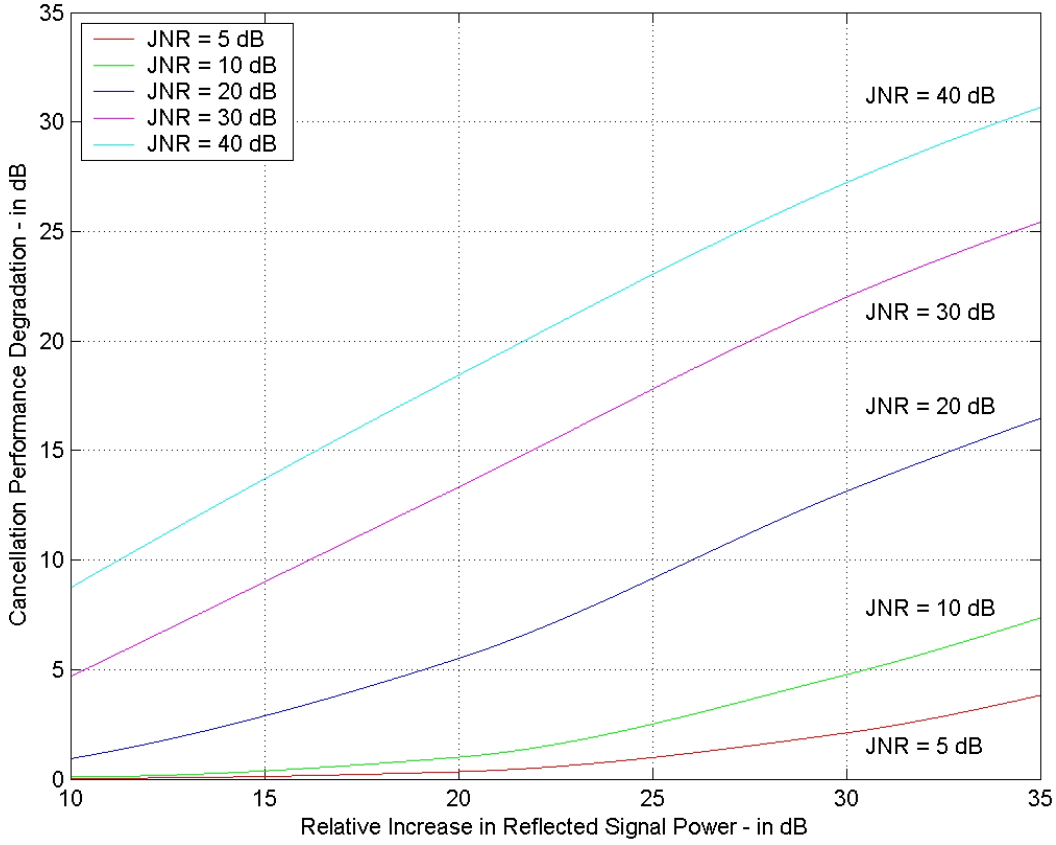

Figure 20. Effects of Increasing Powers of Reflected Signals on Single Canceller Performance

The cancellation performance was degraded by 30.66 dB when multi-path reflected signal power was increased by 35 dB for the most powerful jamming scenario of JNR = 40 dB. 10 dB, 20 dB and 30 dB increments of reflected signal powers degraded the cancellation performance by 8.73 dB, 18.43 dB and 27.219 dB, respectively. The effects of

varying powers of multi-path reflected jamming signals were simulated for the less powerful jamming scenarios of 30 dB, 20 dB, 10 dB and 5 dB JNRs where the cancellation performance was degraded by up to 25.418 dB, 16.462 dB, 7.355 dB and 3.8177 dB, respectively. The operating range was reduced by up to 82.87% owing to a 35 dB increase in the reflected signal powers.

The varying powers of multi-path signals represent the effects of different terrain scattering coefficients. The terrain characteristics between the jammer and the radar platform determine the effectiveness of hot-clutter as well as the distance between the jammer and the victim radar.

This analysis proves that the hot-clutter effect easily undermines the benefits of using a single sidelobe canceller system in every hot-clutter scenario. This kind of vulnerability is due to the number of degrees of freedom of the single sidelobe canceller, which is 1. It is easily overloaded with hot-clutter and the cancellation performance is reduced drastically.

The performance loss in the cancellation ratio affects the relative operating range of radar directly, as plotted in Figure 12. Reduction in the operating range of surveillance radar prevents the early detection of attacking units by a defending missile system. Successful jamming helps the attacking units infiltrate closer to the protected platform without being detected. After detecting the attacking units by tracking radar, the defending missile system may not have enough reaction time if the attacking units are already very close to the platform.

3. Effects of Hot-clutter on Double Sidelobe Canceller Performance

The number of multi-path reflected jamming signals was increased to 6 for a double sidelobe canceller loop simulation. The second canceller loop tried to cancel this extra jamming signal. It also improved the overall cancellation performance since both canceller loops work together to cancel the interference. The simulation results are tabulated in Table 3 and the hot-clutter effect on the cancellation performance is plotted in Figure 21.

JDJR = 5 dB	
JNR (in dB)	**CR (in dB)**
5	1.587
10	5.365
20	9.703
30	10.55
40	10.64

JDJR = 10 dB	
JNR (in dB)	**CR (in dB)**
5	2.35
10	6.489
20	12.89
30	14.83
40	15.08

JDJR = 20 dB	
JNR (in dB)	**CR (in dB)**
5	3.692
10	8
20	16.41
30	22.7
40	24.53

JDJR = 30 dB	
JNR (in dB)	**CR (in dB)**
5	4.218
10	9.052
20	17.97
30	26.32
40	32.27

JDJR = 40 dB	
JNR (in dB)	**CR (in dB)**
5	4.29
10	9.265
20	19.05
30	27.91
40	34.95

Table 3. Double Sidelobe Canceller Performance with the Existence of Hot-clutter

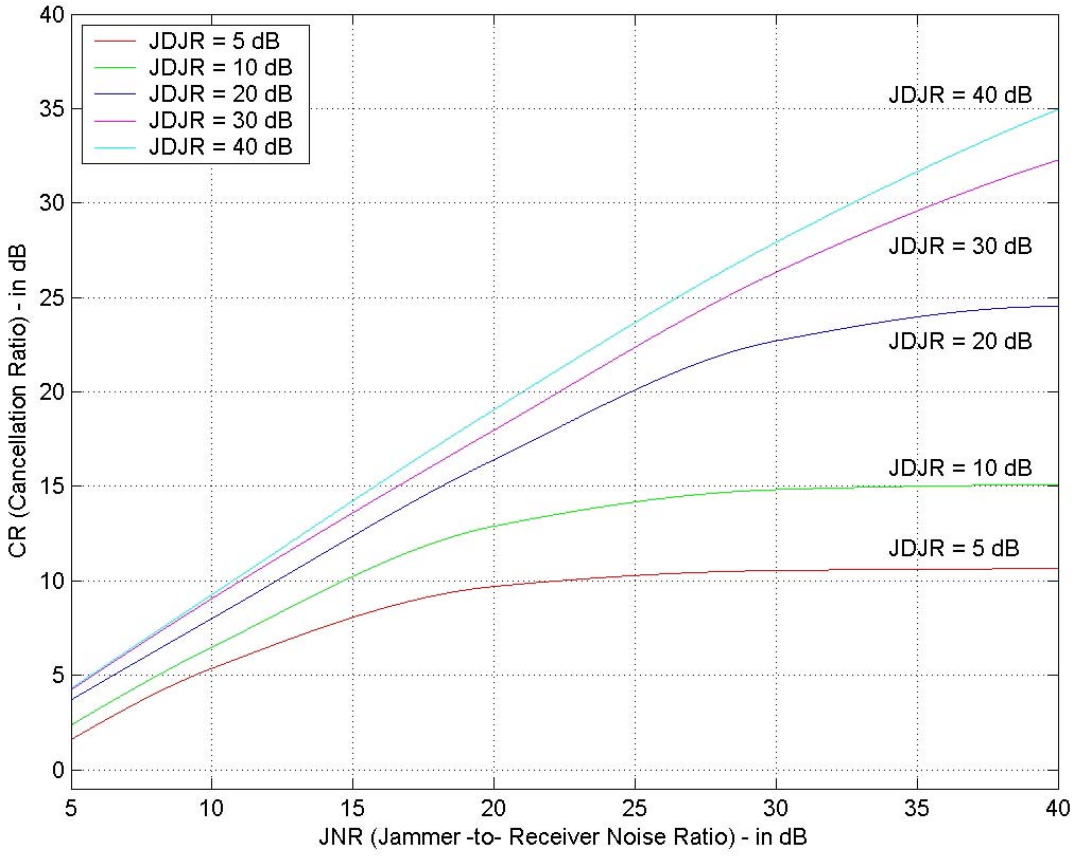

Figure 21. Hot-clutter Effect on Double Sidelobe Canceller Performance

The hot-clutter effect was reduced by up to 9.86 dB as compared to the single sidelobe canceller performance in Figure 16. The least powerful hot-clutter effect reduced the cancellation performance by 3.69 dB. Hot-clutter still effectively reduced the cancellation performance by up to 28 dB. This corresponds to an 80.04% decrease in the operating range of radar.

Clearly, the double sidelobe canceller system is also ineffective at mitigating the negative effects of hot-clutter.

The relative improvement in the cancellation performance of a single sidelobe canceller as a result of a second sidelobe canceller loop is plotted in Figure 22.

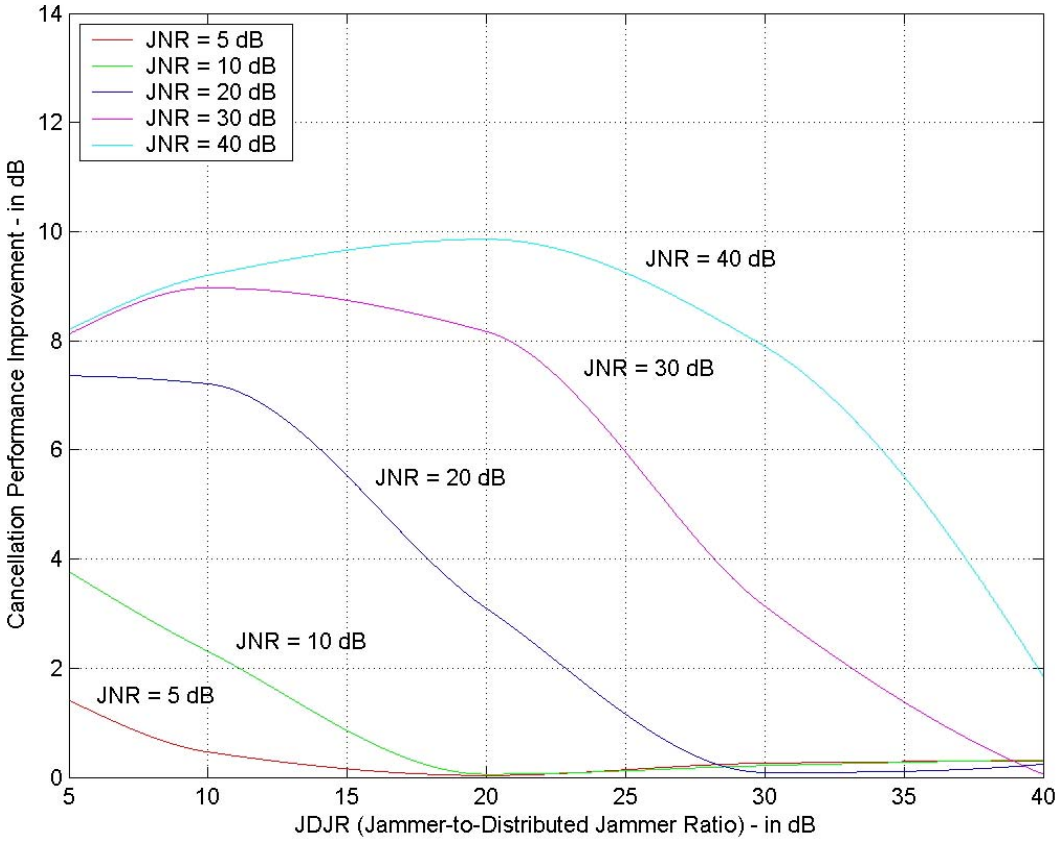

Figure 22. Relative Improvement of a Single Sidelobe Canceller Performance due to a Second Canceller Loop

The second sidelobe canceller improved the cancellation performance increasingly with high-power jamming signals of 30 dB and 40 dB JNRs. But, the varying powers of multi-path reflected jamming signals still degraded the double canceller performance by up to 24.31 dB.

The effects of the varying powers of multi-path reflected signals on the cancellation performance of a double sidelobe canceller are plotted in Figure 23.

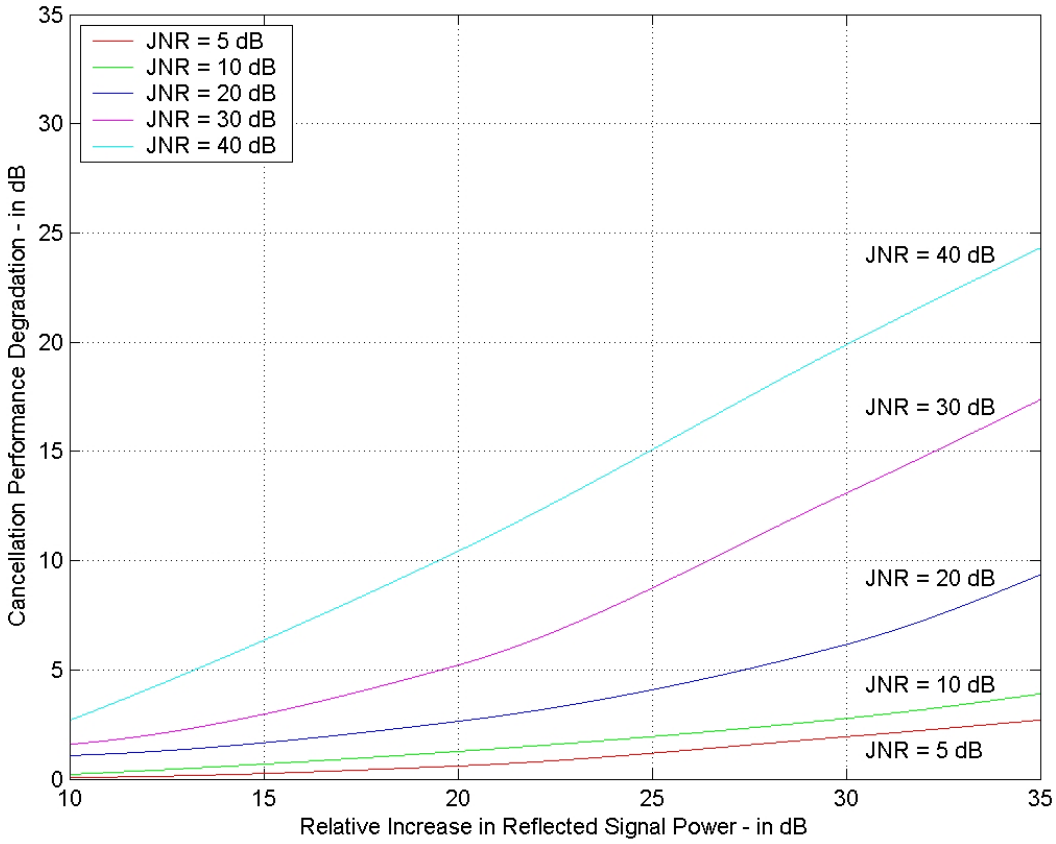

Figure 23. Effects of Varying Powers of Reflected Signals on Double Sidelobe Canceller Performance

The effects of the varying powers of reflected signals were reduced due to a second sidelobe canceller in the system. The maximum degradation effect of 24.31 dB occurred when the distributed jammer powers were increased by 35 dB. The cancellation performance degraded by 2.68 dB, 10.42 dB and 19.87 dB as a result of 10 dB, 20 dB, and 30 dB increments of reflected signal powers, respectively. The effects of the relatively increasing powers of the multi-path reflected jamming signals were simulated for the less powerful jamming signals of 30 dB, 20 dB, 10 dB and 5 dB of JNRs. In this case, cancellation performance was degraded by up to 17.36 dB, 9.347 dB, 3.9 dB and 2.703 dB, respectively. Hot-clutter was still effective in preventing the proper operation of the radar.

The double sidelobe canceller output versus time is plotted in Figure 24 when JNR = 40 dB and JDJR = 20 dB.

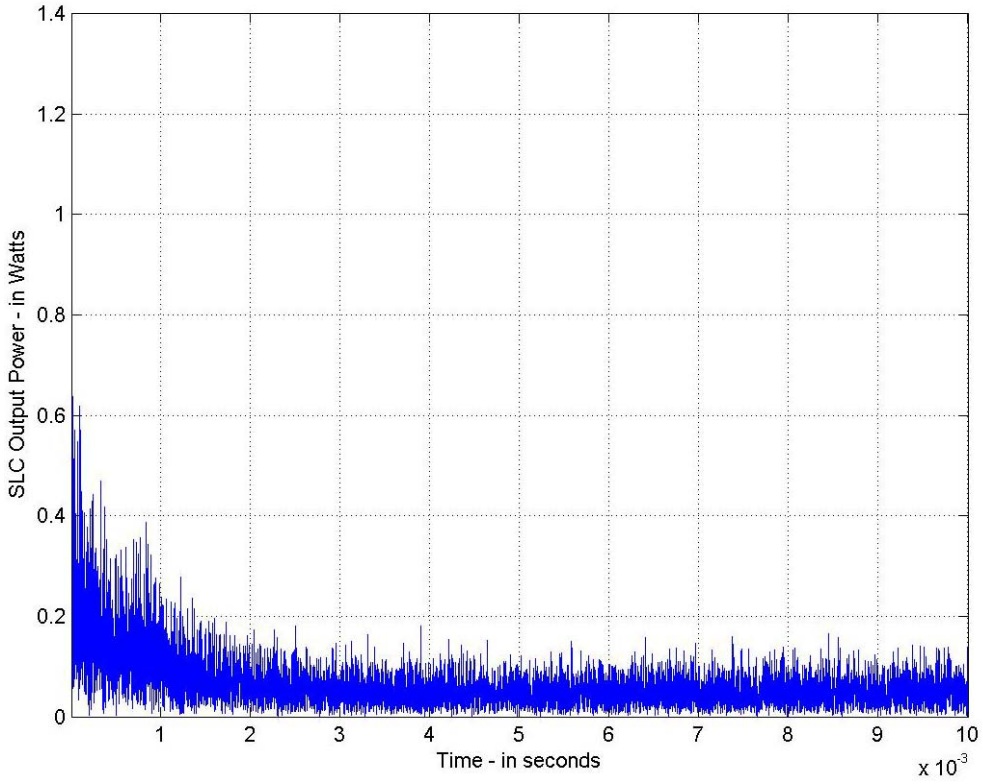

Figure 24. Double Sidelobe Canceller Power Output versus Time with Hot-clutter

The double canceller output is more stable than the single canceller output. The second canceller loop reduced mean output power as compared to Figure 17, but canceller system response time is longer. This is due to the competition between canceller loops. The loops compete with each other at the beginning and then they become stable after a learning time. The weights do not fluctuate around their mean values as much as single canceller configuration. This provides more stable operation and better cancellation in the steady state of the system.

4. Effects of Hot-clutter on Triple Sidelobe Canceller Performance

The third sidelobe canceller loop was added to the simulation to test the effects of hot-clutter on a triple sidelobe canceller system. The number of multi-path reflected jamming signals also increased to 7. The third sidelobe canceller mitigated the effects of hot-clutter more effectively compared to the single and the double sidelobe cancellers. The simulation results are tabulated in Table 4 and plotted in Figure 25.

JDJR = 5 dB	
JNR (in dB)	**CR (in dB)**
5	1.514
10	5.038
20	12.55
30	18.89
40	20.84

JDJR = 10 dB	
JNR (in dB)	**CR (in dB)**
5	2.581
10	6.492
20	14.06
30	21.24
40	25.06

JDJR = 20 dB	
JNR (in dB)	**CR (in dB)**
5	3.673
10	8.229
20	16.47
30	24.52
40	29.87

JDJR = 30 dB	
JNR (in dB)	**CR (in dB)**
5	4.213
10	9.017
20	18.23
30	26.4
40	31.65

JDJR = 40 dB	
JNR (in dB)	**CR (in dB)**
5	4.323
10	9.298
20	19.02
30	28.18
40	35.74

Table 4. Triple Sidelobe Canceller Performance with the Existence of Hot-clutter

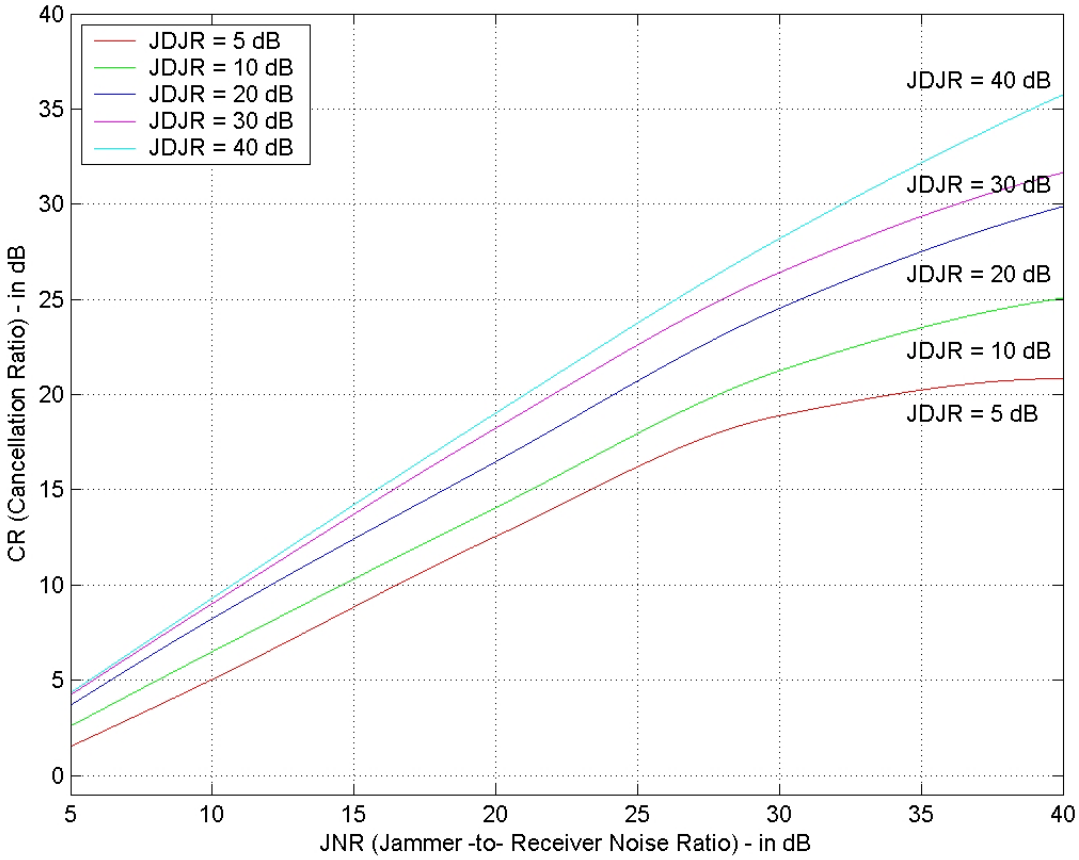

Figure 25. Hot-clutter Effect on Triple Sidelobe Canceller Performance

The third sidelobe canceller reduced the effects of hot-clutter by up to 19.179 dB, as compared to the single sidelobe canceller performance in Figure 16. The maximum benefit of using a third sidelobe canceller against a double sidelobe canceller was that the hot-clutter effect was reduced by up to 10.2 dB. Thus hot-clutter was still effective in reducing the cancellation performance by up to 17.8 dB.

The least powerful hot-clutter effect reduced the cancellation performance by 2.9 dB as compared to the single canceller performance without the hot-clutter effect, as shown in Figure 13. The third canceller loop provided 2.64 dB performance improvement over the single

canceller performance for the least powerful hot-clutter effect.

The relative improvement in the cancellation performance of a single canceller configuration due to the third canceller loop is plotted in Figure 26.

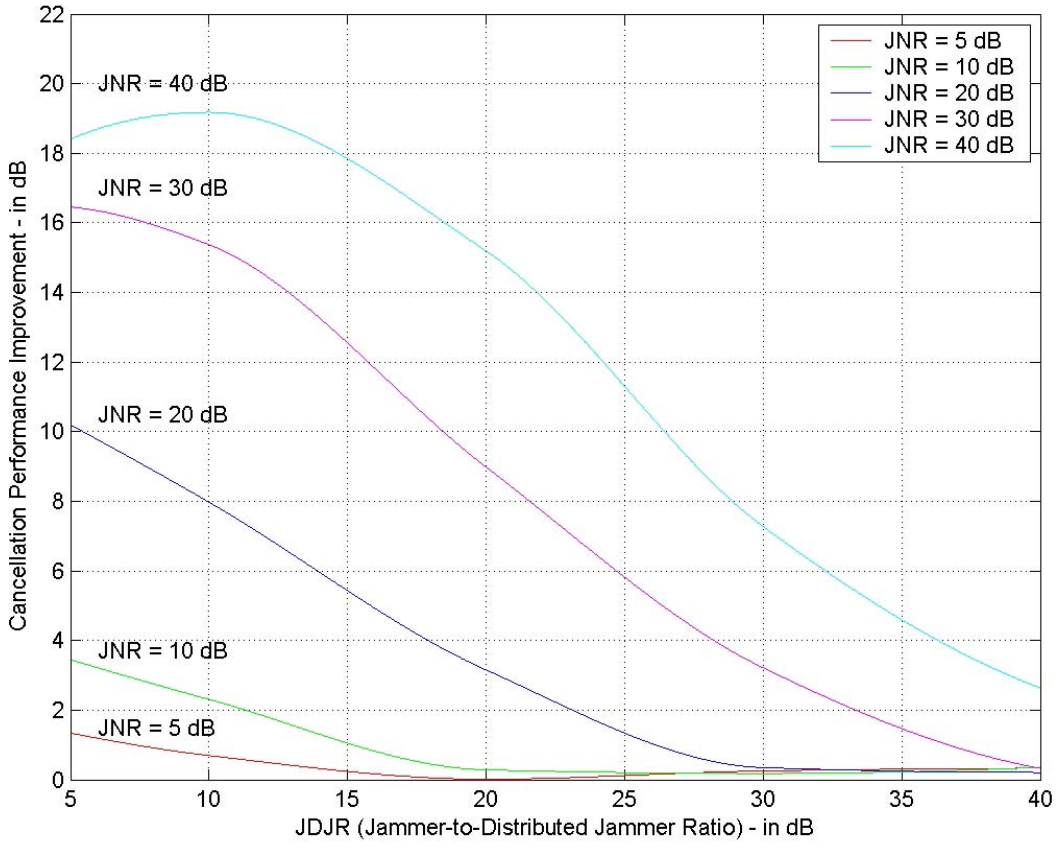

Figure 26. Relative Improvement of Single Canceller Performance due to a Third Canceller Loop

Even with a 19.179 dB increase in the cancellation ratio, hot-clutter still affected the canceller performance by reducing the relative operating range of radar up to 65%. Though the effects of multi-path reflected jamming signal powers decreased, the hot-clutter was still powerful enough to remove the benefits of using a triple sidelobe canceller system.

The effects of the varying powers of multi-path reflected signals on the cancellation performance of a triple sidelobe canceller are plotted in Figure 27.

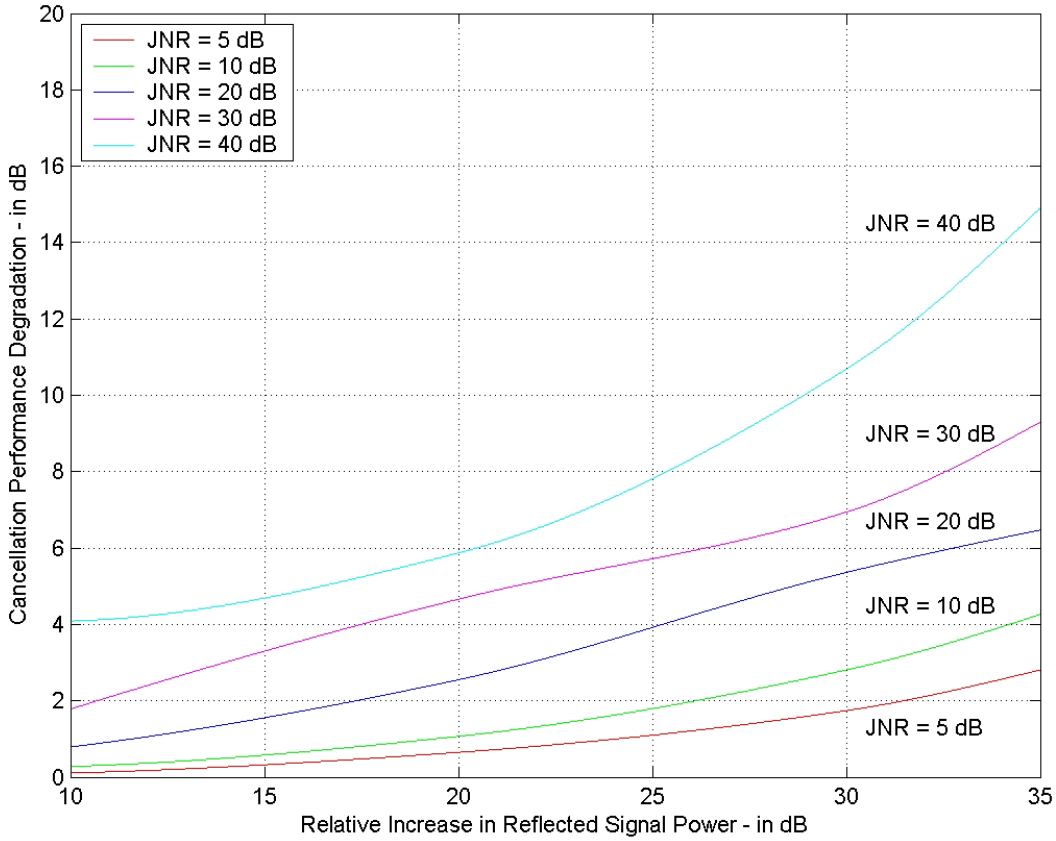

Figure 27. Effects of the Varying Powers of Reflected Signals on a Triple Canceller Performance

The third sidelobe canceller reduced the effects of the varying powers of reflected signals, as compared to single and double canceller loops. The maximum degradation effect of 14.9 dB occurred when distributed jamming signal powers were increased by 35 dB for the most powerful jamming signal of JNR = 40 dB. The cancellation performance degraded by up to 4.09 dB, 5.87 dB and 10.68 dB as a result of 10 dB, 20 dB and 30 dB increments of reflected signal powers, respectively. Just by increasing the multi-path reflected jamming signal powers, the cancellation performance was degraded by up to 9.29 dB, 6.47 dB, 4.26 dB

and 2.809 dB for the less powerful jamming signals of 30 dB, 20 dB, 10 dB and 5 dB of JNRs.

The triple sidelobe canceller output versus time is plotted in Figure 28 when JNR = 40 dB and JDJR = 20 dB.

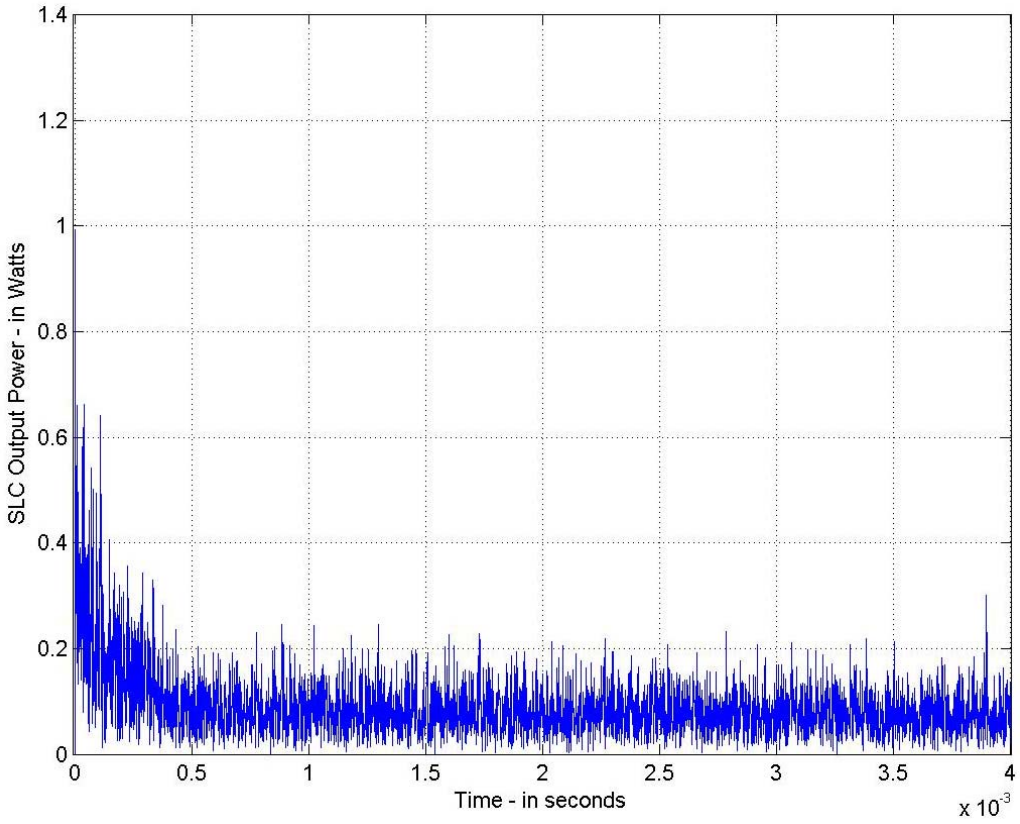

Figure 28. Triple Sidelobe Canceller Power Output versus Time with Hot-clutter

The most stable canceller operation is obtained with the triple sidelobe canceller configuration. The mean output power is reduced as compared to Figure 17, and Figure 24. The weights reach their optimum values slowly owing to the competition between canceller loops but lesser weight variances are obtained in the steady state. So the response time is longer than single and double canceller systems but the power fluctuations are less than these two systems.

5. Effects of Hot-clutter on Quadruple Sidelobe Canceller Performance

The effects of hot-clutter on a quadruple sidelobe canceller system were simulated with 8 multi-path reflected jamming signals, which were distributed at different angles. Four is the practical limit of the number of sidelobe cancellers because of difficult operational design problems. The simulation results are tabulated in Table 5 and the hot-clutter effect is plotted in Figure 29.

JDJR = 5 dB	
JNR (in dB)	**CR (in dB)**
5	1.309
10	5.462
20	12.92
30	18.49
40	22.47

JDJR = 10 dB	
JNR (in dB)	**CR (in dB)**
5	2.369
10	6.471
20	14.7
30	20.78
40	24.58

JDJR = 20 dB	
JNR (in dB)	**CR (in dB)**
5	3.677
10	8.209
20	16.55
30	24.72
40	29.83

JDJR = 30 dB	
JNR (in dB)	**CR (in dB)**
5	4.165
10	8.99
20	18.22
30	26.46
40	33.4

JDJR = 40 dB	
JNR (in dB)	**CR (in dB)**
5	4.285
10	9.261
20	18.99
30	28.18
40	35.33

Table 5. Quadruple Sidelobe Canceller Performance with the Existence of Hot-clutter

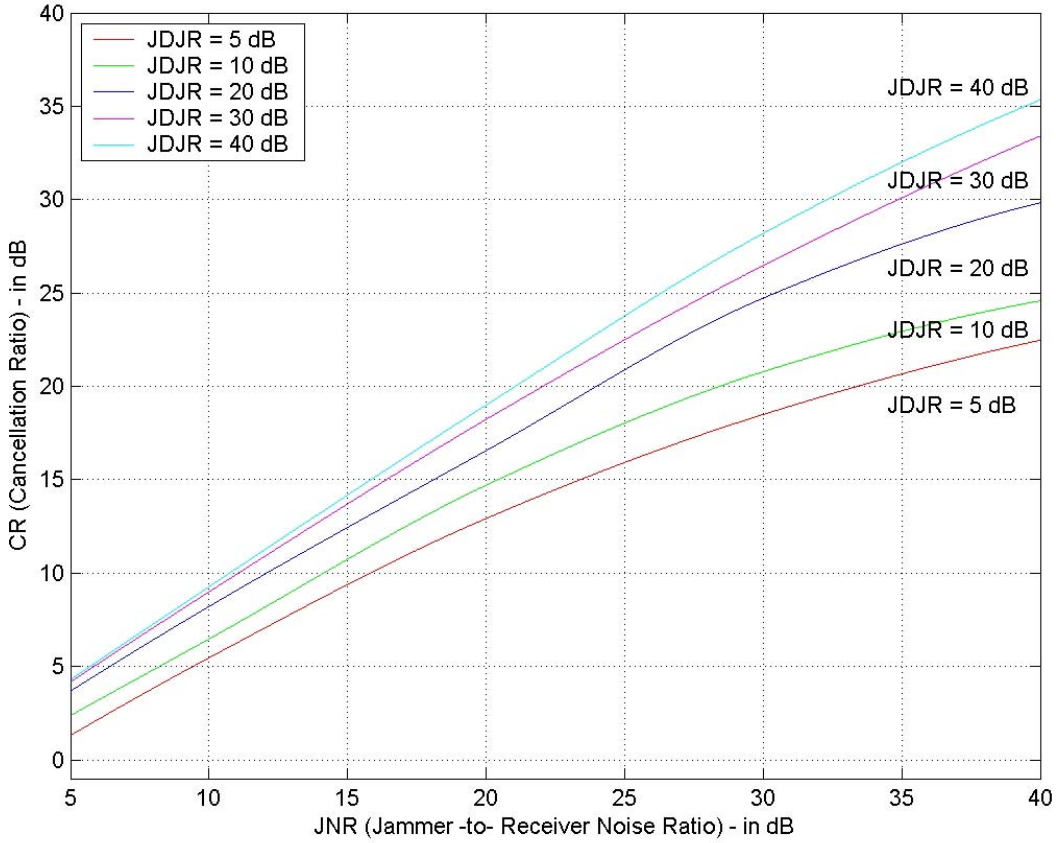

Figure 29. Hot-clutter Effect on Quadruple Sidelobe Canceller Performance

The quadruple sidelobe canceller configuration reduced the effects of hot-clutter by up to 20.03 dB for the most powerful hot-clutter effect of JDJR = 5 dB, as compared to Figure 16. The maximum benefit of using four canceller loops was that the hot-clutter effect is reduced by up to 1.63 dB for JDJR = 5 dB when compared to the triple sidelobe canceller performance. Hot-clutter was still effective at reducing the cancellation performance by up to 16.17 dB, as compared to the single sidelobe canceller performance.

This analysis clearly proved that using more than three sidelobe cancellers did not provide any noticeable

performance improvement because of the strong hot-clutter effect.

The relative improvement in the cancellation performance of a single canceller configuration is plotted in Figure 30.

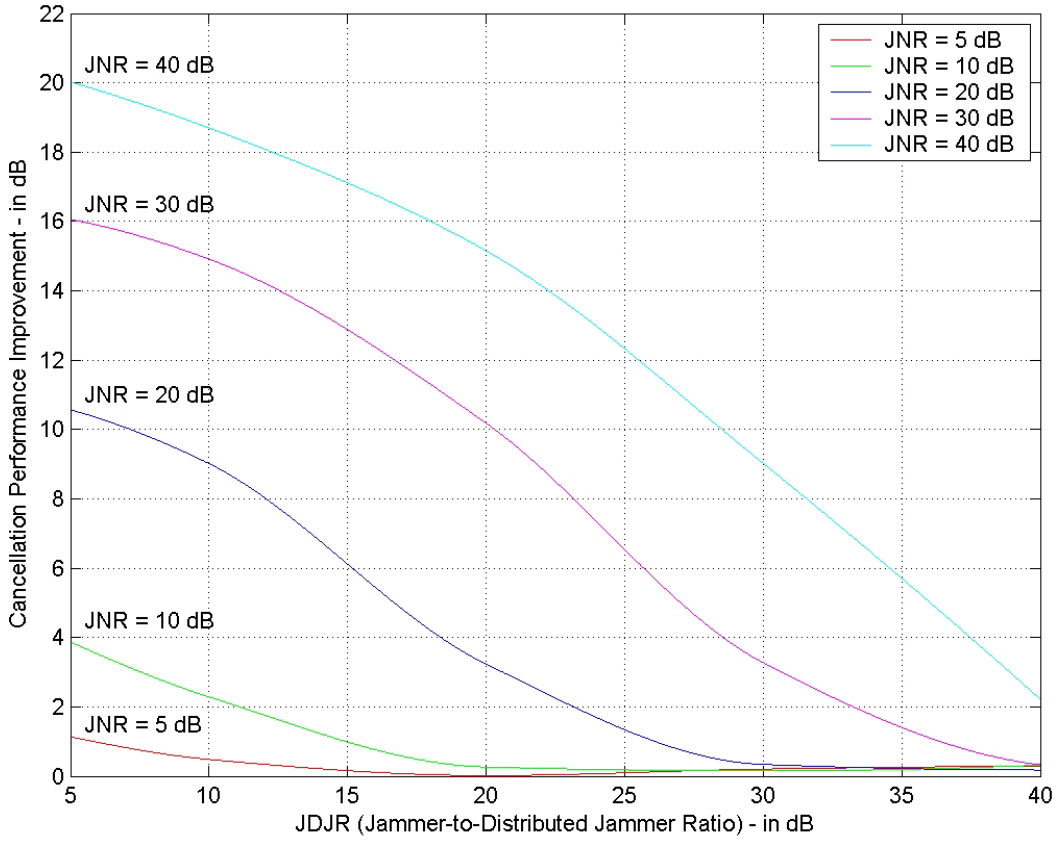

Figure 30. Improvement of Single Canceller Performance due to Fourth Canceller Loop

The best effect of a four canceller loop decreased the JNR from 37.56 dB to 17.53 dB. All against such a high improvement in the cancellation ratio, the hot-clutter effect still reduced the relative operating range of radar by 60.58%.

The effects of the varying powers of the multi-path reflected signals on the cancellation performance of a

quadruple sidelobe canceller system are plotted in Figure 31.

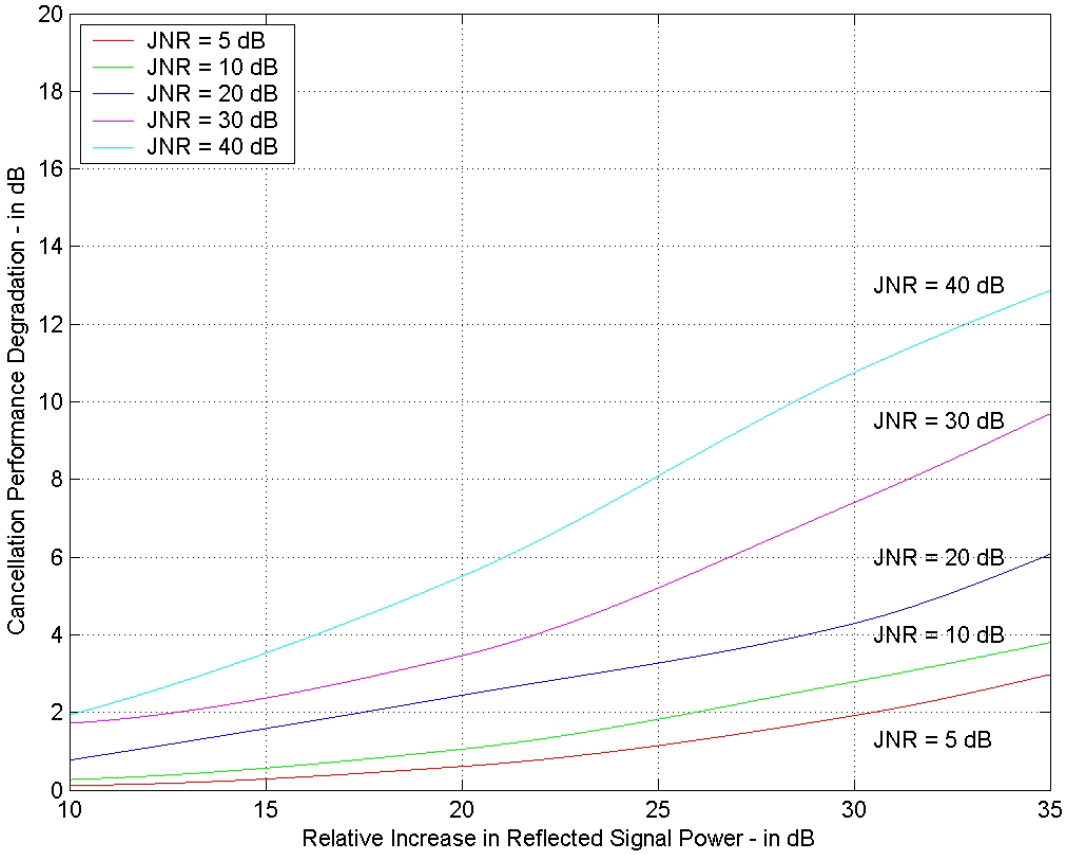

Figure 31. Effects of Varying Powers of Reflected Signals on Quadruple Sidelobe Canceller

The maximum degradation effect of varying powers of multi-path reflected jamming signals was 12.86 dB, where JNR was 40 dB. This degradation effect of hot-clutter decreased with decreasing JNR. Hot-clutter degraded the cancellation performance by up to 9.69 dB, 6.07 dB, 3.799 dB and 2.976 dB with decreasing JNR values of 30 dB, 20 dB, 10 dB and 5 dB, respectively, when multi-path reflected jamming signal powers are increased by 35 dB. A fourth sidelobe canceller loop did not reduce the hot-clutter effect by a considerable amount as compared to triple sidelobe canceller.

D. SUMMARY

The computer simulation result showed that hot-clutter provided a formable threat to limit a sophisticated sidelobe canceller's performance. The number of degrees of freedom of the sidelobe canceller was easily overloaded by the nature of hot-clutter. Hot-clutter reduced the success of a formidable sidelobe canceller system by up to 36.2 dB. Even the multiple sidelobe canceller systems proved very vulnerable to the hot-clutter effect. In fact, increasing the number of degrees of freedom of sidelobe canceller system is not always a useful method to mitigate the negative effects of hot-clutter. Note that increasing the number of sidelobe cancellers from 3 to 4 provided just a 1.63 dB increase in the cancellation performance.

The zero-cost hot-clutter effect easily removed the benefits of using costly and sophisticated sidelobe canceller systems.

THIS PAGE INTENTIONALLY LEFT BLANK

V. CONCLUSIONS

The CSLC has a number of inherent defects that can be exploited by support jammers. The number of degrees of freedom in CSLC is generally limited. Thus, if multiple jamming signals can be induced into the jammer at various angles through, for example, multi-path reflections, then the CSLC becomes overloaded and its performance becomes severely degraded [1].

The mission of stand-off support jamming is to deny, delay, and degrade acquisition of strike aircraft while forcing early turn-on of terminal radars. Current support jamming systems have proven effective in recent conflicts against operational enemy air defense systems that used radar technology of modest capability [1].

It is believed that support jammers can use hot-clutter effects to gain advantage of sending the direct signals as well as reflected signals to the radar. It is known that smooth surfaces improve the hot-clutter effect because of the high reflection coefficients. Especially airborne jammers have the advantage of using smooth sea surfaces to increase the jamming performance. So, the reflected signals can enter the sidelobes at the same power level as the direct jamming signals to degrade the operational capability of the radar.

In this study different parameters were used under a simulation environment to determine the effects of the hot-clutter or multi-path signals against a CSLC. The research results have shown that the hot-clutter saturates the CSLC effectively and removes the beneficial use of the CSLC.

The CSLCs show an outstanding performance in negating and nulling the effects of sidelobe jamming. Using more jammers can defeat CSLCs but this is not always cost effective and almost impossible due to operational needs. Therefore, using the multi-path effect or hot clutter effect is more feasible. Among the many possible solutions, use of the hot clutter effects is the most efficient way to attain a better jammer performance against a CSLC.

This study shows many possibilities of jamming effects that can be applied against a CSLC using hot clutter. Under generic assumptions a model was built to represent an analog system in a digital environment using Simulink. Generic power values for the reflected signals were used to represent different coefficient numbers for different surfaces. So, the hot clutter effects were demonstrated in a generic system. Any future study can focus specifically on the corresponding reflection surfaces to obtain more realistic values.

In the recent era, modern radars are manufactured with one or more CSLC units embedded into the system. So, the radars are designed with maximum protection against jammers. With the availability of the multi-path signals, it is believed that the modern radars are still vulnerable to the noise jammers if the hot clutter effects can be used wisely. It is also believed that future studies will focus more on the real world systems by pointing out further advantages of employing the hot-clutter technique against modern radar systems.

APPENDIX A. HOT CLUTTER

A. GENERAL DEFINITION

The earth's surface and atmosphere cause major effects on radar performance. Since propagation effects might extend the radar range significantly it is important to account for the earth's environment when attempting to predict radar performance [6].

Study of the models used in terrain scattered interference (TSI) simulations and use of these models to assess the performance of adaptive cancellation algorithms in the presence of multipath jamming or "hot clutter" is a difficult subject to deal with [7].

Forward scattering (reflection) of the radar energy from the surface of the earth enhances the radiated energy at some elevation angles. Refraction (bending) of the radar energy by the earth's atmosphere can cause the radar energy to deviate from straight-line propagation. Ducting (trapping) of the radar energy causes extended radar ranges. Diffraction of radar waves by the earth's surface causes energy to propagate beyond the normal radar horizon. It applies mainly at the lower frequencies that are seldom used for radar applications [6].

The difficulty with hot clutter is due to distribution of angle, time delays and powers of the multipath jamming components. Hot clutter effects are more severe with low altitude and short-range jammers due to more spread in angle and time-delays [7].

B. TERRAIN REFLECTION

The field scattered by a rough surface consists of two components: the specular component and the diffuse component. A rough surface is usually defined according to the Rayleigh criterion [7].

1. Smooth Surface

The condition for a smooth surface is

$$\Delta h < \frac{\lambda}{8 \sin \Psi} \tag{A.1}$$

where, Δh is the change in surface height, Ψ is the grazing angle and λ is wavelength. Smooth surface reflection occurs mainly from the first Fresnel zone. The first Fresnel zone is defined as the region on the surface where the distance traveled by any ray from the transmitter to the receiver after reflection from the surface does not differ by more than $\lambda/2$.

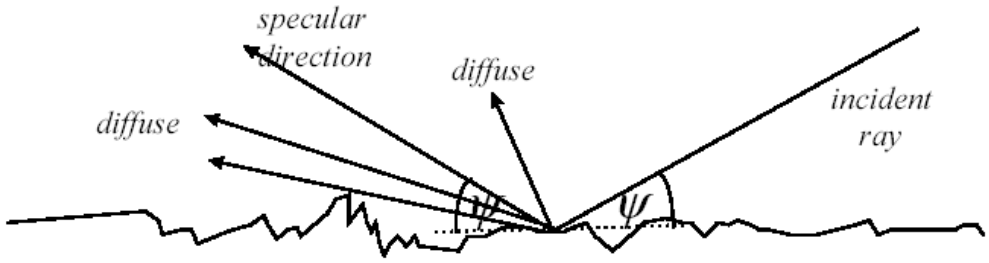

Figure 32. Specular and diffuse reflections [From Ref.7]

Specular reflection is similar to smooth surface reflection in that it is directional and follows the laws of classical optics as shown in Figure 32. It is a result of coherent radiation from points on the first Fresnel

ellipse. These transmitted waves are of approximately equal phase towards the receiver [7].

2. Specular Reflection

The specular scattering coefficient is a factor that multiplies the smooth surface reflection coefficient, which takes into account the surface irregularities. In theory specular reflection is assumed not to be dependent on the physical geometry of the terrain but only the radar and jammer parameters.

The coefficient for specular reflection is:

$$\rho_{sp} = \rho_o . \rho_s \tag{A.2}$$

where, ρ_o is reflection coefficient of a smooth surface and ρ_s is specular scattering coefficient.

σ_h is standard deviation of surface height, Ψ is grazing angle and λ is wavelength.

$$\overline{\rho}_s^2 = e^{-(4\pi g)^2} \tag{A.3}$$

$$g = \frac{\sigma_h \sin\Psi}{\lambda} \tag{A.4}$$

$$\rho_o = \frac{\gamma^2 \sin\Psi - \sqrt{\gamma^2 - \cos^2\Psi}}{\gamma^2 \sin\Psi + \sqrt{\gamma^2 - \cos^2\Psi}} \tag{A.5}$$

$$\gamma = \sqrt{\frac{\varepsilon_{rc}}{\mu_{rc}}} \tag{A.6}$$

where, ε_{rc} is surface complex relative dielectric constant, μ_{rc} is the relative permeability and γ is the interference-to-noise ratio.

3. Diffuse Scattering

The bistatic scattering coefficient is a function of both the geometrical parameters and terrain parameters. We may assume the same terrain exists everywhere in the scattering plane but the geometrical parameters will change. Since diffuse scattering occurs over an extensive region, we expect significant changes to occur for the value of the bistatic scattering coefficient for the scattering surface.

The models developed for computing the bistatic scattering coefficient assume that the geometric parameters do not change over the surface of interest. To apply these models we must divide up the terrain into surface patches over which the geometrical parameters are approximately constant. This would suggest choosing small areas [7].

Choosing small surface patch sizes increases the correlation between the incoherent scatters from different points on the surface. For small surface sizes, correlation between adjacent surfaces should be taken into account.

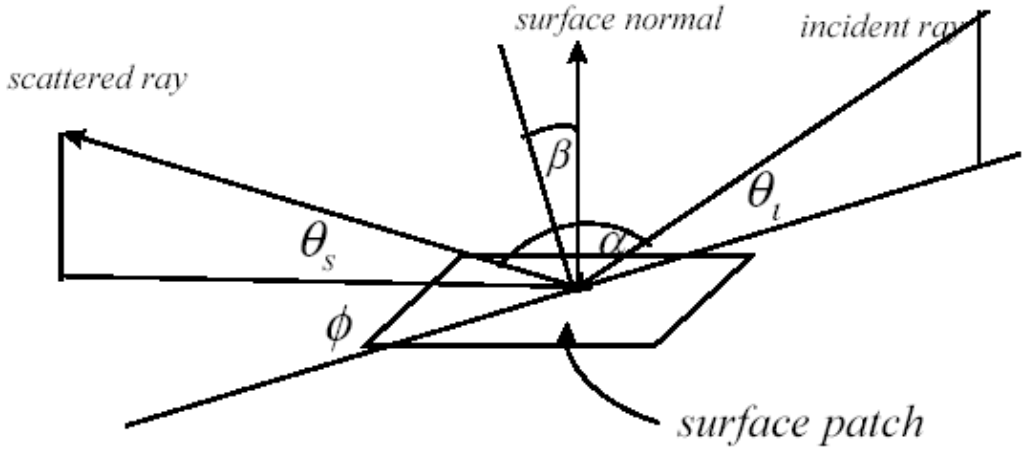

Figure 33. Bistatic Geometry [From Ref.7]

The power received from a differential patch of area as shown in Figure 33 is

$$P_r = \frac{P_J G_J G_R \lambda^2 F_d^2}{(4\pi)^3 R_1^2 R_2^2} \sigma_B^\circ dA \qquad \text{(A.7)}$$

$P_j =$ jammer power
$G_J =$ jammer antenna gain
$G_R =$ radar antenna gain
$F_d =$ pattern propagation factor
$R_1 =$ distance from radar to suface point
$R_2 =$ distance from jammer to surface point
$\sigma_B^\circ =$ bistatic scattering coefficient
$dA =$ surface area

Three regions may be identified in order to calculate the bistatic scattering coefficient:

- Low grazing angle region: θ_i or $\theta_s < 3^\circ$
- Bistatic scatter region: at any angle
- Specular region: $140^\circ \le \theta_i + \theta_s \le 220^\circ$

For each of the three regions different equations apply.

a. Region 1

$$\sigma_B^\circ = \gamma \sin(\frac{\theta_i + \theta_s}{2}) F_{c1}^2 F_{c2}^2 \qquad \text{(A.8)}$$

b. Region 2

$$\sigma_B^\circ = \frac{\rho_\circ^2 F_d^2}{\beta_\circ^2} e^{-\frac{\beta^2}{\beta_\circ^2}} \qquad \text{(A.9)}$$

$$F_d^2 = \sqrt{(1-\overline{\rho}_{s1}^2)}\sqrt{(1-\overline{\rho}_{s2}^2)} \qquad \text{(A.10)}$$

$\beta_\circ$ is terrain dependent and ranges in value between 0.05 and 0.06.

For land terrain we have the following $\beta_\circ$ values:

$\beta_\circ$ = 0.14 radian for desert

$\beta_\circ$ = 0.2 radian for farmland

$\beta_\circ$ = 0.4 radian for woodland

$\beta_\circ$ = 0.5 radian for mountains

For sea surface:

$$\beta_\circ = 2.44(SS+1)^{1.08}(\pi/180) \qquad \text{(A.11)}$$

where SS: Sea state ranges between 0 and 8.

With correlation distance T, the surface slope can be found according to the geometry in Figure 34.

$$\beta_\circ = \tan^{-1}(\frac{2\sigma_h}{T}) \qquad \text{(A.12)}$$

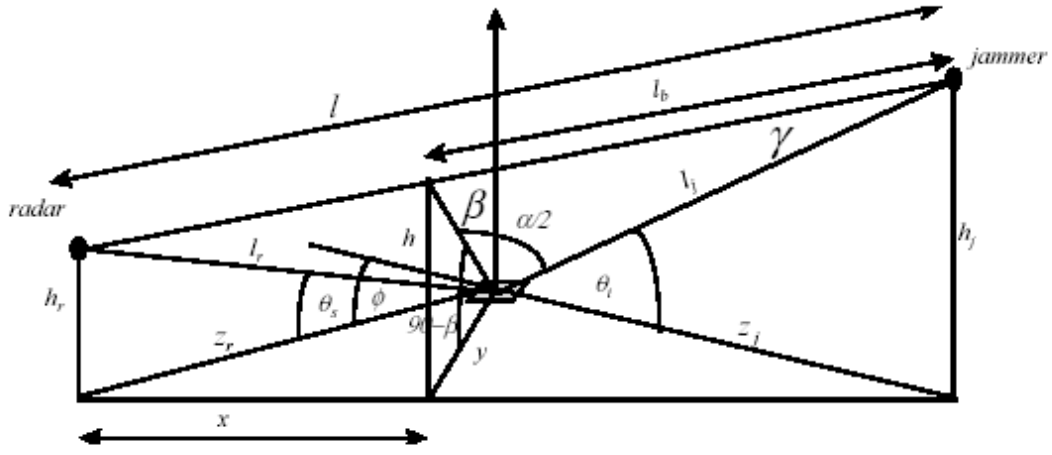

Figure 34. Calculation of Angle β [From Ref.7]

c. Region 3

$$\sigma_B^{\circ} = \gamma\sqrt{\sin\theta_i \sin\theta_s}\, F_{c1}^2 F_{c2}^2 \tag{A.13}$$

For pattern propagation factors F_{c1} and F_{c2}:

$$F_{c1}^4 = [1 + \rho_{\circ}^2 \overline{\rho}_{s1}^2 - 2\rho_{\circ}^2 \overline{\rho}_{s1} \cos(\frac{4\pi\sigma_h}{\lambda}\sin\theta_i)]^2 \tag{A.14}$$

$$F_{c2}^4 = [1 + \rho_{\circ}^2 \overline{\rho}_{s2}^2 - 2\rho_{\circ}^2 \overline{\rho}_{s2} \cos(\frac{4\pi\sigma_h}{\lambda}\sin\theta_s)]^2 \tag{A.15}$$

C. COHERENT SIDELOBE CANCELLER (CSLC)

1. Introduction

When we consider the presence of jamming interference together with the monostatic clutter that is naturally produced by ground reflections of the radar's transmitted signal, we have to deal with an extremely high jammer-to-noise ratio (JNR) by placing an antenna null adaptively in the direction of the jammer.

Energy that arrives at the radar receiver by way of bistatic path is received in the target beam with the receiver's full main beam gain. This interference cannot be mitigated using spatial-only processing, because nulling the jammer would also attenuate target returns [8]. Other terms used for this bistatic path energy are “terrain scattered jamming,” “hot clutter” or “terrain scattered interference (TSI).”

The distinction between *hot clutter* and ordinary *monostatic clutter* is that *cold clutter* or *monostatic clutter* is a reflection of the radiated radar signal, while the hot clutter refers to the multipath scattered jammer signals [8].

Scattering characteristics of the terrain, the jammer and receiver antenna patterns, and the transmitted jammer power cause the problem between antenna and jammer platform. Motion of the radar receiver or jammer platform induces a bistatic Doppler shift for each terrain reflection. This will result in nonstationary TSI, which varies as a function of time. This will result in a severe impact on the mitigation strategy that is employed. Fortunately, both TSI and monostatic clutter can effectively be mitigated using space-time adaptive processing (STAP) techniques [8].

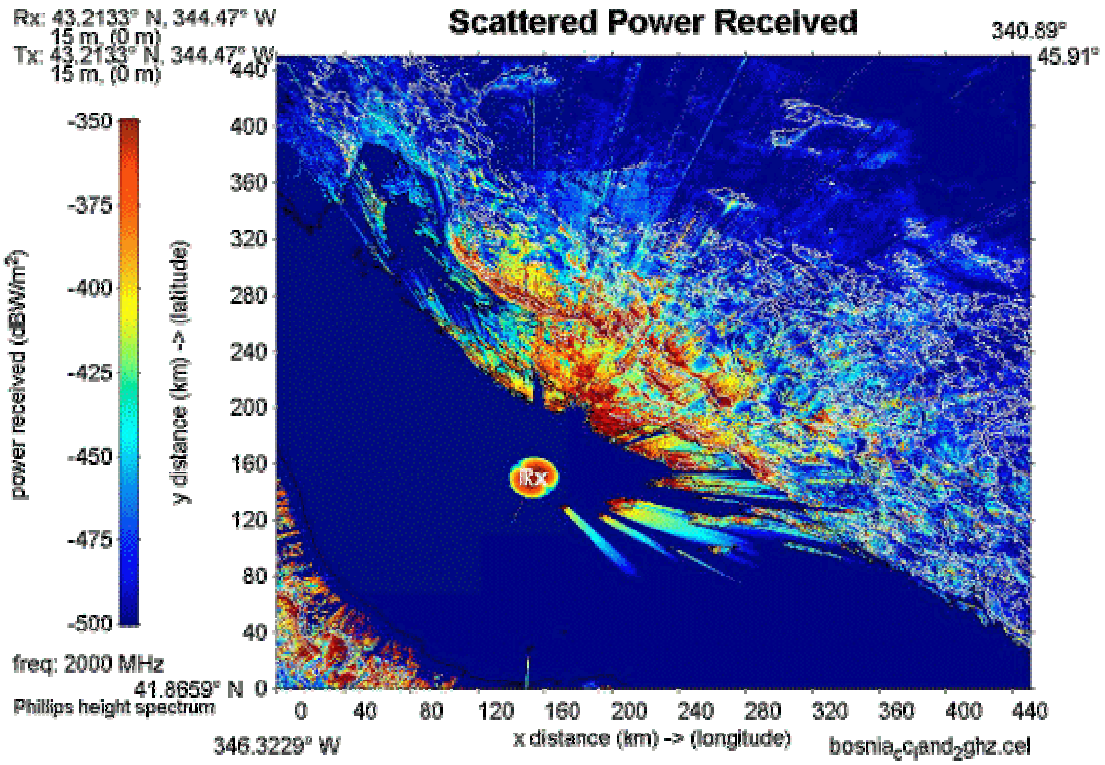

Figure 35. Cold Clutter [From Ref.9]

A CSLC is a signal processor used in conjunction with a set of antenna weights that provides a versatile form of spatial filtering. The processor combines spatial samples

of a propagating field with a variable set of weights. Weights are typically chosen to reject interfering signals and noise. In radar, the spatial filtering capability of the array facilitates cancellation of hostile jamming signals and aids in the suppression of clutter [8].

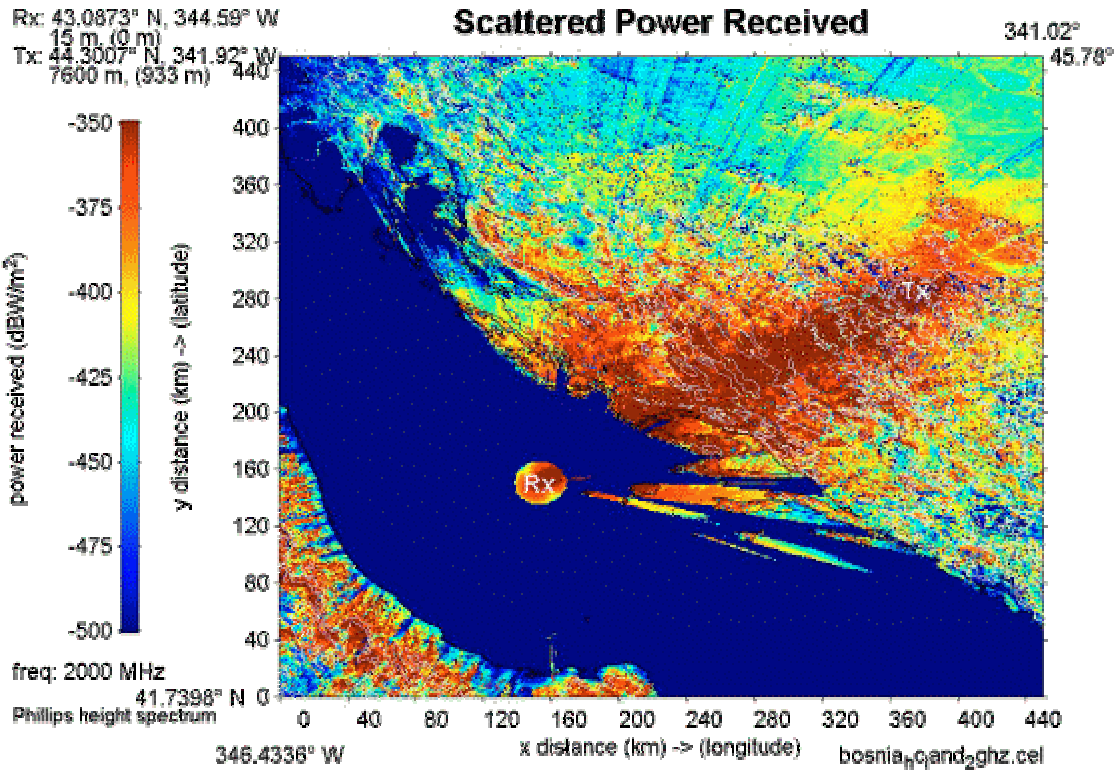

Figure 36. Hot Clutter [From Ref.9]

The practical usefulness of a CSLC is limited by the complexity associated with the computation of the adaptive weights. In an adaptive beamformer only subsets of the available degrees are used adaptively. So, the number of free weights must be computed. The principal benefits associated with reducing the number of adaptive degrees will reduce the computational burden and will improve the adaptive convergence rate.

The computational cost of adaptive algorithms is generally either directly proportional to the number of loops or proportional to the square of the number of adaptive weights.

As a result, the number of data vectors needed for the adaptive weights to converge to their response requirements will dictate reductions in the number of adaptive weights.

2. Conclusions

First of all we expect to see some decrease in the performance of jamming cancellation due to terrain reflection interference. This interference is very much dependent on the altitude of the jammer source. The higher the altitude of the jammer, the less the interference. Any reflection from rough terrain will occur over an extensive region and the amount of data present in the hot clutter is very large. Even though cancellation takes place pulse-by-pulse, each pulse contains a large number of range samples and antenna elements [10].

Hot clutter cancellation techniques rely on the presence of energy produced by the jammer, which is in the angular spectrum. Since the jammer transmitter has a large beamwidth and significant sidelobes, in addition to the main beam interference, the radar receiver will also receive jammer energy from both the direct-path and from hot clutter through the receiver sidelobes.

APPENDIX B. THEORY OF SIDELOBE CANCELLATION

A. JAMMING EFFECTS ON A RADAR

Radars are vulnerable to the negative effects of jammers due to the sidelobes of the radars antenna's radiation pattern. Jamming can affect a search radar in the following ways [14]:

- Reduce the operating range drastically,
- Overload the search Radar with non-existent targets,
- Prevent proper radar operation via saturation.

Of these three effects, reducing the operating range is the most important. The reduction of the relative operating range of a radar versus interference plus noise-to-noise ratio is plotted in Figure 37.

Figure 37 is plotted according to the radar range equation:

$$R_{max}^4 = \frac{P_t G_t G_r \lambda^2 \sigma}{(4\pi)^3 (kT_0 B N_F)(SNR)} \qquad (B.1)$$

where P_t is the transmitter power, G_t is the transmit antenna gain, G_r is the receiver antenna gain, λ is the operating wavelength, σ is the target radar cross section, (kT_0BN_F) is the receiver thermal noise power, the SNR is the signal-to-noise ratio and *R* is the detection range. This equation must be satisfied to achieve the desired detection performance with a given SNR.

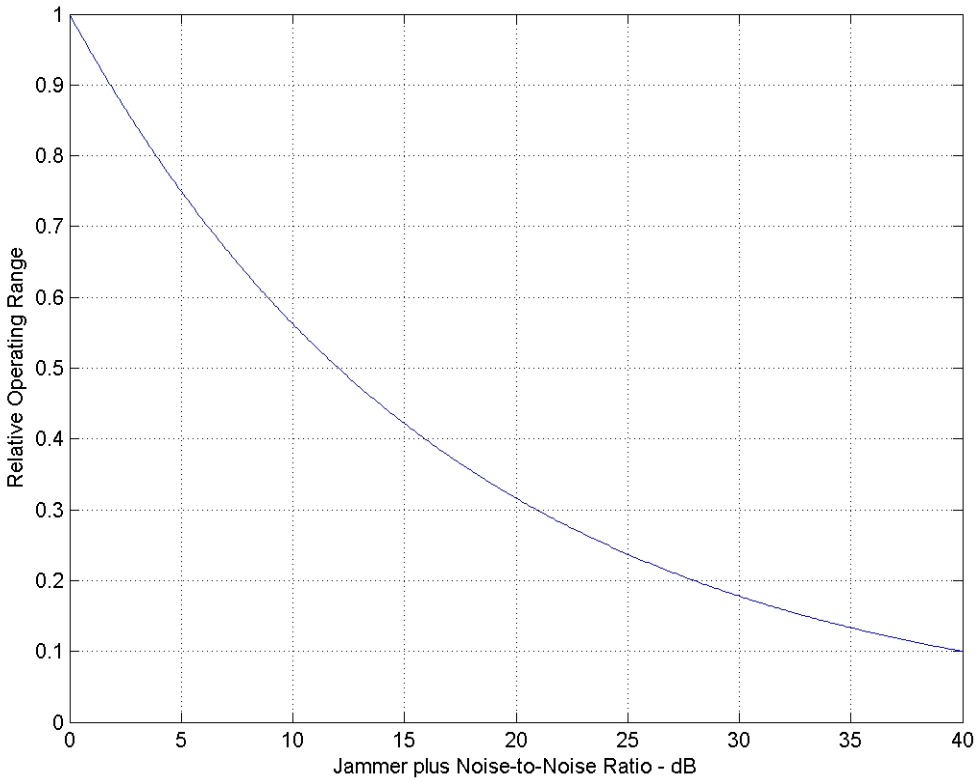

Figure 37. The Relative Operating Range of a Radar versus Interference plus Noise-to-noise Ratio

This kind of vulnerability of a radar system to jamming is due to the one-way and two-way radar range equations [6,13]. In the target case, the two-way range equation applies and the target signal power varies with the inverse of the fourth power of the range:

$$P_{target} = \frac{P_t G_t G_r \lambda^2 \sigma}{(4\pi)^3 R^4}. \qquad (B.2)$$

In the jammer case, the one-way range equation applies and the jamming power varies only with the inverse square range:

$$P_{jammer} = \frac{P_{tj} G_{tj} G_r \lambda^2}{(4\pi)^2 R^2} \qquad (B.3)$$

where P_{tj} is the jammer power, G_{tj} is the jammer antenna gain and R is the distance between the jammer and the radar antenna.

Thus, even a weak jamming power can substantially reduce the operating range of a radar, even if it enters the low gain sidelobe region of the radar antenna. Consequently, the capability of jamming rejection is one of the most desirable features for a Radar system [20].

B. TECHNIQUES TO REDUCE JAMMING EFFECTS

The efforts to reduce the vulnerability of radar systems to intentional, i.e. jamming, and unintentional interference resulted in various interference mitigation methods. Of these methods, antenna sidelobe reduction and adaptive interference cancellation are the most popular [17].

Antenna sidelobe reduction seeks to minimize the interference received beyond the antenna’s field of view by reducing the antenna sidelobe levels via the antenna’s design [17]. The most widely used dish type reflector antenna and phased array antennas can generate considerably low sidelobe levels. But to reach an ultra-low sidelobe level radiation pattern, the dish size should be much larger than the practical limits. In the case of a phased array antenna, many more antenna elements should be used

with correct phasing. Large antennas are not desirable for practical real-time applications, such as shipboard radar. Large phased-array antennas are also not cost-effective.

On the other hand, adaptive interference cancellation by using adaptive array antennas is more cost-effective than ultra-low sidelobe level antenna techniques. It is necessary to build an ultra-low sidelobe level phased-array antenna within very tight mechanical and electrical tolerances. However, for the same accepted level of performance, adaptive antenna arrays with larger mechanical and electrical building tolerances can be used owing to the self-correcting nature of the radiation patterns. As such, adaptive array antennas are more useful and more cost-effective for today's practical applications.

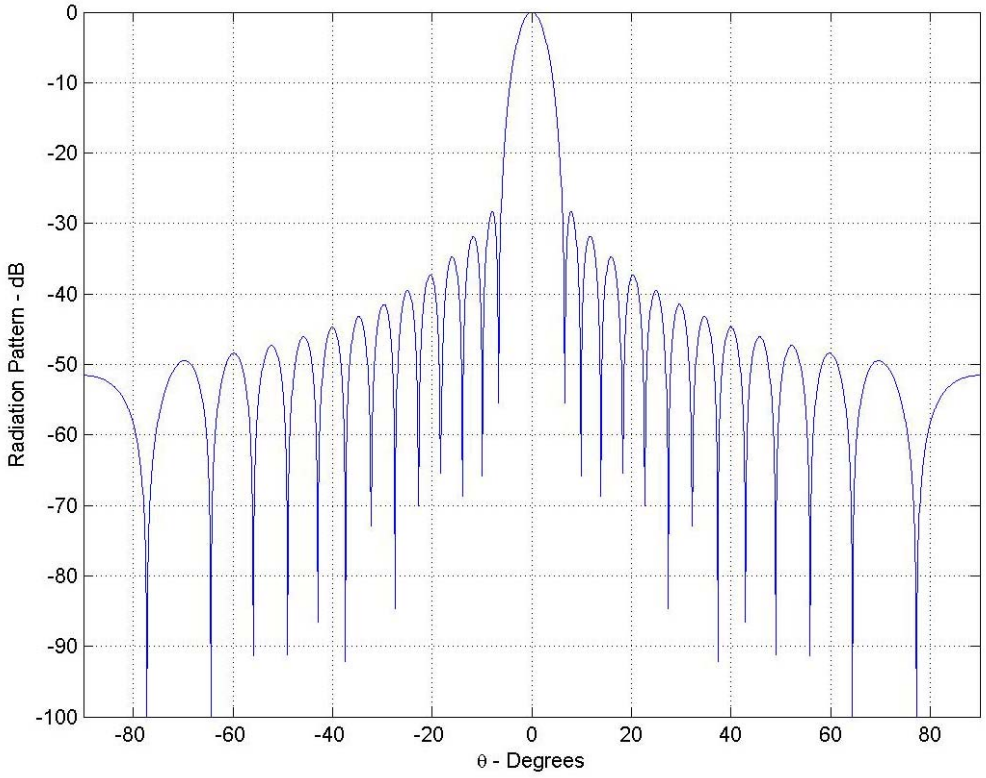

Figure 38. Pattern for an Axisymmetric Reflector Antenna Sidelobe Level = -28.28 dB, HPBW = 5^0

A conventional reflector type antenna might have a maximum ~28 dB of sidelobe level below the peak of the main beam, as seen in Figure 38. But those with sidelobe levels of –50 dB or less can be considered as ultra-low sidelobe level antennas [6].

1. Adaptive Arrays and Sidelobe Cancellers

Undesired noise appears in the signal environment. This negative effect decreases the signal-to-noise ratio and reduces the performance of the radar by reducing the operation range. Adaptive antenna arrays can be used to keep or improve the performance of the radar systems under such conditions. This is true because these antennas automatically respond to unknown interferences by steering nulls in the direction of these undesired interferences without human intervention, thereby maximizing the signal-to-noise ratio and improving the detection probability of the desired signals.

To illustrate the effect of a sidelobe canceller for a radar system, consider Figure 37 again. Suppose that a single jammer is present and it corresponds to a jammer plus noise-to-noise ratio of 28 dB. Under such a condition, the relative operating range of radar would be 0.2 units. But in the presence of a sidelobe canceller system, which has a cancellation ratio of about 16 dB, the jammer plus noise-to-noise ratio would become about 12 dB and the relative operating range would be almost 0.5 units. Here, the sidelobe canceller effect is more than double the existing operating range.

C. SIDELOBE CANCELLER CONFIGURATION

The conventional adaptive sidelobe canceller configuration is shown in Figure 39.

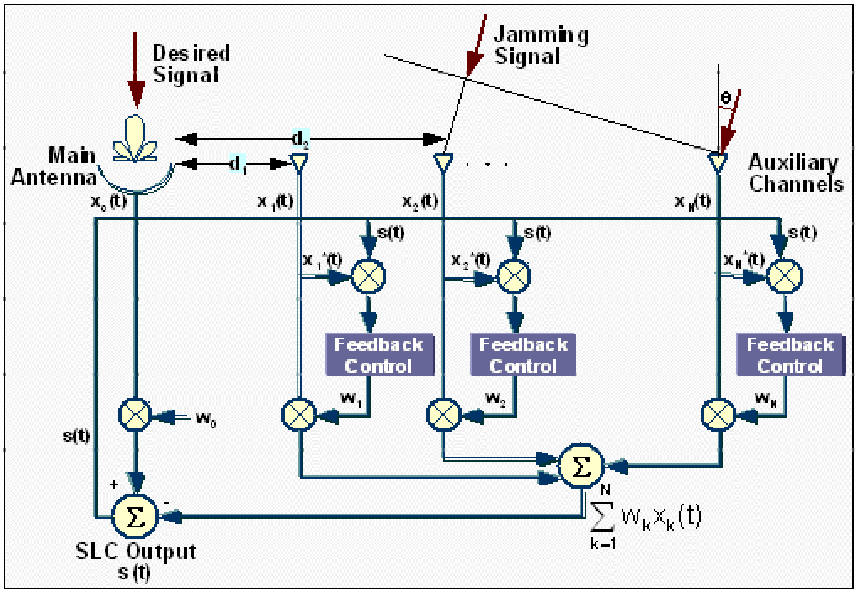

Figure 39. Conventional Sidelobe Canceller Model [From Ref.18]

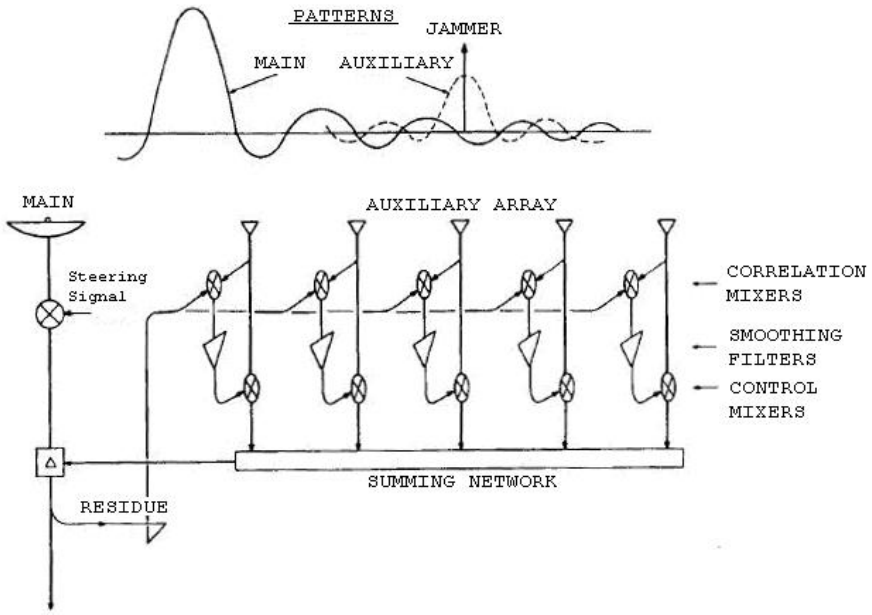

Figure 40. Conventional Adaptive SLC Configuration Analog IF Circuit [From Ref.19]

Paul Howells' text description associated with Figure 40 clearly explains the operation of the configuration:

> The simple parallel arrangement connects the auxiliary channels together as an adaptive array whose summed output is subtracted from the main channel. The complex weighting of each auxiliary is performed by its control mixer, which replaces the usual element phase shifter. A single jammer will appear in all auxiliaries with equal amplitude and a relative phase dependent on its angle of arrival. The main channel residue of that jammer is fed in parallel to all the loops, to be correlated with the jamming present there. As before, the action in each loop is to produce an output to the summing network proportional to jammer power, in phase with the main channel residue, and therefore, in phase with each other. The main channel jamming residue, therefore, serves as a steering signal that produces a uniformly weighted array beam centered on the jammer. Subtracting its output from the main channel creates a narrow null there with only minor perturbations to the pattern elsewhere. The parallel loops behave in a cooperative mode like a single loop with a directive auxiliary: loop voltage gain is increased by the gain of the array, and the auxiliary receiver noise brought over is reduced by that gain [19].

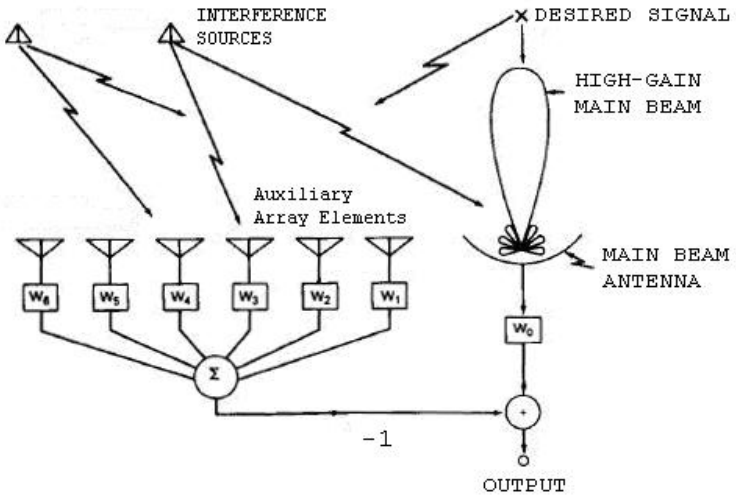

Figure 41. Conventional Adaptive SLC Configuration Nominal Schematic Diagram [From Ref.19]

The sidelobe canceller system consists of a main antenna of reflector type, an array of auxiliary antennas and a number of real-time adaptive processors that adjust the antenna element weights, W_k, to optimize, or maximize, the output signal-to-noise ratio(SNR) with selected control algorithms. The number of deep nulls this system can introduce to the total radiation pattern is equal to the number of auxiliary antennas. So the number of auxiliary antennas together with the control loops determines the degrees of freedom of the sidelobe canceller system. For strong cancellation, the number of auxiliary antennas must be at least equal to the jamming signals to be suppressed.

1. Antenna Element Spacing

The design assumes that interference arrives through the sidelobes of the main antenna and the main antenna receives both the desired signal and the interference signal components. The auxiliary antennas primarily receive interference power because their gain in the direction of the reflector's main beam is much lower. The signals received by auxiliary antennas are the same signals as the signals received by the main antenna, but with different phase shifts. According to Figure 42, the phase difference between the adjacent antenna elements is

$$\phi = 2\pi \frac{d}{\lambda} \sin\theta \qquad \text{(B.4)}$$

where ϕ is the phase difference between the first auxiliary antenna and the main antenna, *d* is the separation between these two antenna phase centers and θ is the jammer incident angle relative to the array bore sight.

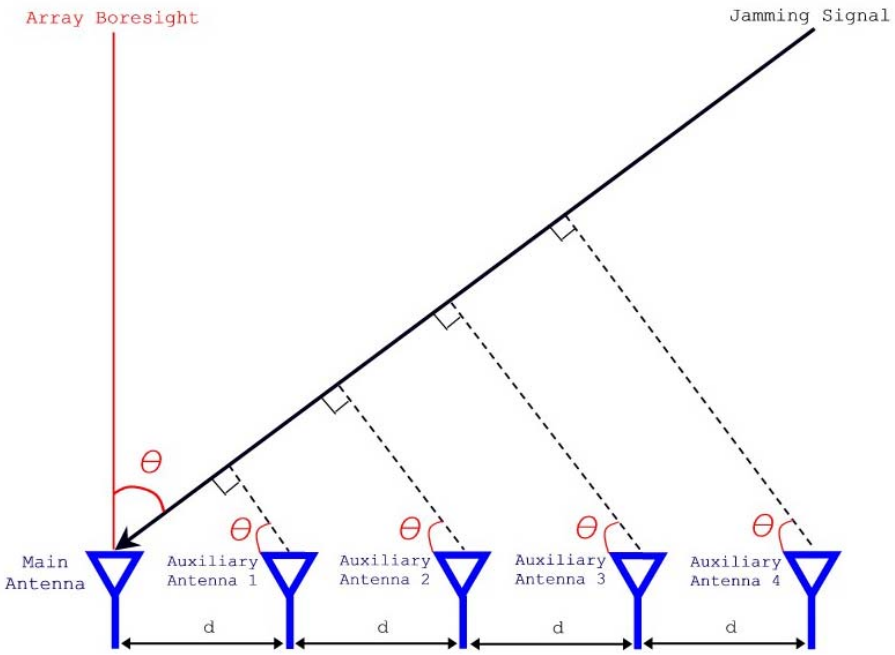

Figure 42. Illustration of Phase Difference between Received Signals in Each Channel

The auxiliary antennas should be placed as close as possible to the phase center of the main antenna. This provides more correlation between the main antenna samples and the auxiliary antenna samples. The sidelobe canceller output is determined by subtracting the auxiliary antenna array output from the main antenna output. The correlation between the main and the auxiliary antenna elements quantifies the received interference power, and this interference power is treated like an error signal in the control loop. Minimizing this error signal is equivalent to minimizing the interference [17]. As a result, higher correlation provides better cancellation performance.

Consider the following relationship for the correlation coeffient, ρ, for the one-pole filter case [21]:

$$\rho(X) = e^{(-\pi|X|)} \tag{B.5}$$

where X is the Time-Bandwidth product, which is given by:

$$X = BT_a \tag{B.6}$$

where B is the filter bandwidth, T_a is the difference between the time of arrival of the interference at the main and at the auxiliary antenna which is given by:

$$T_a = \frac{d}{c} \sin\theta \tag{B.7}$$

where θ is the angle of incidence of the interference and c is the speed of light.

It is obvious from Equation (B.5), Equation (B.6), and Equation (B.7) that a higher correlation is obtained either by reducing the separation between the phase centers of the antennas or by reducing the bandwidth of the receiving channels. Higher correlation is also obtained when the jammer incident angle is close to the array bore sight.

In a more detailed analysis, higher correlation requires the separation d between the phase centers of the main and auxiliary antennas, divided by the velocity of light, to be much less than the smaller of the receiver bandwidths [21]:

$$\frac{d}{c} \ll BW_{c_s} \tag{B.8}$$

where BW_{c_s} is the smaller of the receiver bandwidths.

2. Correlation Effects

The several values of the cancellation ratios versus the jammer-to-noise power ratio is plotted in Figure 43 for the case of one SLC loop with one auxiliary antenna.

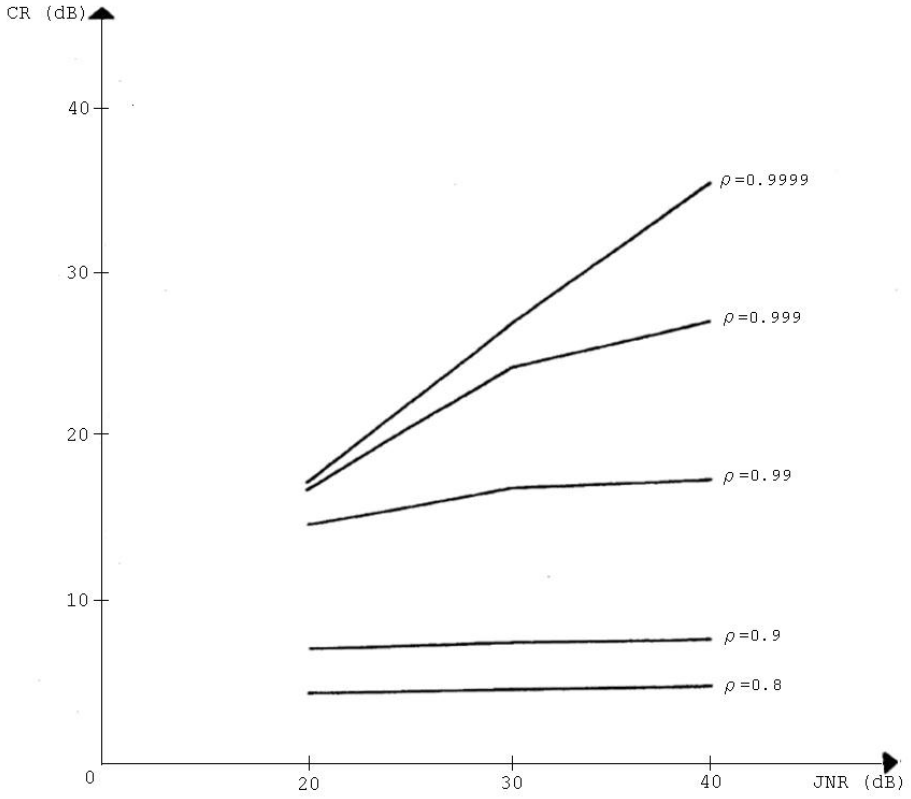

Figure 43. The Cancellation Ratio vs the Jammer-to-noise Ratio Having the Correlation Coeffient, ρ, as a Parameter [From Ref.21]

It is obvious from Figure 43 that the maximum cancellation ratio is obtained with highly correlated signals and the maximum achievable cancellation ratio is limited by the jammer-to-noise power ratio.

3. Antenna Gain Margin

Two states of the sidelobe canceller should be considered when choosing the gain margin of the auxiliary antennas [21]: The transient state and the steady state. The transient sidelobe levels are proportional to the auxiliary antenna's gain margin. A low value of gain margin is better for the transient state. However, a large value of auxiliary antenna gain margin is useful in the steady state. This is true because the weights of the auxiliary channels would be small and the corresponding internal noise powers of the auxiliary channels would be attenuated. The gain margin of the auxiliary antennas should be chosen according to this trade-off analysis. In general, the auxiliary antenna gains should approximate the average sidelobe level of the main antenna pattern [21]. An example pattern is shown in Figure 44.

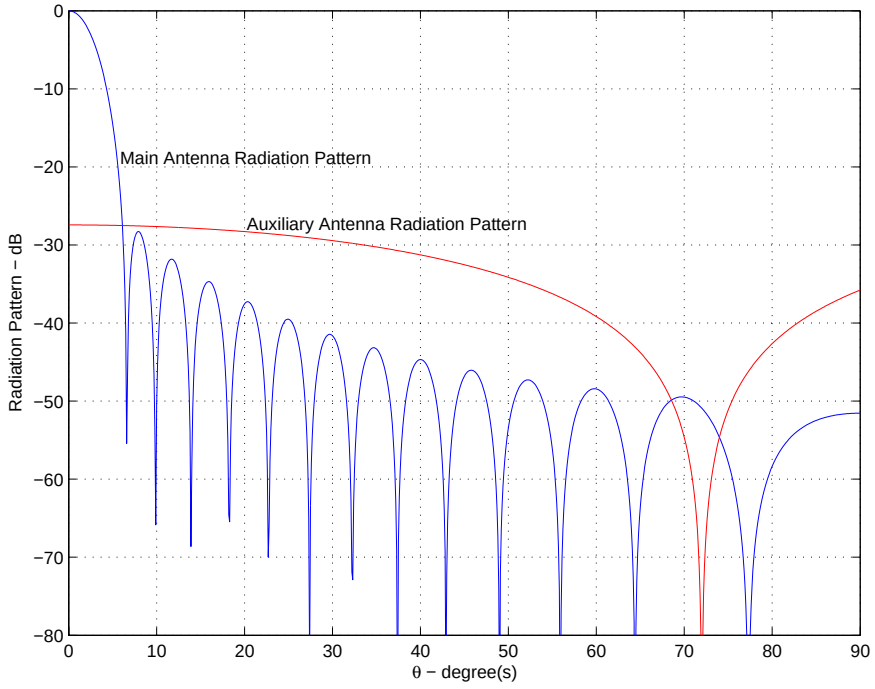

Figure 44. General Main and Auxiliary Antenna Radiation Patterns

Besides the antenna element spacing and the gain margin, finding a suitable way of controlling the auxiliary channel weights is the next major problem for adaptive arrays. The weights should be highly optimized to achieve highly correlated signals.

4. General Control Law for Sidelobe Canceller

Before establishing the general control law for the sidelobe cancellers, it is better to derive the general control law for adaptive arrays because the sidelobe canceller control law can be generated from this control law. The auxiliary channel outputs are weighted and summed and then subtracted from the main channel in the sidelobe canceller configuration.

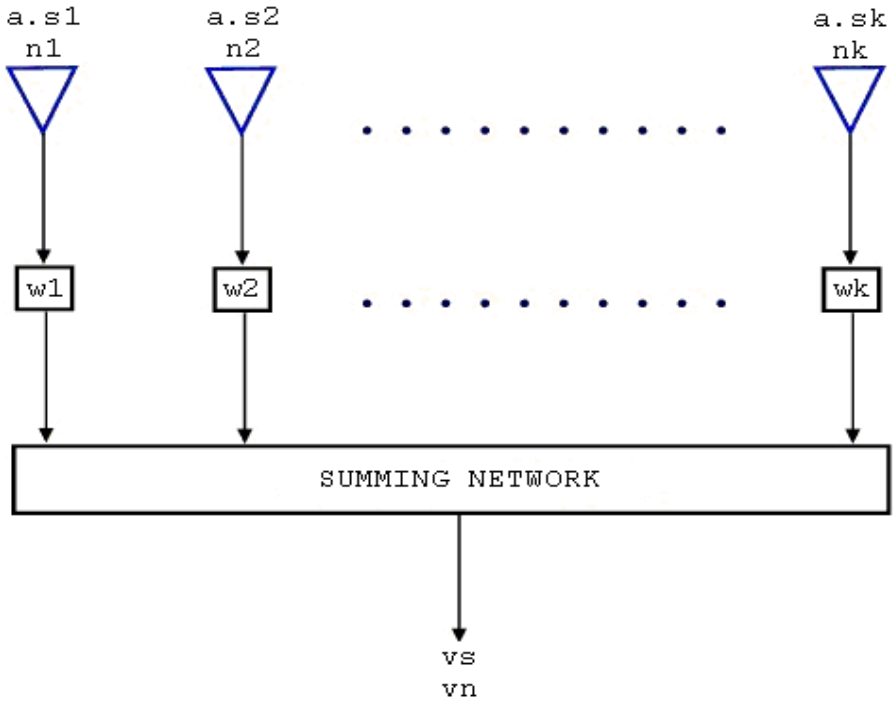

Figure 45. Functional Representation of Optimum Coherent Combiner [From Ref.26]

To derive the control law for adaptive arrays, consider Figure 45. The signal at the k^{th} channel can be represented as the product as_k, where a defines the level and time variation of the arriving signal. The s_k represents the application of the phase difference of the signal at the k^{th} antenna element. This phase difference is due to the extra path length traveled by the signal to reach k^{th} antenna element.

$$s_k = e^{ik\phi} \tag{B.9}$$

where ϕ is defined by Equation (B.4). The w_k represents the weight of k^{th} channel determined by the control law. All these signals, noises, and weights can be represented in matrix form as follows:

$$S = \begin{bmatrix} s_1 \\ s_2 \\ . \\ . \\ . \\ s_k \end{bmatrix}, N = \begin{bmatrix} n_1 \\ n_2 \\ . \\ . \\ . \\ n_k \end{bmatrix}, W = \begin{bmatrix} w_1 \\ w_2 \\ . \\ . \\ . \\ w_k \end{bmatrix}. \tag{B.10}$$

The expressions for the signal and noise outputs of the summing network in Figure 45 are

$$v_s = a\sum_{k=1}^{K} w_k s_k \, . \tag{B.11}$$

$$v_n = \sum_{k=1}^{K} w_k n_k \tag{B.12}$$

where v_s is the signal output and v_n is the noise output. In matrix notation:

$$v_s = aW^T S = aS^T W \, . \tag{B.13}$$

$$v_n = W^T N = N^T W . \qquad \text{(B.14)}$$

The superscript T denotes the matrix transpose in Equation (B.13) and Equation (B.14).

The expected noise power of summing network output is

$$\begin{aligned} P_n &= E\left\{|v_n|^2\right\} = E\left\{\left|W^T N\right|^2\right\} . \\ P_n &= E\left\{(W^T N)^*(N^T W)\right\} . \\ P_n &= E\left\{W^{T^*} N^* N^T W\right\} \end{aligned} \qquad \text{(B.15)}$$

where the asterisk(*) denotes the complex conjugate. The expectation operator will affect only the noise terms in Equation (B.15) [26]. So, P_n can be written as

$$P_n = W^{T^*} E\left\{N^* N^T\right\} W . \qquad \text{(B.16)}$$

$E\{N^* N^T\}$ is the covariance matrix of the noise components [26]. The n_k denotes the complex envelope of the noise component of the k^{th} channel in Figure 45. The covariance of n_k by n_l is

$$\mu_{kl} = E\left(n_k^* n_l\right) . \qquad \text{(B.17)}$$

$$\mu_{lk} = E\left(n_l^* n_k\right) = \mu_{kl}^* . \qquad \text{(B.18)}$$

$$M = [\mu_{kl}] \qquad \text{(B.19)}$$

where M denotes the covariance matrix of the noise outputs. The expression $E\{N^* N^T\}$ in Equation (B.16) can be changed with M in Equation (B.19) and then Equation (B.16) becomes

$$P_n = W^{T^*} M W . \qquad \text{(B.20)}$$

The covariance matrix M will be a diagonal matrix if the noise components are uncorrelated. However, matrix M may have non-zero entries in any position. Matrix M is

Hermitian, that is $M^T = M^*$ [26], from Eq.(B.18) and Eq.(B.19).

Covariance matrix M is also positive definite since the output noise power is greater than zero unless $W \neq 0$ [26].

Matrix M can be diagonalized by a nonsingular coordinate transformation since M is a positive definite Hermitian matrix. All channels will have equal power uncorrelated noise components by diagonalization of the covariance matrix M [26].

A transformation matrix A can be defined to diagonalize the covariance matrix M, as in Figure 46.

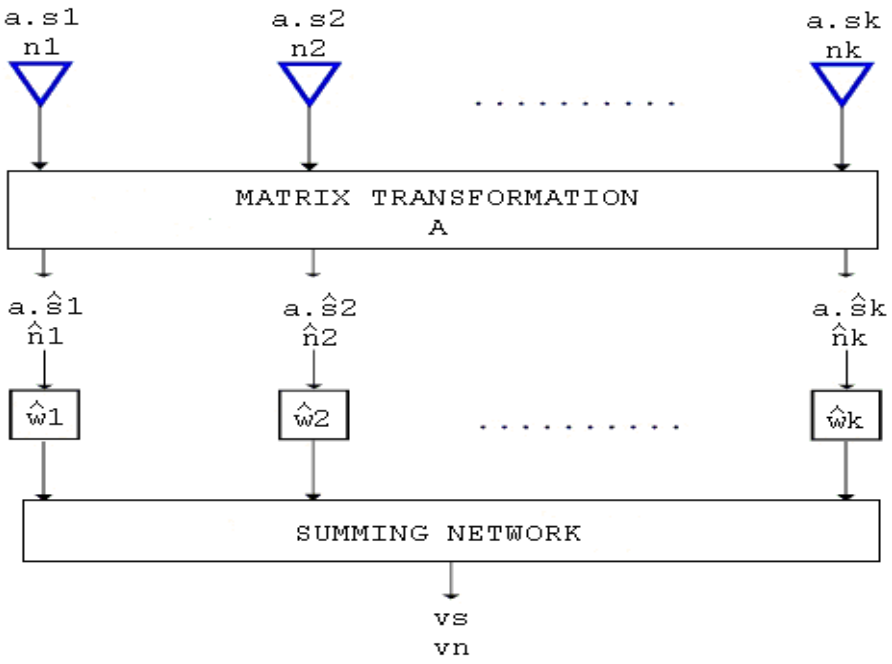

Figure 46. Use of Transformation Matrix *A* to Diagonalize Covariance Matrix M [From Ref.26]

After the transformation shown in Figure 46, the signal and noise components, respectively, become

$$\hat{S} = AS. \tag{B.21}$$

$$\hat{N} = AN \tag{B.22}$$

where the caret(^) represents the quantities after the transformation and matrices S and N are as defined in Equation (B.10). When the results of the transformation are combined with the weights, $\hat{W}$, the output signal and noise of the summing network becomes:

$$v_s = a\hat{W}^T\hat{S} = a\hat{W}^TAS. \tag{B.23}$$

$$v_n = \hat{W}^T\hat{N} = \hat{W}^TAN. \tag{B.24}$$

If Equation (B.13) and Equation (B.14) are compared with Equation (B.23) and Equation (B.24), it is obvious that combining the channels after the transformation matrix A with the weight vector $\hat{W}$ is equivalent to using the weight vector $A^T\hat{W}$ without the transformation. Thus, for equivalent outputs:

$$W = A^T\hat{W}. \tag{B.25}$$

If W in Equation (B.13) and Equation (B.14) is replaced with the expression in Equation (B.25), then Equation (B.23) and Equation (B.24) are obtained.

From Equation (B.15) and Equation (B.24), the expression for the output noise power becomes:

$$\begin{aligned} P_n &= E\left\{|v_n|^2\right\} = E\left\{\left|\hat{W}^T\hat{N}\right|^2\right\}. \\ P_n &= E\left\{(\hat{W}^T\hat{N})^*(\hat{N}^T\hat{W})\right\}. \\ P_n &= \hat{W}^{T^*}E\left\{\hat{N}^*\hat{N}^T\right\}\hat{W}. \end{aligned} \tag{B.26}$$

The covariance matrix of the noise components is simply the identity matrix of order K because the transformation matrix A decorrelates and equalizes the noise components powers [26]. Thus,

$$E\left\{\hat{N}^{*}\hat{N}^{T}\right\} = 1_{K}\,. \tag{B.27}$$

The expression for the output noise power becomes:

$$P_{n} = \hat{W}^{T^{*}}\hat{W} = \|W\|^{2}\,. \tag{B.28}$$

Since the configurations of Figure 45 and Figure 46 are equivalent, the output noise power from Equation (B.20) and Equaiton(B.25) can be written as

$$P_{n} = \hat{W}^{T^{*}}A^{*}MA^{T}\hat{W}\,. \tag{B.29}$$

Comparing Equation (B.28) and Equation (B.29), it obvious that

$$A^{*}MA^{T} = 1_{K}\,. \tag{B.30}$$

Equation (B.30) expresses that the transformation matrix A diagonolizes the covariance matrix M.

It is well known that the optimum choice for the weighting vector $\hat{W}$ in Figure 46 is given by

$$\hat{W}_{opt} = \mu\hat{S}^{*} \tag{B.31}$$

where μ is an arbitrary constant [26]. The optimum value of W may be obtained from Equation (B.25) and Equation (B.31) as

$$W_{opt} = A^{T}\hat{W}_{opt} = A^{T}\mu\hat{S}^{*}\,. \tag{B.32}$$

By changing $\hat{S}^*$ with the expression in Equation (B.21), W_{opt} in Equation (B.32) becomes:

$$W_{opt} = \mu A^T A^* S^*, \tag{B.33}$$

and finally from Equation (B.30)

$$W_{opt} = \mu M^{-1} S^*. \tag{B.34}$$

Thus the optimum weight vector for the combiner in Figure 45 is the value of weight vector W that satisfies the equation:

$$MW = \mu S^*. \tag{B.35}$$

a. Application of Control Law to Sidelobe Cancellers

In case of a sidelobe canceller system, the summing network output is subtracted from the main channel. The rejection of disturbance in the main channel is achieved by subtracting the estimate of the jamming signal from the main channel signal. So the noise power of sidelobe canceller output is

$$P_n = E\left\{\left|V_{m_n} - v_n\right|^2\right\} \tag{B.36}$$

where V_{m_n} is the noise output of the main channel and $V_{m_n} = n_m$. Replacing v_n in Equation (B.36) with the expression in Equation (B.14) gives:

$$P_n = E\left\{\left|V_{m_n} - W^T N\right|^2\right\}. \tag{B.37}$$

From Equation (B.16) and Equation (B.20), the covariance matrix M is

$$M = E\left\{N^{*}N^{T}\right\}, \tag{B.38}$$

and the cross-correlation vector, R, between the main and the auxiliary channel noises is

$$R = E\left\{n_{m}N^{*}\right\} = E\left\{V_{m_n}N^{*}\right\}. \tag{B.39}$$

The equation of the noise output of the sidelobe canceller, Equation (B.37), is a quadratic function of W with parameters M and R:

$$P = E\left\{\left|V_{m_n}\right|^{2}\right\} - W^{T^{*}}R - W^{T}R^{*} + W^{T^{*}}MW. \tag{B.40}$$

By taking the gradient of P_n with respect to W (Haykin, 1986, pp. 105-108):

$$\begin{aligned} \nabla_{w}P_{n} &= \left[\frac{\partial P_{n}}{\partial w_{1}}\ \frac{\partial P_{n}}{\partial w_{2}}\ \ldots\ \frac{\partial P_{n}}{\partial w_{K}}\right] \\ \nabla_{w}P_{n} &= 2\left[MW - R\right], \end{aligned} \tag{B.41}$$

and equating it to zero, the following equation is obtained for the optimum weights (Brennan and Reed, 1973)

$$W_{opt} = \mu M^{-1}R. \tag{B.42}$$

D. SIDELOBE CANCELLER IMPLEMENTATION

The methods for implementing the SLC can be divided into two main categories: Closed-loop or feedback control techniques and open-loop or direct solution methods. Closed-loop methods are well suited to analog implementation owing to their self-correcting nature and they do not require wide dynamic range or highly linear components. However, the main limitation of the closed-loop methods is that their speed of convergence must be restricted to achieve stable operation. Direct solution

methods require wide dynamic range and highly linear components that can only be realized digitally. But direct solution methods do not suffer from convergence speed and stability problems [21].

1. The Howells-Applebaum Closed-Loop Approach

The Howells-Applebaum control loop is the conventional analog adaptive processor for implementing the sidelobe canceller. This configuration tries to find the optimum weights in a closed-loop fashion.

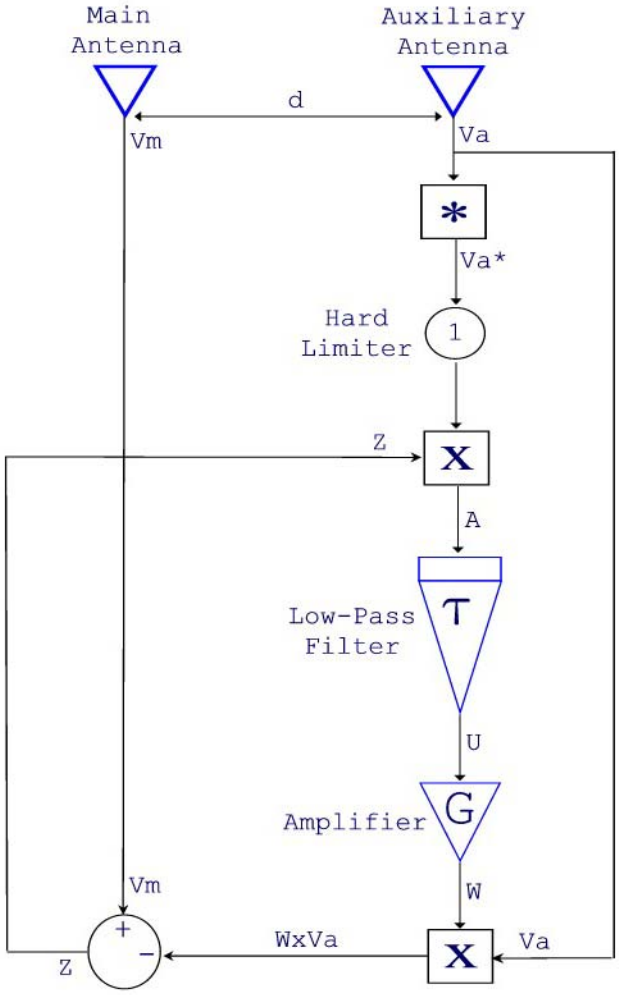

Figure 47. Functional Block Diagram of Howells-Applebaum Canceller

The equations describing the operation of Howells-Applebaum control-loop are

$$V_m = G_m A_i . \tag{B.43}$$

$$V_a = G_a A_i s_1 \tag{B.44}$$

where A_i is the arriving signal at the main antenna, s_1 is as defined by Equation (B.9), G_m and G_a are the gains of the main and auxiliary antennas at the direction of arrival of the signal, respectively [14][21].

$$Z = V_m - WV_a \tag{B.45}$$

where Z is the output of the sidelobe canceller and W is the complex weight determined by the control loop.

$$A = ZV_a^* \tag{B.46}$$

where A is the input to the low-pass filter. From Equation (B.45) and Equation (B.46), A can be written as

$$A = V_m V_a^* - W(V_a V_a^*) \tag{B.47}$$

$$A = V_m V_a^* - W|V_a|^2 . \tag{B.48}$$

The output of the low-pass filter is U. So the equation for U is

$$\tau_{LPF} \frac{dU}{dt} + U = A \tag{B.49}$$

where τ_{LPF} is the integration time constant of the low-pass filter. Weight is calculated by amplifying U with a high-gain amplifier:

$$W = GU \tag{B.50}$$

where G is the amplifier gain.

If Equations (B.48), (B.49) and (B.50) are combined, then Equation (B.49) can be written in the following form:

$$\tau_{LPF} \frac{dW}{dt} \frac{1}{G} + \frac{W}{G} = V_m V_a^* - W |V_a|^2 . \qquad \text{(B.51)}$$

Equation (B.51) can be rearranged as:

$$\frac{dW}{dt} + \frac{W}{\tau_{LPF}} = \frac{G}{\tau_{LPF}} \left(V_m V_a^* - W |V_a|^2 \right), \qquad \text{(B.52)}$$

$$\frac{dW}{dt} + W \left(\frac{1 + G |V_a|^2}{\tau_{LPF}} \right) = \frac{G}{\tau_{LPF}} \left(V_m V_a^* \right) \qquad \text{(B.53)}$$

where $G |V_a|^2$ is the closed-loop gain [21]. Equation (B.53) is the stochastic non-linear differential equation describing the weights.

In the Howells-Applebaum control-loop, the weighting signal is developed in a closed-loop fashion, which causes the power of residual signal, Z, to be a minimum [21].

a. Weight Mean and Variance

It is necessary to solve the stochastic non-linear differential equation, Equation (B.53), to evaluate the sidelobe canceller performance properly. The presence of the stochastic processes, V_m and V_a, makes the weight a stochastic process itself [21]. The calculation of weights according to their stochastic nonlinear differential equation has been considered in reference 22 and accurate expressions for the mean, $\bar{W}$, and the variance, σ_w^2, of $W(t)$ have been obtained in the following forms:

$$\bar{W}(t) = e^{\left(\frac{-t}{\tau_{SLC}}\right)} W_0 + \rho \left\{ e^{\left(\frac{-t}{\tau_{SLC}}\right)} - 1 \right\} \qquad \text{(B.54)}$$

where W_0 is the statistics of the initial value of $W(t)$ and ρ is the correlation coefficient between the signals at the main and the auxiliary antenna elements, V_m and V_a [22]. According to statistics [22]

$$\rho = \frac{E\{V_m V_a\}}{p^2} \tag{B.55}$$

where p^2 denotes the power of V_a and V_m:

$$p^2 = |V_a|^2 = |V_m|^2 . \tag{B.56}$$

In the steady-state condition, the mean value of the weight approaches the limit value of

$$\bar{W}_{t\to\infty} = \frac{\rho G V_a^2}{1 + G V_a^2} \tag{B.57}$$

whereas, in the least-mean-square sense, the optimal value of W is

$$W_{opt} = \rho . \tag{B.58}$$

This is an unbiased estimate of W_{opt} considering that $GV_a^2 \gg 1$. However, $\bar{W}_{t\to\infty}$ is a random variable with a variance of

$$\sigma^2_{\bar{W}_{t\to\infty}} = (1 + \rho^2) F(\alpha) \tag{B.59}$$

where α is defined as:

$$\alpha = \frac{BW_{SLC}}{2BW_C} = \frac{\tau_c}{2\tau_{SLC}}, \tag{B.60}$$

which is the ratio of the sidelobe canceller bandwidth to twice the receiver channel bandwidth [22].

F is a function that takes α as the parameter [22] and F is defined as:

$$F(\alpha) = \sqrt{\frac{\pi}{2}}\alpha e^{\left(\frac{\alpha^2}{2}\right)}\left[\frac{1}{2} - \left|\mathrm{erf}(\alpha)\right|\right] \qquad \text{(B.61)}$$

where the error function $\mathrm{erf}(X)$ is

$$\mathrm{erf}(X) = \frac{1}{\sqrt{2\pi}}\int_0^X e^{\left(-\frac{1}{2}y^2\right)}dy\,. \qquad \text{(B.62)}$$

b. Performance Evaluation

Two figures of merit define the sidelobe canceller performance [21]: the time required to compute the estimated weights and the power cancellation ratio at the steady-state condition. These two figures compete with each other.

First, the steady-state performance of the circuit should be explained.

The sidelobe canceller output signal, which is defined by Equation (B.45), is a zero-mean process. The facts that $E\{V_m\} = 0$ and $E\{WV_a\} = 0$ make the output signal a zero-mean process [22].

The cancellation ratio is defined as the ratio of input jamming power to the output residual power:

$$CR = \frac{E\{V_m^2\}}{E\{Z^2\}} \qquad \text{(B.63)}$$

where $E\{Z^2\}$ is the output residual power.

The uncancelled output power is

$$E\{Z^2\} = E\{V_m^2\} + E\{W^2V_a^2\} - 2E\{V_m W V_a\}. \qquad \text{(B.64)}$$

Assuming that weight is a gaussian process [22], then

$$\begin{aligned} E\{V_m^2\} &= p^2. \\ E\{W^2V_a^2\} &= E\{V_m^2\}\,E\{W^2\} = p^2E\{W^2\}. \\ E\{V_m W V_a\} &= E\{V_m V_a\}\,E\{W\} = p^2\rho E\{W\}. \end{aligned} \qquad \text{(B.65)}$$

In the steady-state condition, the cancellation ratio in Equation (B.63) follows from Equations (B.57), (B.59) and (B.64) as

$$CR = \frac{1}{(1-\rho^2) + (1+\rho^2)\,F(\alpha)} \qquad \text{(B.66)}$$

where α and $F(\alpha)$ are defined by Equations (B.60) and (B.61) , respectively, [21,22].

It is obvious that the effect of the variance of the weight, $\sigma^2_{w_{t\to\infty}}$, on the system cancellation can be evaluated as a function of α, which is the ratio of the sidelobe canceller bandwidth to twice the receiver channel bandwidth, as in Equation (B.60). Here, α is the key parameter of the system. The cancellation ratio versus α is plotted in Figure 48 for some values of correlation coeffient ρ.

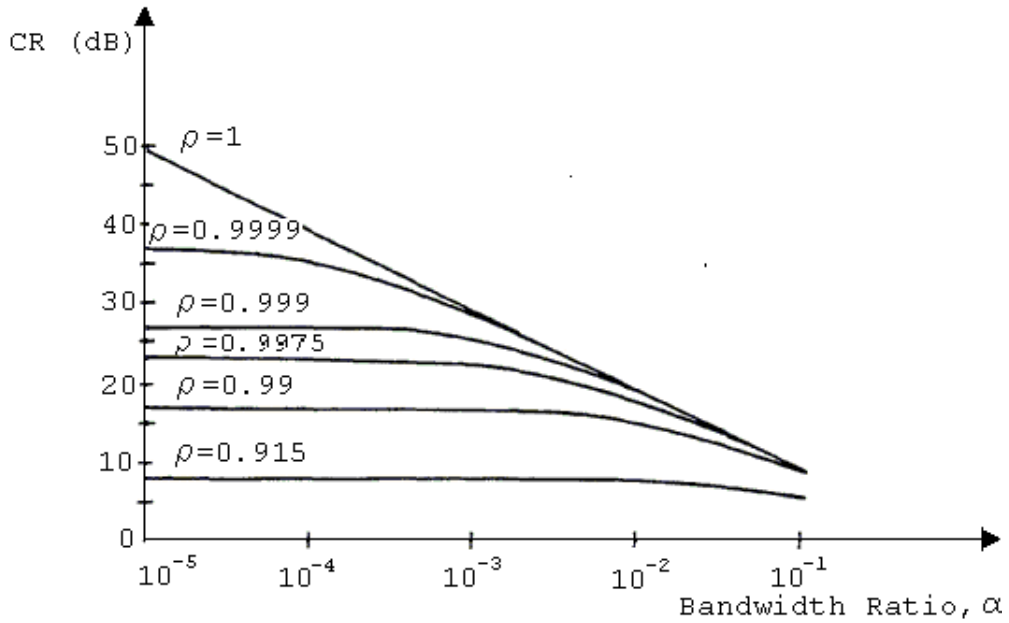

Figure 48. Cancellation Ratio versus α for Single Sidelobe Canceller [From Ref.22]

Figure 48 illustrates the importance of keeping α as low as possible to obtain high cancellation performance, even at the expense of a slower circuit response [21][22]. When α reaches zero, the cancellation ratio approaches its ideal value because canceller loop time constant reaches to infinity as $\alpha \rightarrow 0$ and an infinite time of observation is spent to obtain a precise estimate of the correlation coefficient ρ. The effect of the correlation coefficient on the cancellation ratio was discussed in Appendix-A section C-2 and shown in Figure 43. To reach the optimum value of the weight, which is defined in Equation (B.57), the transient time constant of the sidelobe canceller loop should be [21]

$$\tau_{SLC} = \frac{\tau_{LPF}}{\left(1 + G\left|\bar{V}_a\right|^2\right)} . \qquad (B.67)$$

c. Trade-off Analysis

The weight reaches its ideal value when $GV_a^2 \gg 1$. It seems that increasing $G\left|\overline{V}_a^2\right|$ is a good strategy to reach the ideal cancellation. But, according to Equation (B.67), increasing $G\left|\overline{V}_a\right|^2$ reduces the sidelobe canceller loop time constant and a decrease in τ_{SLC} increases the sidelobe canceller loop bandwidth, BW_{SLC}. Thus, this increases the amount of interference power transferred to the output and worsens the cancellation. In other words, a decrease in τ_{SLC} causes an increase in α and worsens the cancellation. In fact, the mean value of the weight would quickly reach the steady-state condition with increasing $G\left|\overline{V}_a\right|^2$, but the variance of the weight, $\sigma^2_{w_{t\to\infty}}$, would also be increased, thus reducing the efficiency of the jammer cancellation. This is called the loop-noise effect and this is the main limitation of the Howells-Applebaum control loop [21][22].

The loop noise effect requires a careful design of the circuit parameters of the amplifier gain and low-pass filter time constant so that the canceller loop functions properly. The canceller loop time constant should be kept within the limits of $\tau_{SLC} \geq 10\tau_c$ by choosing the appropriate values for the circuit parameters, as explained below.

Since the bandwidth of the receiver channels are generally fixed, τ_c cannot be readily changed. So, the sidelobe canceller loop bandwidth should be adjusted to reduce α according to Equation (B.60).

To obtain a good average of the weight process, the sidelobe canceller loop bandwidth should not exceed one-tenth of the receiver channel bandwidth [14,24]:

$$BW_{SLC} \leq \frac{BW_c}{10}, \tau_{SLC} \geq 10\tau_c . \qquad \text{(B.68)}$$

Higher loop time constant causes a longer response time, but better cancellation owing to a decrease in the weight variance and loop bandwidth, as discussed earlier.

The minimum value of the loop gain can be calculated by using the quiescent receiver noise level. In the minimum conditions, there will be no external interference source and the output of the receiving channel equals the receiver self noise:

$$V_a = n_a \qquad \text{(B.69)}$$

where n_a is the receiver self noise. To obtain the ideal condition for the weight, the following condition should be met: $G\left|\bar{V}_a\right|^2 \gg 1$. See Equation (B.57) and Equation (B.58).

To obtain $G\left|\bar{V}_a\right|^2 \gg 1$ for the minimum condition, the amplifier gain should be chosen to satisfy Equation (B.70):

$$G \geq \frac{1}{\left|\bar{n}_a\right|^2} . \qquad \text{(B.70)}$$

This is the minimum value condition for the amplifier gain.

Loop gain, $G|\bar{V}_a|^2$, will be increased due to an increase in V_a as the external interference power increases. The low-pass filter time constant should be chosen according to the level of maximum interference power that the loop handles. Clearly, an increase in the external interference power decreases the sidelobe canceller loop time constant. To keep τ_{SLC} within the limits defined by Equation (B.68) a proper value should be chosen for the low-pass filter time constant. The τ_{SLC} reaches its minimum value when $G|\bar{V}_a|^2$ reaches its maximum value. The low-pass filter time constant should be high enough to keep τ_{SLC} within its limits as the external interference power increases.

To address the maximum condition, the closed loop gain can be expressed in terms of the minimum loop gain, $G|\bar{n}_a|^2$, and the interference power ratio [24].

$$\frac{G|\bar{V}_a|^2}{G|\bar{n}_a|^2} = \frac{G\left(|\bar{n}_a|^2 + |\bar{J}|^2\right)}{G|\bar{n}_a|^2} = 1 + \frac{|\bar{J}|^2}{|\bar{n}_a|^2}. \qquad \text{(B.71)}$$

The ratio of the squares of the voltage magnitudes, $\frac{|\bar{J}|^2}{|\bar{n}_a|^2}$, is equal to the ratio of the interference power-to-receiver noise power, P_i. Then the closed loop gain is

$$G|\bar{V}_a|^2 = G|\bar{n}_a|^2(1 + P_i) \qquad \text{(B.72)}$$

where the minimum loop gain can be fixed at any desired value by choosing an appropriate value for the amplifier gain, as discussed previously. The maximum interference

power to be handled by the loop, $P_{i_{max}}$, determines the maximum loop gain [24], $\left(G\left|\bar{V}_a\right|^2\right)_{max}$:

$$\left(G\left|\bar{V}_a\right|^2\right)_{max} = G\left|\bar{n}_a\right|^2\left(1 + P_{i_{max}}\right) = \left(G\left|\bar{V}_a\right|^2\right)_{min}\left(1 + P_{i_{max}}\right). \quad \text{(B.73)}$$

All the discussions above define the minimum value of the low-pass filter time constant in relation to the maximum interference power to be handled by the loop

$$\tau_{SLC} \geq 10\tau_C, \tau_{SLC_{min}} = 10\tau_C. \quad \text{(B.74)}$$

The maximum closed loop gain defines $\tau_{SLC_{min}}$:

$$\tau_{SLC_{min}} = \frac{\tau_{LPF}}{1 + \left(G\left|\bar{V}_a\right|^2\right)_{max}}. \quad \text{(B.75)}$$

From Equation (B.73)

$$\tau_{LPF_{min}} = \tau_{SLC_{min}}\left(1 + \left(G\left|\bar{V}_a\right|^2\right)_{min} + \left(G\left|\bar{V}_a\right|^2\right)_{min} P_{i_{max}}\right). \quad \text{(B.76)}$$

$$\tau_{LPF_{min}} = 10\tau_C\left(1 + \left(G\left|\bar{V}_a\right|^2\right)_{min} + \left(G\left|\bar{V}_a\right|^2\right)_{min} P_{i_{max}}\right). \quad \text{(B.77)}$$

$$\tau_{LPF} \geq 10\tau_C\left(1 + \left(G\left|\bar{V}_a\right|^2\right)_{min} + \left(G\left|\bar{V}_a\right|^2\right)_{min} P_{i_{max}}\right). \quad \text{(B.78)}$$

It is evident from Equation (B.67) and Equation (B.75) that the sidelobe canceller loop time constant, or in other words, the response time of the canceller loop depends on the external excitation conditions. The variance of the weight in the steady state is also related to this external power level. This dependence can cause wide variations in the canceller’s performance, ranging from excessive control loop noise when the interference is strong, or very slow convergence time when the interference is small [23].

d. Hard-limiter Modification

The envelope limiting technique can help reduce the effects of the varying external noise intensity without degrading the loop performance [23]. Inserting a coherent hardlimiter at point 1 of Figure 47 is likely to reduce such dependence [14,24]. After the hardlimiting, the signal at the mixer input becomes

$$\text{Output}_{\text{Hard limiter}} = \frac{V_a^*}{|V_a|} . \tag{B.79}$$

The amplitude variation in the conjugate signal has been removed and only the phase variation is retained. The mixer output is sensitive to the phase of its input, but not to its input amplitude. Thus, limited signals can be used without loss of information [13]. After the hardlimiter modification, the closed loop gain becomes

$$G|\bar{V}_a|^2 \Rightarrow G|\bar{V}_a| . \tag{B.80}$$

At the minimum conditions, when there is no external interference power, the loop gain will be equal to

$$\left(G|\bar{V}_a|\right)_{min} = G|\bar{n}_a| . \tag{B.81}$$

The minimum loop gain should be fixed at any desired value by choosing an appropriate value for the amplifier gain to satisfy $GV_a \gg 1$.

Addressing the maximum condition after hardlimiting, Equation (B.71) can be written as

$$\frac{G|\bar{V}_a|}{G|\bar{n}_a|} = \frac{G\sqrt{|\bar{n}_a|^2 + |\bar{J}|^2}}{G\sqrt{|\bar{n}_a|^2}} = \sqrt{1 + \frac{|\bar{J}|^2}{|\bar{n}_a|^2}} = \sqrt{1 + P_i} . \tag{B.82}$$

$$G|\bar{V}_a| = G|\bar{n}_a|\sqrt{(1 + P_i)} . \tag{B.83}$$

The Maximum loop gain is determined by the maximum interference power to be handled by the loop.

$$\left(G\left|\bar{V}_a\right|\right)_{max} = G\left|\bar{n}_a\right|\sqrt{\left(1 + P_{i_{max}}\right)} = \left(G\left|\bar{V}_a\right|\right)_{min}\sqrt{\left(1 + P_{i_{max}}\right)}. \quad \text{(B.84)}$$

To keep the canceller loop time constant within limits defined by Equation (B.74), the minimum value of the low-pass filter time constant should be

$$\tau_{SLC_{min}} = \frac{\tau_{LPF}}{1 + \left(G\left|\bar{V}_a\right|\right)_{max}}. \quad \text{(B.85)}$$

$$\tau_{LPF_{min}} = \tau_{SLC_{min}}\left(1 + \left(G\left|\bar{V}_a\right|\right)_{min}\sqrt{\left(1 + P_{i_{max}}\right)}\right). \quad \text{(B.86)}$$

$$\tau_{LPF_{min}} = 10\tau_C\left(1 + \left(G\left|\bar{V}_a\right|\right)_{min}\sqrt{\left(1 + P_{i_{max}}\right)}\right). \quad \text{(B.87)}$$

$$\tau_{LPF} \geq 10\tau_C\left(1 + \left(G\left|\bar{V}_a\right|\right)_{min}\sqrt{\left(1 + P_{i_{max}}\right)}\right). \quad \text{(B.88)}$$

Note that because of the square root of $P_{i_{max}}$, the low-pass filter time constant is faster now owing to the factor determined by this square-root process. The effective time constants that determine the rate of convergence and control loop noise are changed by this square-root factor, thus reducing the dependence of loop performance on the intensity of the external noise field.

THIS PAGE INTENTIONALLY LEFT BLANK

LIST OF REFERENCES

[1] D.C.Schleher, “Electronic Warfare in the Information Age”, Norwood, MA: Artech House, 1999.

[2] D.C.Schleher, “Introduction to Electronic Warfare”, Norwood, MA: Artech House, 1986.

[3] B.R.Mahafza, “Introduction to Radar Analysis”, CRC Press LLC, 1998.

[4] W.L.Stutzman, G.A.Thiele, “Antenna Theory and Design”, 2nd Edition, John Wiley & Sons, Inc., 1998.

[5] S.Kingsley, S.Quegan, “Understanding Radar Sysytems”, SciTech Publishing, Inc., 1999.

[6] M.L.Skolnik, “Introduction to Radar Systems”, Third Edition, Mc Graw Hill, 2001.

[7] K-B. Yu, S.Sowelam, “Modeling and Mitigation of Terrain Scattered Interference for Advanced Shipboard Radar”, GE Research & Development Center, June 2000.

[8] U.G.Arrazola, “Adaptive Array Processing for Airborne Radar”,Research Page of U.Garro, February 2000, http://www.see.ed.ac.uk, last accessed May 3rd 2004.

[9] Space-Time Adaptive Processing (STAP) for Advanced Phased Array Radars, http://www.navysbir.brtrc.com, last accessed June 11th 2004.

[10] S.M.Kogon, D.B.Williams, E.J.Holder, “Beamspace Techniques for Hot Clutter Cancellation”, IEEE, 1996.

[11] P.M.Techau, “Effects of Receiver Filtering on Hot Clutter Mitigation”, Information Systems Laboratories, Inc., IEEE, 1999.

[12] P.Parker, A.L.Swindlehurst, “A Parametric Approach to Hot Clutter Cancellation”, IEEE, 2001.

[13] E.Nicolau, D. Zaharia, “Adaptive Arrays”, Elsevier, 1989.

[14] A.Farina, “Single Sidelobe Canceller: Theory and Evaluation”, IEEE, VOL.AES-13, No.6, November 1977.

[15] M.C.Wicks, B.Himed, “Four Problems in Radar”, NATO Advanced Study Institute, Computational Noncommutative Algebra and Applications, July 6--19, 2003, http://www.prometheus-inc.com, last accessed August 12th 2004.

[16] Royal School of Artillery, “Electronic Warfare” Basic Science & Technology Section Gunnery Staff/Career Courses, 20 May 1995.

[17] D.J.Hinshilwood, R.B.Dybdal, “Adaptive Nulling Antennas for Military Communications”, http://www.aero.org, last accessed June 15th 2004.

[18] F.Wright, “ Electronic Countermeasures (ECM) Analysis”, Georgia Tech Research Institute,2003.

[19] W.F. Gabriel, “Adaptive Processing Array Systems”, Proceedings of IEEE, Vol. 80, No.1, January 1992.

[20] Z.Fu, “Adaptive Arrays Antenna Systems”, http://www.people.cornell.edu, last accessed 9 May 2004.

[21] A.Farina, “Antenna-Based Signal Processing Techniques for radar Systems”, Artech House, Inc. 1992.

[22] A.Farina, F.A.Studer, “Evaluation of sidelobe-canceller performance”, IEE Proceedings, Vol. 129, Pt. F, No.1 February 1982.

[23] L.E.Brennan, I.S. Reed, “Effect of Envelope Limiting in Adaptive Array Control Loops”, IEEE Transactions on Aerospace and Electronic Systems, July 1971.

[24] W.F. Gabriel, “Adaptive Arrays–An Introduction”, Proceedings of IEEE, Vol. 64, No.2, February 1976.

[25] L.E.Brennan, E.L.Pugh, I.S.Reed, “Control-Loop Noise in Adaptive Array Antennas” IEEE Transactions on Aerospace and Electronic Systems,Vol. AES-7, No.2, March 1971.

[26] S.P Applebaum, “Adaptive Arrays”, IEEE Transactions on Antennas and Propagation, VOL. AP-24, NO.5, September 1976.

[27] J.E. Hudson, “Adaptive Array Principles”, The Institution of Electrical Engineers, London and New York, 1981.

THIS PAGE INTENTIONALLY LEFT BLANK

INITIAL DISTRIBUTION LIST

1. Defense Technical Information Center
   Ft. Belvoir, Virginia

2. Dudley Knox Library
   Naval Postgraduate School
   Monterey, California

3. Chairman
   Information Sciences Department
   Monterey, California

4. Professor Daniel C. Schleher
   Information Sciences Department
   Monterey, California

5. Professor David C. Jenn
   Department of Electrical and Computer Engineering
   Monterey, California

6. MAJ. Sargun Goktun
   Hava Kuvvetleri Plan Prensipler Bsk.ligi
   Ankara, Turkey

7. LTJG. Ercan Oruc
   Genelkurmay Baskanligi Elektronik Harp Subesi
   Ankara, Turkey

8. Hava Harp Okulu Komutanligi
   Hava Harp Okulu Kutuphanesi
   Yesilyurt, Istanbul Turkey

9. Deniz Harp Okulu Komutanligi
   Deniz Harp Okulu Kutuphanesi
   Tuzla, Istanbul Turkey

10. Hava Kuvvetleri Komutanligi
    Elektronik Harp Subesi
    Ankara, Turkey

11. Deniz Kuvvetleri Komutanligi
    Elektronik Harp Subesi
    Ankara, Turkey